Cold and trapped metastable noble gases

Vassen, W.; Cohen-Tannoudji, C.; Leduc, M.; Boiron, D.; Westbrook, C.I.; Truscott, A.; Baldwin, K.; Birkl, G.; Cancio, P.; Trippenbach, M.

published in
Reviews of Modern Physics
2012

DOI (link to publisher)
10.1103/RevModPhys.84.175

document version
Publisher's PDF, also known as Version of record

Cold and trapped metastable noble gases

Wim Vassen[*]

LaserLaB Vrije Universiteit, De Boelelaan 1081, 1081 HV Amsterdam, The Netherlands

Claude Cohen-Tannoudji and Michele Leduc[†]

Ecole Normale Superieure and College de France, Laboratoire Kastler Brossel, 24 rue Lhomond, 75231 Paris Cedex 05, France

Denis Boiron and Christoph I. Westbrook[‡]

Laboratoire Charles Fabry de l'Institut d'Optique, CNRS, Univ Paris-Sud, Campus Polytechnique RD128 91127 Palaiseau France

Andrew Truscott and Ken Baldwin[§]

ARC Centre of Excellence for Quantum-Atom Optics Research School of Physics and Engineering, Australian National University, Canberra, ACT 0200, Australia

Gerhard Birkl[‖]

Institut für Angewandte Physik, Technische Universität Darmstadt, Schlossgartenstraße 7, 64289 Darmstadt, Germany

Pablo Cancio[¶]

Istituto Nazionale di Ottica (INO-CNR) and European Laboratory for Non-linear Spectroscopy (LENS), Via N. Carrara 1, 50019 Sesto Fiorentino FI, Italy

Marek Trippenbach[**]

Wydzial Fizyki, Uniwersytet Warszawski, ul. Hoza 69, 00-681 Warszawa, Polska

(published 24 February 2012)

Experimental work on cold, trapped metastable noble gases is reviewed. The aspects which distinguish work with these atoms from the large body of work on cold, trapped atoms in general is emphasized. These aspects include detection techniques and collision processes unique to metastable atoms. Several experiments exploiting these unique features in fields including atom optics and statistical physics are described. Precision measurements on these atoms including fine structure splittings, isotope shifts, and atomic lifetimes are also discussed.

DOI: 10.1103/RevModPhys.84.175 PACS numbers: 03.75.−b, 67.85.−d, 34.50.−s, 32.30.−r

CONTENTS

I. Introduction 176
II. Production and Detection 178
A. Discharge sources 179
B. Intense and slow beams of metastable atoms 179
C. Magneto-optical trapping 180
D. Magnetic trapping 181
E. Optical dipole trapping 181
F. Evaporative cooling and quantum degeneracy 182
G. Detection of metastable noble gas atoms 183
1. Optical detection 183
2. Direct detection using electron multipliers 184
3. Detection by use of Penning ionization 185
III. Cold Collisions 185
A. Elastic collisions of He 186
B. Ionizing collisions in He 186
1. Measurement of ionizing collisions in a MOT 187
2. Two-body and three-body losses for spin-polarized $^4He^*$ 188
3. Collisions in the presence of light 189
C. Elastic and inelastic collisions in Ne 189
D. Ionizing collisions in Ar, Kr, and Xe 190
E. Mixtures 190
1. $^3He/^4He$ 191
2. $^4He/^{87}Rb$ and $^{40}Ar/^{85}Rb$ 191
F. Feshbach resonances 191
IV. Photoassociation 192

[*]w.vassen@vu.nl
[†]leduc@lkb.ens.fr
[‡]christoph.westbrook@institutoptique.fr
[§]kenneth.baldwin@anu.edu.au
[‖]gerhard.birkl@physik.tu-darmstadt.de
[¶]pablo.canciopastor@ino.it
[**]matri@fuw.edu.pl

A. General features for metastable atoms 192
B. One-photon photoassociation of metastable helium 192
C. Formation of long-range helium molecules 192
V. Scattering Length Measurements 193
A. Determinations from collisional properties 193
B. Determinations using photoassociation 193
VI. Spectroscopic Measurements of Atomic Properties 194
A. Metastable state lifetimes 194
B. Precision spectroscopy of atomic structure 195
1. Precision spectroscopy on triplet levels of He^* 195
2. Precision spectroscopy on heavier metastable noble gases 197
VII. Atom Optics Experiments 197
A. Interferometry 197
B. Metastable helium atom laser 197
1. Atom laser spatial profiles 198
2. Feedback control of an atom laser beam 199
VIII. Pair Correlation Experiments 199
A. Correlation effects in equilibrium ensembles 199
B. Four-wave mixing of matter waves 201
1. Pair production in the spontaneous regime 201
2. Paired atom laser beams in the stimulated regime 202
IX. Other Experiments Using Cold, Metastable Noble Gases 203
A. Reflection of slow metastable atoms from surfaces 203
B. Birth and death of a Bose-Einstein condensate 203
C. Hydrodynamic regime close to the bosonic degenerate regime 204
X. Outlook 204

I. INTRODUCTION

Cold atom physics came to life three decades ago and has been expanding ever since. It started as a subfield of atomic physics and now extends to other domains such as molecular physics, statistical physics, condensed matter, and quantum information [see Chu (2002), for an introduction to these topics]. The field began with the demonstration of cooling and trapping methods based on the light-matter interaction. This work was recognized in 1997 by a Nobel physics prize (Chu, 1998; Cohen-Tannoudji, 1998; Phillips, 1998). The achievement of Bose-Einstein condensation (BEC) in cold dilute gases (Anderson *et al.*, 1995; Bradley *et al.*, 1995; Davis *et al.*, 1995; Cornell and Wieman, 2002; Ketterle, 2002), followed by the realization of degenerate Fermi gases (DeMarco and Jin, 1999; Schreck *et al.*, 2001; Truscott *et al.*, 2001), opened up new perspectives to study situations in which particle statistics and interactions play a central role (Pethick and Smith, 2002; Stringari and Pitaevskii, 2003). In addition to providing new connections between atomic and condensed matter physics, it has long been recognized that the production of cold atoms is useful for improving atomic spectroscopy and atomic clocks (Chu, 2002; Lemonde, 2009; Derevianko and Katori, 2011). Another broadening of the field came a few years ago with the extension of cooling methods to molecules of two or three atoms, including cooling molecules in their ground state (Carr *et al.*, 2009).

Two major advances of the past decade have provided particularly interesting possibilities. First, it became possible to modify the interaction strength between ultracold atoms by simply tuning a magnetic field, taking advantage of Feshbach resonances (Köhler, Góral, and Julienne, 2006; Chin *et al.*, 2010). Second, one can now manipulate cold atoms in optical potentials, change the dimensionality of the system, and load the gas into tailored periodic potentials (optical lattices), created by pairs of counterpropagating laser beams, offering the opportunity to simulate condensed matter systems (Jessen and Deutsch, 1996; Bloch, 2005; Bloch, Dalibard, and Zwerger, 2008).

For noble gases in their ground state, the powerful laser cooling and manipulation methods that have been developed cannot, unfortunately, be easily applied because the wavelengths of the resonance lines are far in the ultraviolet. These atoms, however, have metastable excited states which are connected to higher-lying levels by allowed transitions and are accessible with current lasers. With lifetimes ranging from 15 to 7870 s (see Table I for a summary of atomic data of the most common metastable noble gases), these metastable states serve as effective ground states for optical manipulation and detection. Figures 1 and 2 show the relevant level structure of helium and neon.

Metastable noble gas cooling began in the 1980s, with pioneering experiments on helium (Aspect *et al.*, 1988) and neon (Shimizu, Shimizu, and Takuma, 1987). The initial work on helium concentrated on velocity selective coherent population trapping (Aspect *et al.*, 1988; Hack *et al.*, 2000), a technique which permits cooling below the single photon recoil velocity. The experiments raise interesting issues in statistical physics because the behavior of the velocity distribution is dominated by rare events and can be interpreted with the theory of Lévy flights. This field was reviewed by Cohen-Tannoudji (1998) and Bardou *et al.* (2002) and we will not discuss this work in great detail in this review.

In 2001 Bose-Einstein condensation of metastable helium atoms was demonstrated (Pereira Dos Santos, Léonard *et al.*, 2001; Robert *et al.*, 2001) and 2006 saw the realization of the first degenerate Fermi gas of metastable helium (McNamara *et al.*, 2006). It is remarkable that these gases can be cooled to or close to quantum degeneracy (kinetic energy $\approx 10^{-10}$ eV) in spite of their large internal energy (≈ 20 eV). In that sense, they are rather exotic and offer unusual features that have produced many results complementary to those with other atoms, as outlined in this article.

At first sight the internal energy of a metastable atom is primarily a drawback, because it makes them difficult to produce and intrinsically fragile. They tend to deexcite in collisions with surfaces as well as with other atoms. Two colliding identical metastable noble gas atoms Ng^* (we use an asterisk to denote an atom in a metastable state) have a large probability of undergoing Penning ionization, resulting in the destruction of the metastable atoms and the production of one ion, one atom in the ground state, and one electron (normal Penning ionization) or a molecular ion and an electron (associative ionization):

TABLE I. Atomic data of some common metastable noble gases. The energy of the metastable state is given with respect to the ground state. The wavelength λ and lifetime τ refer to the most commonly used laser cooling transition. The Doppler limit is $\hbar/(2\tau k_B)$ and the recoil limit is $h^2/(2m\lambda^2 k_B)$. "Lifetime" refers to the lifetime of the metastable state. Loss rate (Pol. and Unpol.) refer to the two-body inelastic rate constants $\beta(=2K_{SS})$ for a polarized or unpolarized sample in the absence of any resonant light. References for energies and vacuum wavelengths: NIST Atomic Spectra Database (http://www.nist.gov/physlab/data/asd.cfm).

Atom species	^{3}He*	^{4}He*	^{20}Ne*	^{22}Ne*	^{40}Ar*	^{84}Kr*	^{132}Xe*
Abundance	0.01	99.99	90.48	9.25	99.60	57.00	26.91
Metastable state	2^3S_1	2^3S_1	$3s[3/2]_2(^3P_2)$	$3s[3/2]_2(^3P_2)$	$4s[3/2]_2(^3P_2)$	$5s[3/2]_2(^3P_2)$	$6s[3/2]_2(^3P_2)$
Energy (eV)	19.820	19.820	16.619	16.619	11.548	9.915	8.315
Laser cool. wavelength λ (nm)	1083.46	1083.33	640.40	640.40	811.75	811.51	882.18
Upper state lifetime τ (ns)	97.89	97.89	19.5	19.5	30.2	28.0	33.03
Doppler limit (μK)	38.95	38.95	196	196	140.96	133.4	115.64
Recoil limit (μK)	5.433	4.075	2.337	2.125	0.727	0.346	0.186
Exp. lifetime (s)	-	7870(510)[a]	14.73(14)[b]	···	38^{+8}_{-5} [c]	28.3(1.8),[d] 39^{+5}_{-4},[c]	42.9(9)[e]
Theory lifetime (s)	7860[f]	7860[f]	22,[g] 17.1,[h] 24,[i]	22,[g] 17.1,[h] 24,[i]	56,[g] 51,[i]	85,[g] 63,[i]	150[g], 96[i]
Scat. length (nm)	···	7.512[j]	$-9.5(2.1)$[k]	$7.9^{+4.2}_{-2.7}$[k]	···	···	···
Pol. loss rate (10^{-14} cm^3/s)	···	2(1)[l]	650(180)[k]	1200(300)[k]	···	40 000[m,n]	6000[e,o]
Unpol. loss rate (10^{-11} cm^3/s)	38(6)[p]	20(4)[p]	50(30)[q]	100^{+40}_{-50}[r]	58(17)[s]	40[m]	6(2)[e]

[a] Hodgman *et al.* (2009b).
[b] Zinner *et al.* (2003).
[c] Katori and Shimizu (1993).
[d] Lefers *et al.* (2002).
[e] Walhout, Sterr, Orzel *et al.* (1995).
[f] Łach and Pachucki (2001).
[g] Indelicato *et al.* (1994).
[h] Tachiev and Froese Fischer (2002).
[i] Small-Warren and Chiu (1975).
[j] Moal *et al.* (2006).
[k] Spoden *et al.* (2005).
[l] Tychkov *et al.* (2006) (see Sec. III.B.2).
[m] Katori and Shimizu (1994).
[n] Katori, Kunugita, and Ido (1995).
[o] Orzel *et al.* (1999).
[p] Stas *et al.* (2006) (see Fig. 10).
[q] Kuppens *et al.* (2002).
[r] van Drunen (2008).
[s] Busch *et al.* (2006), value obtained in a MOT without extrapolation to vanishing light intensity.

$$\mathrm{Ng}^* + \mathrm{Ng}^* \rightarrow \begin{cases} \mathrm{Ng} + \mathrm{Ng}^+ + e^- \\ \mathrm{Ng}_2^+ + e^-. \end{cases} \quad (1)$$

In most experiments we do not discriminate between these two processes, so we often refer to both of them as Penning ionization in the following. A review of the general field of Penning ionization can be found by Siska (1993). The existence of strong Penning ionization was initially thought to hinder the production of dense samples of metastable atoms, but, as discussed in Sec. III, an effective way to overcome this disadvantage was demonstrated, at least for helium and to some extent for neon: ionization is strongly suppressed in a spin-polarized sample (Shlyapnikov *et al.*, 1994; Vassen, 1996; Spoden *et al.*, 2005). Furthermore, the study of Penning collisions with ultracold atoms has turned out to be a fruitful domain in itself.

On the other hand, dealing with metastable atoms offers unique advantages. It provides new observation methods which are not possible with ground-state atoms. Metastable atoms hitting a surface lose their energy, expelling an electron which can be detected with good efficiency using electron multipliers. This detection scheme provides both spatial and temporal resolution as well as single atom sensitivity. Thus the study of two-particle correlations is natural (see Sec. VIII). In addition, Penning collisions in the gas result in emission of ions and electrons which can also be detected with electron multipliers. This feature gives information about the dynamics of the atoms in real time, while keeping them trapped. Real time, *in situ* detection is sometimes advantageous compared to the usual time-of-flight methods used for detecting cold atoms, and we give some examples in later sections.

In this review, metastable helium plays a special role. This is in part because it is the only metastable atom to date in which quantum degeneracy has been achieved. This success is partly due to its simplicity: The absence of orbital angular momentum in the ground state and its low mass means that relativistic effects are not important and that electron spin is nearly conserved in collisions. The simplicity of the helium atom has other ramifications which we illustrate in this review. Helium is the simplest atom after hydrogen, composed of only three particles (one nucleus and two electrons), and its atomic structure can be calculated *ab initio* with great accuracy. Atomic spectroscopy using cold helium is of great interest because of our ability to make precision measurements of lifetimes, Lamb shifts, and the fine structure. The latter is especially important because it leads to a spectroscopic method to determine the fine structure constant.

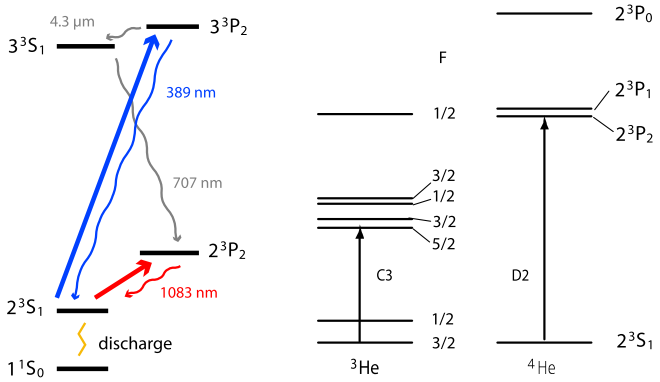

FIG. 1 (color online). Energy levels for helium: (left) principal helium transitions for laser cooling and trapping. The long-lived metastable $2\,^3S_1$ state (20 eV above the ground state) is used as an effective ground state and the $2\,^3S_1 - 2\,^3P_2$ transition at 1083 nm transition is used for laser cooling and trapping. The $2\,^3S_1 - 3\,^3P_2$ transition at 389 nm is used in some studies. (right) Excited-state manifold for the 1083 nm cooling transition in both ^{3}He and ^{4}He (not to scale). For ^{4}He, the $2\,^3S_1 - 2\,^3P_2$ $D2$ transition is used and for ^{3}He, which shows a hyperfine structure as a result of the $I = 1/2$ nuclear spin, the $C3$ transition ($F = 3/2 - F = 5/2$) is used.

Molecular potentials between interacting helium atoms can also be calculated *ab initio* with great precision, meaning that collisions between two helium atoms in the $2\,^3S_1$ metastable state can be accurately described theoretically. Metastable helium dimers can be created by photoassociation and their spectra provide accurate methods for measuring the s-wave scattering length between two colliding atoms, a quantity of critical importance for understanding the properties of interacting ultracold atoms.

In this article we emphasized the specific features of cold metastable noble gas atoms and described the great variety of experiments that they have enabled. Our emphasis is on experiments and we therefore do not discuss exhaustively the theoretical literature, especially that on collisions of cold metastable atoms. Even with respect to experiments, we do not cover all possible topics; ultracold neutral plasmas and atom lithography are not discussed and atom interferometry is discussed only briefly. Discussions of these three topics can be found elsewhere (Baldwin, 2005; Cronin, Schmiedmayer, and Pritchard, 2009; Killian and Rolston, 2010).

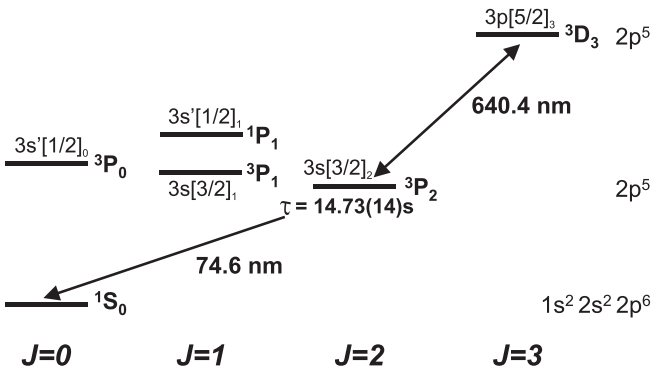

FIG. 2. Neon energy levels (not to scale). The metastable $^3P_2$ state can be manipulated by light on a transition to the upper ^3D states.

Section II is devoted to the production and detection of cold clouds of metastable noble gas atoms, describing metastable production, beam slowing, and trapping. Detection techniques which are often what distinguishes cold, metastable atom experiments from others in the field are also discussed in some detail. Section III gives a detailed description of the different types of collisions taking place between cold metastable noble gases from helium to xenon, distinguishing between inelastic collisions resulting in atom losses, and elastic ones that help thermalizing the cloud at each step of the evaporation process. Sections IV and V deal with photoassociation experiments leading to the formation of exotic giant helium dimers as well as to an accurate determination of the s-wave scattering length of He*. We then turn to precision measurements of atomic properties, in particular, of atomic lifetimes, fine structure and isotope shifts (Sec. VI). Sections VII, VIII, and IX discuss several experiments in atom optics and statistical physics which have been enabled by our ability to produce cold samples of metastable atoms and to detect them often on a single atom basis. Section X outlines what appears to us to be the most promising avenues for future research.

II. PRODUCTION AND DETECTION

The experimental techniques for producing cold (mK) and ultracold (μK) samples of metastable noble gas atoms are similar to the ones developed since the 1980s for alkali atoms. Important steps are (1) slowing, cooling, and trapping of gas-phase atoms with near-resonant laser light (Chu, 1998; Cohen-Tannoudji, 1998; Phillips, 1998; Metcalf and van der Straten, 1999); (2) transfer of the atoms to conservative trapping potentials, such as magnetic traps or optical dipole traps; and (3) evaporative or sympathetic cooling for a further reduction of the sample temperature and an increase in its phase-space density. This sequence is followed by a determination of the final sample parameters, such as temperature, density, and phase-space density, and in the case of aiming at quantum degeneracy, by obtaining evidence for the transition to BEC or to Fermi degeneracy.

We mentioned in the Introduction the necessity of studying noble gas atoms in metastable states. This fact has some essential consequences for experimental implementations: (1) atoms in a metastable state have to be created in a discharge or by electron bombardement rather than being evaporated in an oven as for other atomic species, and the efficiency of exciting the atoms into the metastable state in the discharge is low with a large number of atoms remaining in the ground state; (2) inelastic collisions between metastable noble gas atoms present a strong additional loss mechanism since the metastable state energy exceeds half of the ionization energy; but also (3) the high internal energy allows the implementation of highly sensitive electronic detection techniques not available for alkali atoms.

Figure 3 presents a schematic overview of a typical experimental setup for the production of ultracold noble gas atoms. Some details may vary between different realizations and atomic species, but the general configuration remains the same. Noble gas atoms (Ng*), excited to a metastable state by means of an electric discharge in a liquid nitrogen or liquid

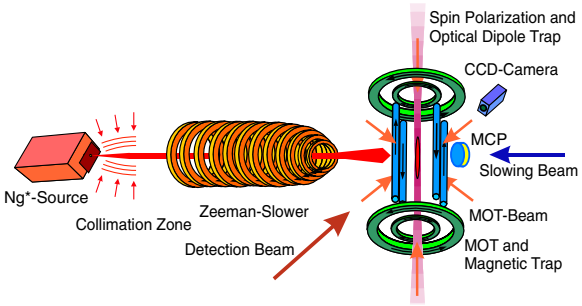

FIG. 3 (color online). Example of an experimental setup for producing ultracold metastable noble gas (Ng^*) atoms. A more detailed example of a source is shown in Fig. 4. After the source comes a region of transverse collimation using radiation pressure from resonant laser beams, and a Zeeman slower in which the atomic beam is slowed down. Specific for research on metastable noble gases is the microchannel plate (MCP) detector, which allows detection of ions (produced by Penning ionization) or metastable atoms, released from a trap. This particular setup is used with neon atoms.

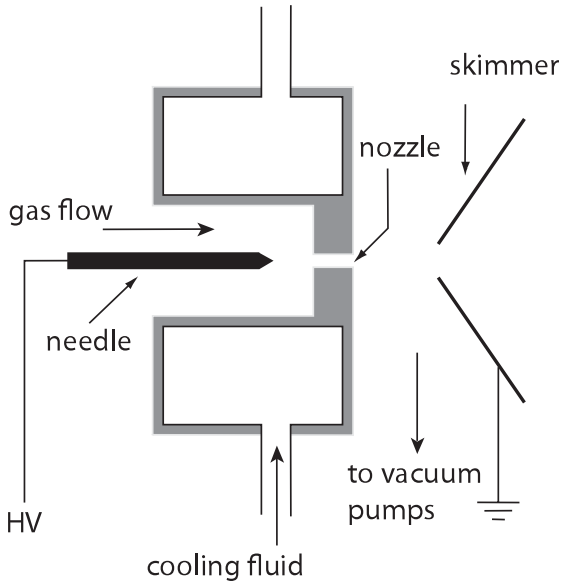

FIG. 4. Example of a simple discharge source to produce a beam of metastable atoms, showing a high voltage (HV) needle cathode, a cooled nozzle, and a grounded skimmer.

helium cooled gas source, are collimated by radiative pressure forces in a transverse laser field. The collimated beam of metastable atoms is then slowed in a Zeeman slower and used to load a magneto-optical trap (MOT). After the laser cooling phase, the atoms are spin polarized by optical pumping and loaded into a static magnetic trap or into an optical dipole trap. Radio-frequency (rf) forced evaporative cooling (in magnetic traps) or evaporation by lowering the trap depth (in dipole traps) enables a further cooling of the atomic cloud. After switching off the trap, the atoms are detected either optically by fluorescence and absorption imaging or electronically on an electron multiplier detector.

In the following sections, the different stages in this production process are described in more detail. The parameters given are typical values and may vary for the different noble gas species and for different experimental realizations.

A. Discharge sources

For the investigation and manipulation of cold metastable noble gas atoms, a long-lived metastable triplet state has to be populated. Excitation to the metastable state can be achieved by collisions with electrons in an electric discharge (Gay, 1996). Different types of discharge sources, such as needle-type cathode dc discharge sources (Kawanaka *et al.*, 1993; Rooijakkers, Hogervorst, and Vassen, 1995), hollow cathode dc discharge sources (Swansson *et al.*, 2004), or rf-driven discharge sources (Carnal and Mlynek, 1991; Chen *et al.*, 2001) are used routinely. A quantitative comparison of different types of dc sources can be found in Lu *et al.* (2001), Palmer, Baker, and Sang (2004), and Swansson *et al.* (2004). Figure 4 shows a typical example of a needle-type discharge source. The discharge runs between the cathode and an anode close to it or through a nozzle of typically 0.3–2 mm diameter to an external anode, in some cases serving as a skimmer in addition (see Fig. 4). The source is cooled by liquid nitrogen (Kawanaka *et al.*, 1993) or in some cases even by liquid helium (Aspect *et al.*, 1988; Carnal and Mlynek, 1991; Woestenenk *et al.*, 2001; Swansson *et al.*, 2004) for a reduction of the initial mean velocity of the resulting atomic beam.

Only a fraction of 10^{-5} to 10^{-4} (Metcalf and van der Straten, 1999; Stas *et al.*, 2006) of the atoms leaving the discharge are in the metastable state. For this reason, efficient removal of the unwanted load of ground-state atoms is required. A skimmer transmits only a small fraction of the solid angle of the atomic beam and serves as the first differential pumping stage. The large remaining gas load is pumped away by oil-diffusion or turbomolecular pumps backed by rotary vane vacuum pumps. After the skimmer, one or more additional differential pumping stages with turbomolecular pumps are implemented before the atom beam reaches the low pressure region of the main vacuum chamber. Maximum beam intensities of 10^{15} metastable atoms $sr^{-1}s^{-1}$ can be achieved (Lu *et al.*, 2001).

B. Intense and slow beams of metastable atoms

Because of the low fraction of metastable atoms and the long distance between the source and the main vacuum chamber, an increase in luminance of the atomic beam is desirable. This is achieved by transverse collimation of the beam of metastable atoms using two-dimensional (2D) transverse radiative pressure forces (Shimizu, Shimizu, and Takuma, 1987, 1990; Aspect *et al.*, 1990; Morita and Kumakura, 1991; Vansteenkiste *et al.*, 1991; Hoogerland, Milic *et al.*, 1996; Rooijakkers, Hogervorst, and Vassen, 1996; Metcalf and van der Straten, 1999; Rasel *et al.*, 1999; Partlow *et al.*, 2004), focusing in a hexapole (Woestenenk *et al.*, 2001) or 2D magneto-optical compression (Scholz *et al.*, 1994; Schiffer *et al.*, 1997; Labeyrie *et al.*, 1999). For maximum efficiency, the collimation zone, which has a typical length of several to a few tens of cm, has to be implemented as close as possible to the source, typically directly after the skimmer. With collimation, an increase of

the atom flux up to a factor of 150 has been reported (Hoogerland, Driessen *et al.*, 1996).

In order to prevent ground-state atoms from entering the main ultrahigh vacuum (UHV) section, the axis of the collimation zone can be tilted with respect to the axis of the Zeeman slower (Vansteenkiste *et al.*, 1991; Scholz *et al.*, 1994). The collimated metastable atoms follow this bend and propagate through an aperture, but the ground-state atoms continue along a straight path which is then blocked. An alternative way to reduce the gas load in the UHV chamber is to use a shutter that blocks the atomic beam.

Atoms emerging from a liquid nitrogen cooled discharge, with a typical mean velocity of 900–1300 m/s in the case of helium and 300–700 m/s in the case of neon and the heavier rare gases, are too fast to be trapped directly in an optical or magnetic trap or even a MOT. They are therefore slowed by spontaneous light forces (Phillips, 1998; Metcalf and van der Straten, 1999) induced by a counterpropagating laser beam. To remain resonant during the deceleration process, the change in Doppler shift in the atoms' rest frame is compensated by a position-dependent Zeeman shift of the corresponding cycling transition (Phillips and Metcalf, 1982; Metcalf and van der Straten, 1999). The respective Zeeman slowing sections typically have a length between 40 cm for krypton and more than 2 m for helium, although even for helium, a liquid helium source and careful optimization of the coil design permitted a length of less than 1 m (Dedman *et al.*, 2004). After the slowing section, the mean velocity of the atoms is reduced to a few tens of m/s (Morita and Kumakura, 1991). An alternative slowing (and collimation) technique for He^* was proposed and demonstrated by the group of Metcalf (Cashen and Metcalf, 2001, 2003; Partlow *et al.*, 2004). Applying a bichromatic force at high power around 1083 nm, a record-high capture angle from the discharge source of $\sim$0.18 rad was demonstrated over the unprecedentedly small distance of 5 cm, albeit with considerable losses. To date, only slowing by 325 m/s has been demonstrated. It remains to be seen whether an atomic beam of He^* atoms can be slowed down efficiently over a much larger velocity range and down to a few tens of m/s, suitable for trapping in a MOT.

Because of the importance of loading a large number of atoms into a MOT, the production of slow and dense beams of metastable noble gas atoms has been thoroughly optimized in recent years (Morita and Kumakura, 1991; Rooijakkers, Hogervorst, and Vassen, 1997b; Rauner *et al.*, 1998; Tol *et al.*, 1999; Milic *et al.*, 2001; Kuppens *et al.*, 2002; Tempelaars *et al.*, 2002; Swansson *et al.*, 2007). Experiments with metastable atoms are clearly at or near the state of the art of high flux beam preparation techniques. Beams of metastable noble gas atoms with up to 2×10^{12} atoms s^{-1} (Hoogerland, Driessen *et al.*, 1996) and intensities on the order of 10^{10} atoms s^{-1} mm^{-2} (Rooijakkers, Hogervorst, and Vassen, 1996) have been achieved.

The celebrated experiments on velocity selective coherent population trapping using metastable helium were also performed, in their first generation, as transverse beam cooling experiments (Aspect *et al.*, 1988; Hack *et al.*, 2000). In these experiments velocity widths below the single photon recoil are possible. The technique has been generalized to two and three dimensions and these experiments as well as the many associated theoretical issues have been ably reviewed by Cohen-Tannoudji (1998) and Bardou *et al.* (2002). We will therefore not discuss velocity selective population trapping further in this review except to point out that for the purposes of the production of intense atomic beams, minimizing the transverse velocity of a beam is not equivalent to maximizing the flux through a given area downstream from the source (Aspect *et al.*, 1990). Maximum flux is generally attained by maximizing the range of transverse velocities which can be brought sufficiently close to zero. Thus, sub-Doppler or subrecoil cooling techniques are less important than having sufficient laser power, curved wave fronts, and long interaction regions to optimize beam flux as described in the references at the beginning of this section.

C. Magneto-optical trapping

For the creation of cold and ultracold samples of gas-phase atoms, laser cooling and trapping techniques (Metcalf and van der Straten, 1999) have of course been remarkably successful. In particular, the MOT (Raab *et al.*, 1987; Metcalf, 1989) has turned out to be the workhorse for almost all of these experiments.

The principle of the MOT is based on cooling via radiative pressure forces of laser light. Superimposed with a magnetic field, the MOT combines the cooling effect of a three-dimensional optical molasses with confinement using the spatial dependence of the radiative pressure force due to Zeeman shifts. The MOT consists of three pairs of circularly polarized laser beams for the three dimensions and two coils with antiparallel currents, which produce a quadrupole magnetic field. For red detuning (laser frequency below the atomic resonance frequency), both atom trapping and cooling are achieved by radiation pressure forces at the same time.

The MOT has been studied both experimentally and theoretically in depth for alkali atoms (Walker, Sesko, and Wieman, 1990; Lindquist, Stephens, and Wieman, 1992; Townsend *et al.*, 1995; Metcalf and van der Straten, 1999). However, different limitations arise in the case of metastable noble gas atoms: The high internal energy leads to Penning ionization [Eq. (1)], a two-body loss process which is particularly rapid in the presence of near-resonant light. Several observations of the loss processes are discussed in Sec. III. Here we emphasize that this loss process puts specific contraints on the design and operation of a MOT for metastable noble gas atoms. The MOT has to be operated under conditions of high loading and low two-body loss rates (Rooijakkers, Hogervorst, and Vassen, 1997b; Kuppens *et al.*, 2002; Swansson, Dall, and Truscott, 2006). For optimizing loading, the incoming flux of trappable atoms has to be maximized (see Sec. II.B) and large MOT beams are applied for achieving a large capture region. For minimizing losses, on the other hand, the MOT is operated in a low-density regime and with low excitation rates to higher states during loading. For increasing the final atom density, at the end of the loading phase, the atom cloud may be compressed to a high-density nonequilibrium situation. With this procedure, MOTs of metastable noble gas atoms can be filled with up to 10^{10} atoms at a peak density of about 10^{10} atoms cm^{-3}

and a temperature of around 1 mk within a loading phase of a few 100 ms to 5 s (Tol *et al.*, 1999; Kuppens *et al.*, 2002; Zinner *et al.*, 2003).

The innovations in the operation of MOTs for metastable noble gas atoms include the use of four beams rather than the usual six (Shimizu, Shimizu, and Takuma, 1991), the application of laser cooling light resonant with transitions to a higher-lying state (Koelemeij *et al.*, 2003; Koelemeij *et al.*, 2004; Tychkov *et al.*, 2004), in some cases applying Stark slowing instead of Zeeman slowing (Schumann *et al.*, 1999; Jung *et al.*, 2003), the simultaneous application of two-color laser fields for improved MOT performance (Kumakura and Morita, 1992; Rooijakkers, Hogervorst, and Vassen, 1995, 1997a), as well as the simultaneous trapping of multiple-bosonic mixtures (Feldker *et al.*, 2011; Schütz *et al.*, 2011), Bose-Fermi mixtures (Stas *et al.*, 2004; Feldker *et al.*, 2011; Schütz *et al.*, 2011), and metastable-alkali mixtures (Sukenik and Busch, 2002; Busch *et al.*, 2006; Byron *et al.*, 2010; Byron, Dall, and Truscott, 2010).

D. Magnetic trapping

After capturing and cooling atoms in a MOT, it is necessary to implement evaporative cooling to further increase the phase-space density of the gas (see Sec. II.F). At the same time, a nondissipative trapping potential is needed to keep the atoms at high phase-space density. For metastable noble gas atoms, in most cases, this is based on the Zeeman shift experienced in an inhomogeneous magnetic field (Nowak *et al.*, 2000; Herschbach *et al.*, 2003). During transfer of the atoms to the magnetic trap, additional laser fields are applied temporarily, in order to optically pump the atoms into the desired Zeeman substate.

Static magnetic traps, such as the Ioffe-Pritchard trap (Ketterle, Durfee, and Stamper-Kurn, 1999) (see Fig. 5) and its variation the ''cloverleaf'' trap (Mewes *et al.*, 1996), are used almost exclusively [for an exception see Doret *et al.* (2009)]. Because of the above described requirements for optimized beam slowing and MOT loading, the layout of the magnetic trapping coils has to be rather evolved.

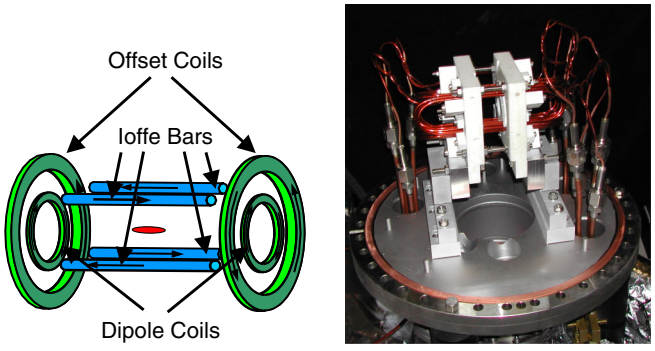

FIG. 5 (color online). Left: Schematic view of a Ioffe-Pritchard trap configuration. Right: Photograph of an actual magnetic trap. The current carrying coils and bars are created from hollow copper tubes mounted on two ceramic plates. Between the plates, the Ioffe bars are visible. The trap coils are water cooled through the hollow copper tubes. The whole assembly has a linear dimension of about 15 cm.

Configurations with the field coils inside or outside the vacuum chamber have been used. In any case the required currents are large, although the high magnetic moment of the metastable triplet states helps to reach strong confinement. Specific numbers vary for each implementation, but typical currents are in the range of a few hundred amperes (electrical power: 1–10 kW) giving axial and vibrational frequencies in the ranges of a few hundred hertz and a few tens of hertz, respectively. After loading atoms in a magnetic trap, it is also often desirable to further laser cool the gas. This additional cooling is achieved with two, red-detuned, circularly polarized laser beams, propagating in opposite directions along the magnetic field axis. This configuration preserves the magnetic sublevel of the atom. Along the radial directions cooling relies on reabsorption of scattered light by the optically thick cloud (Schmidt *et al.*, 2003; Spoden *et al.*, 2005; Tychkov *et al.*, 2006).

Figure 5 shows an example for an Ioffe-Pritchard trap as used for trapping of metastable neon atoms (Zinner *et al.*, 2003; Spoden *et al.*, 2005). On the left, the schematic view is shown: The dipole coils give the axial and the Ioffe bars give the radial confinement. The additional offset coils are used to define the magnetic field bias at the trap center for selecting the trap symmetry and, for nonzero bias field, providing a quantization axis which prevents atom losses due to depolarization and Majorana spin flips. The photograph on the right shows a view of the actual trap as installed inside a vacuum chamber.

E. Optical dipole trapping

The second variant of an almost conservative trapping potential is based on the position-dependent energy shift experienced by atoms in inhomogenous light fields (Dalibard and Cohen-Tannoudji, 1985; Grimm, Weidemuller, and Ovchinnikov, 2000). This energy shift, the so-called dynamic Stark shift or ac Stark shift, is used for the realization of trapping potentials of flexible geometries. In addition, trapping of atoms in internal states that do not experience a sufficient magnetic energy shift, such as neon atoms in the ^{3}He* state, or atoms that experience an antitrapping magnetic energy shift, such as atoms in high-field seeking states can be achieved as well (van Drunen, 2008; Dall *et al.*, 2010; Partridge *et al.*, 2010; van Drunen *et al.*, 2011).

The most common realizations are based on focused, red-detuned Gaussian laser beams. These can be used in the form of a single beam as a trapping or guiding potential (Dall *et al.*, 2010; Partridge *et al.*, 2010). Superimposing two Gaussian beams under a finite angle and preventing interference effects through an appropriate choice of orthogonal laser polarizations or different detunings leads to a straightforward extension of the single-beam trap to a crossed dipole trap (Fig. 6). The main advantage of this configuration is the stronger confinement along the nonradial dimension with an improved performance, e.g., for evaporative cooling. Optical dipole potentials have been applied recently to the investigation of the collisional properties of neon atoms in the $^3P_0$ state (van Drunen, 2008; van Drunen *et al.*, 2011) and the demonstration of Bose-Einstein condensates of spin mixtures of metastable helium atoms (Partridge *et al.*, 2010).

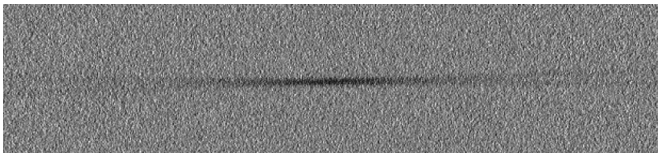

FIG. 6. Absorption image of a cold sample of neon atoms trapped in an optical dipole trap formed by two intersecting red-detuned Gaussian laser beams at a wavelength of 1064 nm. The small intersection angle results in a strongly elongated crossed dipole trap.

On the other hand, the explicit application of interference effects between multiple laser beams leads to dipole potentials with periodically varying potential surfaces. These so-called optical lattices (Jessen and Deutsch, 1996) can be operated in one, two, or three dimensions with structure sizes of the individual potential wells on the order of the wavelength of the light producing the interference pattern. In the lattice, atoms spend considerable time trapped in individual potential wells of the lattice. At low filling factors, they therefore encounter each other less often and it is possible to observe a reduction of the Penning ionization rates when metastable atoms are loaded into an optical lattice (Kunugita, Ido, and Shimizu, 1997; Lawall, Orzel, and Rolston, 1998).

F. Evaporative cooling and quantum degeneracy

As phase-space densities increase, laser cooling techniques cease to be effective in further cooling and compressing a cold gas, and thus quantum degeneracy has never been achieved with laser cooling alone. To cool further it is necessary to turn to evaporative cooling techniques (Hess, 1986; Ketterle and van Druten, 1996; Luiten, Reynolds, and Walraven, 1996; Nguyen *et al.*, 2005). Evaporative cooling consists of having the high energy tail of the distribution of a trapped gas escape and then allowing the remaining atoms to reequilibrate. The new equilibrium temperature is lower and under the right circumstances, the phase-space density increases. In magnetic traps, evaporation is induced with an ''rf knife'' which expels atoms by causing transitions to untrapped states, while in optical traps, the trapping potential is simply lowered (Barrett, Sauer, and Chapman, 2001).

An important condition for successful evaporation is that the ratio of good (elastic) to bad (inelastic) collisions remains high enough. Thus, a high elastic collision rate is desirable, and in the cases that have been studied so far, the elastic cross sections are indeed quite high. Experiments to determine elastic scattering cross sections are described in Secs. III and V. Inelastic loss processes present a more serious problem in metastable gases: Penning ionization is the most rapid loss process and evaporative cooling is possible only if it can be suppressed. In Sec. III we describe in detail how Penning ionization can be suppressed in spin-polarized samples. In helium, the suppression factor is of order 10^4, and this has permitted efficient thermalization and evaporative cooling (Browaeys *et al.*, 2001; Herschbach *et al.*, 2003; Tol, Hogervorst, and Vassen, 2004; Nguyen *et al.*, 2005). The supression factor is of the order of 100 in neon (Spoden *et al.*, 2005; Schütz *et al.*, 2011) and has thus far prevented the attainment degeneracy with this atom. For the even heavier noble gas atoms no suppression of Penning ionization has been reported.

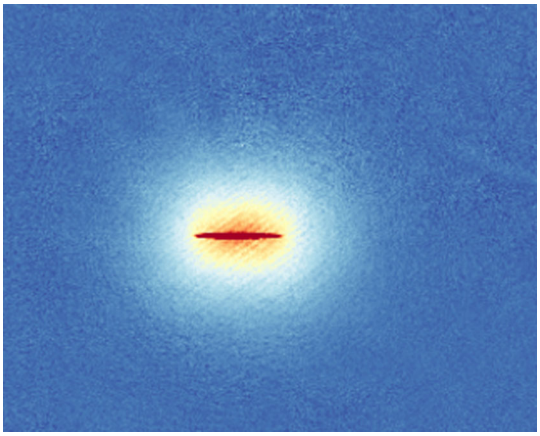

FIG. 7 (color online). Observation of Bose-Einstein condensation of metastable ^{4}He. An image of an expanding cloud of ultracold atoms after expansion from a magnetic trap is shown. The elongated core shows the BEC whereas the circular cloud with larger diameter corresponds to the thermal cloud of not-condensed atoms. The image was acquired with an InGaAs CCD camera.

For a dilute gas of bosons, the achievement of quantum degeneracy corresponds to BEC which was experimentally observed for the first time in 1995 for ensembles of alkali atoms (Cornell and Wieman, 2002; Ketterle, 2002). BEC was observed in metastable helium in 2001 (Pereira Dos Santos, Léonard *et al.*, 2001; Robert *et al.*, 2001; Westbrook *et al.*, 2002), and since then three more experiments have reported this achievement (Tychkov *et al.*, 2006; Dall and Truscott, 2007; Doret *et al.*, 2009). The experiment of Doret *et al.* (2009) is notable because it uses no laser cooling at all. Metastable helium atoms are loaded into a magnetic trap and cooled by collisions with ground-state helium at a temperature of 200 mK. This sample is the starting point for purely evaporative cooling down to BEC. This experiment is the first example of achievement of BEC by buffer gas cooling (Doyle *et al.*, 1995). Another experiment (Tychkov *et al.*, 2006) produced condensates with more than 10^7 condensed atoms.

In Fig. 7, we show an absorption image of a BEC after its release and expansion from a magnetic trap. Techniques of optical detection are discussed briefly in Sec. II.G. The various length scales in the image can be used to extract parameters such as the temperature and the chemical potential of the sample. Another signature of BEC is the change in ellipticity of an expanding BEC which was created in an asymmetric trapping potential (see Fig. 8). In contrast to alkali atoms, electronic detection is also available for the investigation of condensates of metastable atoms (see Sec. II.G). Time resolved detection of the arrival of metastable atoms gives data similar to that of an image integrated in one direction (see Fig. 9). A BEC signature which is unique to metastable atoms is the observation of an abrupt increase in the ionization rate as the gas passes through the BEC transition (Seidelin *et al.*, 2003; Tychkov *et al.*, 2006). This type of observation is described in more detail in Sec. IX.

Simple evaporative cooling cannot be used to produce a degenerate Fermi gas, since the elastic collision cross section

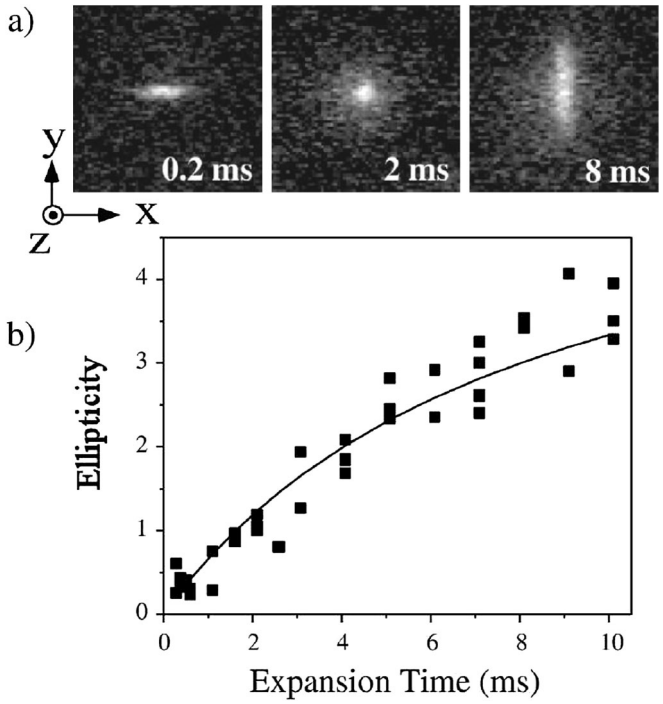

FIG. 8. Direct evidence of the occurrence of a BEC of ^{4}He (Pereira Dos Santos, Léonard *et al.*, 2001): (a) images of a BEC for the given expansion times; (b) ellipticity extracted from the images. Because of the asymmetric potential surface of the magnetic trap used for condensation, the ellipticity of the expanding cloud of condensed atoms changes from below 1 to above 1 for increasing expansion times. This behavior is in contrast with that of a thermal cloud whose ellipticity approaches unity for long expansion times.

between identical low energy fermions vanishes at low temperature. Some form of "sympathetic cooling," in which one species cools another, must be applied. In the case of helium, sympathetic cooling of ^{3}He* atoms (the fermionic isotope) has been implemented by making them interact with an evaporatively cooled sample of the bosonic isotope ^{4}He*. The two isotopes were held simultaneously in the same magnetic trap (McNamara *et al.*, 2006; Vassen *et al.*, 2007). In Sec. VIII we describe experiments on such a mixture to directly compare the quantum statistical behavior of bosons and fermions.

G. Detection of metastable noble gas atoms

1. Optical detection

Almost all cold atom experiments have relied on atom laser interactions to detect the atoms. In the most common technique a near-resonant "probe" laser beam traverses a sample of cold atoms which in turn scatter the light. One can then either collect the scattered light and form a positive image of the sample ("fluorescence" imaging) or use the unscattered light in which case the sample appears as a shadow in the beam ("absorption" imaging). A third possibility is to tune the probe laser far enough from resonance that dispersive effects dominate. The atomic sample acts as a transparent medium with a real index of refraction. Phase contrast techniques then allow one to form an image. Imaging

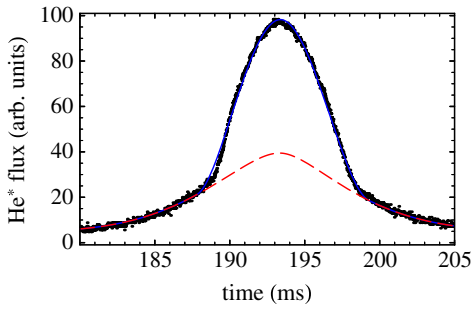

FIG. 9 (color online). Detection of Bose-Einstein condensation of metastable helium via the electron current induced in a MCP detector. The internal energy of the metastable atoms expels electrons when hitting the surface of the detector mounted below the trap after falling under gravity. The electrons are amplified in the MCP and the temporal distribution of the detected current can be used to extract the parameters of the BEC (narrow distribution, fit in solid line) and the thermal atom fraction (wide distribution, fit in dashed line).

methods involve many subtleties and tradeoffs, and some of them are reviewed by Ketterle, Durfee, and Stamper-Kurn (1999).

One can also glean information from nonimaging techniques using laser interactions. As an example, a laser standing wave can form a diffraction grating for matter waves and thus act as a sort of spectrometer. This technique is often referred to as "Bragg spectroscopy" (Stenger *et al.*, 1999). Optical detection of the atoms however is still used in such experiments, although the ability to image the atoms plays only a minor role.

All these techniques are in principle also available when using metastable atoms. To date only imaging techniques have been used with metastable atoms, and we will not attempt to review the use of optical probing of cold metastable samples since most examples do not differ substantially from their use in other atomic species. We only comment on one case, metastable helium, which presents some particularities because of its small mass, small natural linewidth, and primary transition wavelength (see Table II). This $\lambda = 1083$ nm wavelength is poorly adapted to conventional CCD detectors based on silicon. The best measured quantum efficiencies are of order 1% (Tychkov, 2008). CCD detectors based on InGaAs technology are becoming available. These detectors have reported much higher quantum efficiencies, and first results have become available and are promising (see Fig. 7 for a sample image).

The optical detection process depends on the scattering of nearly resonant light by the atoms, and of course the more

TABLE II. Lifetime of ^{4}He states for decay to the ground state, deduced from MOT measurements.

^{4}He state	$2\,^3P_1$	$2\,^3P_2$	$2\,^3S_1$
Exp. lifetime (s)	$5.66(25) \times 10^{-3}$[a]	3.09(15)[b]	7870(510)[c]
Theory lifetime (s)	5.63×10^{-3}[d]	3.06[d]	7860[d]

[a] Dall *et al.* (2008).
[b] Hodgman *et al.* (2009a).
[c] Hodgman *et al.* (2009b).
[d] Łach and Pachucki (2001).

that light is scattered, the greater the signal available for detection. The scattering, however, is accompanied by the acceleration of the atoms along the laser propagation direction due to radiation pressure. At some point the Doppler shift associated with the increased velocity becomes comparable to the natural linewidth $\Gamma/(2\pi)$. Unless the laser's frequency is swept to compensate this Doppler shift, the light ceases to be resonant and the scattering rate drops. The typical number of scattered photons is given by $\Gamma/k\upsilon_{\mathrm{rec}}$, where $\upsilon_{\mathrm{rec}} = \hbar k/m$ is the velocity transfer associated with the absorption or emission of one photon of wave vector k by an atom of mass m. For He^* this quantity is about 20 for the $2^3S - 2^3P$ transition at $\lambda = 1083$ nm. For comparison, the same quantity for Ne^* atoms and the $2p^5\,3s\,^3P_2 - 2p^5\,3p\,^3D_3$ transition at $\lambda = 640$ nm is about 170 while for Rb atoms and the $5S - 5P$ transition at $\lambda = 780$ nm, $\Gamma/k\upsilon_{\mathrm{rec}}$ is about 800. This effect severely limits the available signal for He^*, and this limitation is compounded by a poor quantum efficiency when using Si based CCD cameras.

Acceleration of the atoms is not the only difficulty related to the large recoil velocity in He^*. Successive absorption and emission processes also increase the three-dimensional momentum spread due to fluctuations in the direction of absorbed and scattered photons. Cold atoms thus necessarily heat during optical imaging. For long exposures this heating can result in a loss of signal, but an additional difficulty is that the atoms will also move in space during imaging and smear out their positions so as to mimic a loss in optical resolution.

One example of circumventing the large recoil issue is found in the work of Pereira Dos Santos, Léonard *et al.* (2001). They used two counterpropagating beams for imaging to ensure a zero net radiation pressure on the atoms. Indeed they tuned the lasers so as to have a net cooling effect. As shown in Fig. 8, this technique realized good quality absorption images. A similar technique was used in the work of Tol (2005), with the difference that the lasers were tuned on resonance and had an intensity far below saturation. This technique provides a reliable determination of the number of trapped atoms.

An alternative approach for imaging might be to use light resonant with the $2^3S - 3^3P$ transition at $\lambda = 389$ nm. Although the figure of merit $\Gamma/k\upsilon_{\mathrm{rec}}$ is a factor of 8 smaller than for the $2^3S - 2^3P$ transition, the increased quantum efficiency of Si detectors may compensate the loss of photons. Koelemeij *et al.* (2003) created a MOT using the $2^3S - 3^3P$ but they did not attempt to perform absorption imaging at the 389 nm wavelength.

2. Direct detection using electron multipliers

The large internal energy stored in a metastable noble gas atom (see Table II) has naturally led to the introduction of techniques exploiting this energy and which are not available when using ground-state atoms. Metastable atoms can ionize other atoms or eject electrons from a solid. These processes therefore lead to the emission of charged particles which can be electronically multiplied and easily detected.

When a metastable atom comes into contact with a metal surface, an electron can be ejected. Electron ejection probabilities are difficult to measure absolutely and Siska (1993), Hotop (1996), and Harada, Masuda, and Ozaki (1997) reviewed some of these measurements, which we summarize here. For He^* electron ejection probabilities in the range of 50%–70% have been reported for various metals (gold, stainless steel). In Ne^* the probability is in the range of 30%–50%. For the other metastable noble gas atoms, this probability can be much smaller. Roughly speaking, the probability goes down as the metastable state energy decreases, resulting in values on the order of 1% for Kr^* and Xe^*. The electron ejection process, however, is complex and does not depend exclusively on the metastable energy (Hotop, 1996).

Even with small electron yields, electron multiplier techniques are an attractive alternative to the use of optical detection methods, because of their low background and fast (subnanosecond) response. They can also have sufficient gain to be sensitive to individual atoms. A simple detector is the discrete dynode electron multiplier, essentially a photomultiplier without a photocathode. Laser-cooled He^* (Aspect *et al.*, 1988; Bardou *et al.*, 1992), Ne^* (Shimizu, Shimizu, and Takuma, 1989), Ar^* (Faulstich *et al.*, 1992), and Kr^* (Katori and Shimizu, 1994; Kunugita, Ido, and Shimizu, 1997) have been detected in this way. Katori and Shimizu (1994) estimated a quantum efficiency of 2.7% for Kr^* on their detector, consistent with data in the reviews above.

Channel electron multipliers (or "channeltrons") operate on a slightly different principle. Instead of having discrete dynodes, the multiplication structure is a coiled, highly resistive tube along which a potential is applied. Electrons travel down the tube colliding with the wall of the tube creating secondary electrons. We refer the interested reader to Samson and Ederer (2000) for a technical discussion of electron multiplication techniques. As an example, atom interferometry experiments have used channeltron detection of Ar^* (Rasel *et al.*, 1995). Metastable Ne atoms in a MOT were also detected with a channeltron (Kuppens *et al.*, 2002). Closely related to the channeltron is the microchannel plate (MCP) detector. In such a detector, the tube is scaled down to micron size and instead of a single tube, one has an array of thousands or millions of tubes. The electron amplification principle is similar. An MCP in which the front face served as a simple ionizing surface was used to observe the BEC transition in Robert (2001) as well as in Tychkov *et al.* (2006). Quantum efficiencies for He^* on microchannel plates of 10% have been reported (Tol, 2005; Jaskula *et al.*, 2010). MCPs have also been used to detect laser-cooled metastable neon (Shimizu, Shimizu, and Takuma, 1992; Spoden *et al.*, 2005) and xenon (Lawall, Orzel, and Rolston, 1998).

An example of the use of electronic detection to achieve fast, low background single atom detection can be found in the work of Yasuda and Shimizu (1996) (see Sec. VIII.A). In this experiment a set of four MCPs was used to observe correlations of individual atoms in a beam of Ne^* atoms released from a MOT. Atoms fell onto a gold surface and produced electrons. The MCPs collected electrons from different parts of the surface and coincident atoms were detected with nanosecond timing resolution, allowing a correlation time of 100 ns to be demonstrated.

MCPs come in many shapes and sizes and also have imaging capability (Lapington, 2004). Thus MCPs have been widely used in the cold metastable atom community as an alternative or a complement to optical imaging. Imaging

is possible by placing a phosphor screen behind the MCP and recording the phosphorescence with a camera (Shimizu, Shimizu, and Takuma, 1992; Lawall *et al.*, 1994; Lawall and Prentiss, 1994; Rauner *et al.*, 1998; Dall *et al.*, 2009). A drawback to the phosphor screen method is that it relies on a video camera to acquire the data, and thus the frame rate or temporal resolution is necessarily limited by the video frame rate, typically 20 ms.

An MCP imaging technique that is not limited by CCD camera technology involves the use of a resistive anode. The anode collects the charge from the MCP at the four corners of a square. Analysis of the ratios of the charge at each anode allows one to isolate the position of the source of the charge. Such a detector has been used with He^* (Lawall *et al.*, 1995; Koolen *et al.*, 2002). Spatial resolution of several tens of microns has been reported using this technique with cold metastable atoms. The timing resolution of the technique can be as small as 1 μs, although in the experiments of Lawall *et al.*, the time resolution was 5 μs, limiting the rate of detection events. Thus the detector must be used in situations of low atom flux.

Another imaging technique uses an MCP in connection with a delay line anode (Jagutzki *et al.*, 2002). In this technique, the anode is configured as a transmission line with a well-defined propagation speed. The charge travels to opposite ends of the line and high-precision time to digital conversion provides the position information. This technique was used with He^* (Schellekens *et al.*, 2005; Jeltes *et al.*, 2007; Perrin *et al.*, 2008; Manning *et al.*, 2010). Pulse widths with such anodes are typically in the few nanosecond range, and thus the detectors can be extremely fast. Simultaneous, multiple hits can in principle be detected (Jagutzki *et al.*, 2002). This capability has not yet been used with metastable detection. In experiments with metastable atoms to date, a typical dead time of at least 100 ns is imposed to simplify the software reconstruction of events. The permissible atom flux is thus somewhat higher than for an MCP with a resistive anode. When the flux of detected atoms approaches 10^6 s^{-1}, however, the MCPs, which must be used in pulse counting mode (applying close to the maximum allowable voltage), can exhibit saturation effects (Schellekens, 2007; Krachmalnicoff, 2009). Thus the maximum flux with an MCP + delay line detector is only about an order of magnitude higher than for an MCP + resistive anode.

The spatial resolution of a delay-line anode detector depends on the precision of the timing electronics. The larger the MCP the better the position determination because the timing accuracy generally does not depend on the size of the MCP. Using He^*, FWHMs of 500–700 μm (Schellekens *et al.*, 2005; Schellekens, 2007) and 100 μm (Manning *et al.*, 2010) have been reported. Workers using other particles (ions, etc.) have reported resolutions of a few tens of microns (Jagutzki *et al.*, 2002).

3. Detection by use of Penning ionization

We already mentioned that a significant, indeed often dominant, decay mechanism for cold samples of metastable atoms involves the production of ions by Penning ionization [see Eq. (1)]. In Sec. III, we discuss the physics of these collisions. Here we concentrate on the use of the ionization signal as a diagnostic. Almost all residual gases can be ionized by Penning ionization and one metastable atom can ionize another. If one collects the ions or the electrons from these ionization processes on an electron multiplier, one also has a fast, low noise signal to herald the presence of metastable atoms. In a low-density sample the ion signal is primarily due to ionization of residual gas. Thus the signal is proportional to the number of trapped atoms (Nowak *et al.*, 2000). This signal was used as a real time monitor of the trapped atom number in recent measurements of metastable state lifetimes (Dall *et al.*, 2008).

When the density is high enough, ionizing collisions among the trapped atoms (two-body collisions) become important. In this situation the ion signal is proportional to the density squared, integrated over the trap volume, and leads to a nonexponential decay of the trapped atom number. For metastable atoms in a MOT, light assisted collisions between the trapped atoms can have large rate constants and the two-body losses are often dominant. This phenomenon was observed in every metastable noble gas MOT equipped with an ion detector (Shimizu, Shimizu, and Takuma, 1989; Bardou *et al.*, 1992; Walhout, Witte, and Rolston, 1994; Kunugita, Ido, and Shimizu, 1997; Rooijakkers, Hogervorst, and Vassen, 1997b; Mastwijk *et al.*, 1998; Kumakura and Morita, 1999; Tol *et al.*, 1999; Spoden *et al.*, 2005). The experiment of Bardou *et al.* demonstrated that the ion rate could be a probe of the local density of atoms. A cloud of atoms in MOT was allowed to expand briefly by turning off the laser beams. When the beams were turned on again, the recompression of the cloud was observed as an increase of the ionization rate over about 1 ms.

In a magnetically trapped BEC, light assisted collisions are absent, but the high density nevertheless results in Penning ionization. Both two-body and three-body collisions can contribute to ionization signals (Sirjean *et al.*, 2002; Tychkov *et al.*, 2006). As in a MOT, the ionization signal can be used as a real time probe of the local atomic density. As one crosses the BEC threshhold, the abrupt increase in density due to condensation results in a corresponding increase in ionization (Robert *et al.*, 2001; Tychkov *et al.*, 2006). A detailed analysis of such signals can be found in Seidelin *et al.* (2003) and is discussed further in Sec. IX. In Sec. VII we describe the use of a Penning ionization signal to stabilize an atom laser (Dall, Dedman, and Truscott, 2008).

III. COLD COLLISIONS

When the atomic de Broglie wavelength is comparable to or larger than the range of the interatomic potential between two metastable atoms, collisions are defined as cold collisions (Julienne and Mies, 1989; Weiner *et al.*, 1999). In that case only a few partial waves contribute to the collision cross section, either elastic or inelastic. Quantum threshold rules are then valid for collisions in the absence of light close to an atomic resonance. In the presence of near-resonant light, such as in a MOT, the interaction potential becomes long range due to the resonant dipole interaction, and higher-order partial waves need to be included. At the temperatures relevant for this review, i.e., around or below 1 mK, one is in the cold

collision regime. Weiner *et al.* (1999) provided an excellent review of cold collision theory, both in the presence of light and in the dark. That review also discussed experiments in noble gas MOTs on ''optical shielding,'' in which the control of collision dynamics by near-resonant light is studied. We will not cover this topic again here and primarily restrict ourselves to research performed after that review was published.

Collisions between metastable atoms are different from those between alkali atoms because inelastic effects play an even more important role (Julienne and Mies, 1989). Penning ionization [Eq. (1)] is generally rapid and limits the densities that can be obtained in a MOT. Only under specific conditions can these Penning ionization losses be suppressed (see Sec. III.B). Penning ionization thus limits the options for realizing cold and dense gases of metastables and hampers realization of quantum degeneracy in most noble gas atoms.

The interaction that drives the autoionizing transitions of Eq. (1) is electrostatic and induces transitions only between molecular states of equal total electronic spin. For all noble gas atoms, the left-hand side of Eq. (1) contains two $s = 1$ atoms with total spin $S = 0$, 1, or 2, while the right-hand side, with $s = \frac{1}{2}$ (twice) and $s = 0$, can form states only with $S = 0$ or 1. Clearly, the total electronic spin can be conserved only if $S = 0$ or 1, and a Penning ionization reaction with $S = 2$ would involve a violation of spin conservation. If spin conservation in collisions holds (Wigners spin-conservation rule), it is only the fully spin-stretched states of the metastable atoms that may show suppression of Penning ionization, as these add up to an entrance channel with one unit of total electron spin higher than the maximum spin of the product states.

For He^* this is the full argument as there is no orbital angular momentum to consider. The suppression of Penning ionization [first observed by Hill *et al.* (1972)] turns out to be 4 orders of magnitude, limited by the weak spin-dipole interaction, discussed in Sec. III.B.2. In all other noble gas atoms the metastable state has orbital angular momentum $l = 1$: the excitation of one p electron out of the np^6 ground state creates a metastable state $np^5(n + 1)s$ ($n = 2$, 3, 4, and 5 for Ne, Ar, Kr, and Xe). The LS coupling scheme is expected to break down for heavier atoms. Only for the fully spin-stretched states, however, is S a good quantum number and spin conservation in collisions [Eq. (1)] will still hold if there are no additional spin-state changing interactions. On the other hand, as the core is anisotropic, interactions that depend on the relative orientations of the colliding atoms may induce a spin flip to a state in which ionization can occur. These interactions can be so strong that spin polarization of a gas may even increase the Penning ionization rate (Orzel *et al.*, 1999).

In the remainder of this section we further elaborate on elastic and inelastic collision properties, first for helium, for which we discuss a simple model to understand Penning ionization losses, and later for the other noble gas atoms and mixtures. We primarily focus on comparison with theory and comparison of the observed loss rates for the different noble gas atoms. In Table I we compiled atomic data and collisional properties of all noble gases as we found in the literature.

A. Elastic collisions of He

The s-wave scattering length is the most important property in cold collision physics. At low enough temperatures, for bosons we only need to take s-wave interactions into account while for fermions p-wave interactions are the lowest allowed by symmetrization requirements. The s-wave elastic cross section becomes a constant approaching $T = 0$, while the p-wave elastic cross section goes to zero as T^2. As discussed, for the noble gases only spin-polarized atoms may show sufficient suppression of Penning ionization to allow long enough lifetimes to reach BEC. For spin-polarized $^4He^*$ atoms, the interaction potential is $^5\Sigma_g^+$ ($S = 2$), as both atoms have the maximum $m = +1$. Since the beginning of the 1990s theorists (Stärck and Meyer, 1994; Dickinson, Gadea, and Leininger, 2004; Przybytek and Jeziorski, 2005) calculated this $^5\Sigma_g^+$ potential to determine the energy of its least-bound state as well as the scattering length. From these calculations it was predicted (Stärck and Meyer, 1994) that the $^4He^*$ scattering length should be large and positive (+ 8 nm), stimulating experimental research toward BEC in metastable helium. Apart from calculating the scattering length, in the last 10 years experimentalists have tried to measure this number, using a BEC, measuring evaporation in a magnetic trap, and later spectroscopically by actually measuring the energy of the least-bound state in the $^5\Sigma_g^+$ potential (Moal *et al.*, 2006). The latter determination is by far the most accurate and agrees well with the latest quantum chemistry calculations (Przybytek and Jeziorski, 2005; Przybytek, 2008). These experiments are discussed in Sec. IV.

B. Ionizing collisions in He

In an unpolarized gas, such as a MOT, atoms populate all magnetic substates, and collisions therefore proceed on many interatomic potentials. In this case, Penning ionization is a major loss process. Also, in a MOT, the presence of light with a frequency close to an atomic resonance complicates the analysis of experimental data on trap losses. In this section we restrict ourselves first to collisions in the dark between unpolarized atoms, where a partial wave analysis suffices. Many experimental data, however, are for losses in a MOT, i.e., in the presence of near-resonant light. These results are discussed in Sec. III.B.3. As experimental data and theory are best for helium we focus on helium here. In the following, we will not distinguish Penning ionization and associative ionization [see Eq. (1)]. But before proceeding, we point out that the experiment of Mastwijk *et al.* (1998) included a quadrupole mass spectrum analyzer which permitted the identification of the reaction products of the ionizing collisions. They showed that about 5% of the ionizing collisions in a He^* MOT come from the associative ionization process. To our knowledge this is the only such experiment using cold atoms.

The possible values $S = 0$, $S = 1$, and $S = 2$ for collisions between $s = 1$ He^* atoms correspond to the singlet, triplet, and quintet potentials $^1\Sigma_g^+$, $^3\Sigma_u^+$, and $^5\Sigma_g^+$, respectively. As the helium atom, with only two electrons and a nucleus, has a relatively simple electronic structure, interatomic potentials can be calculated with high accuracy. Müller *et al.* (1991) performed *ab initio* calculations in the Born-Oppenheimer

approximation, where the total electronic spin S is a good quantum number. They also included Penning ionization assuming a complex potential.

At the mK temperatures of a laser-cooled sample of He^* atoms, the collision process can be described conveniently using the partial wave method: The ionization cross section, written as a sum of partial wave contributions, is dominated by only a few partial waves ℓ. In a sufficiently cold sample of He^* atoms in the dark, the cross section for Penning ionizing collisions is dominated by the s-wave contribution. For collisions of He^* atoms, partial wave cross sections $\sigma_\ell^{\rm ion}$ can be derived from the solution of an effective one-dimensional potential scattering problem (Orzel *et al.*, 1999; Stas *et al.*, 2006). Restrictions imposed by symmetry on the partial waves that contribute to the cross section can be taken into account thereafter, thus accounting for the different quantum statistics of ^{4}He and ^{3}He. From a semiclassical point of view, the cold ionizing collision can be described as a two-stage process: (1) elastic scattering of the atoms by the interaction potential at large internuclear distance, and (2) Penning ionization at a short distance, when the electron clouds of both collision partners start to overlap. These successive processes can be treated separately. The ionization cross section for collisions with total electronic spin S can be written as the product of the probability for the atoms to reach a small internuclear distance, and the probability for ionization to occur at that place. As the total spin S is conserved during ionization, the latter is small for collisions that violate Wigner's spin-conservation rule. The calculation becomes simple because, for $S = 0$, one ionization occurs with essentially unit probability [Müller *et al.* (1991) reported an ionization probability of 0.975], and the calculation of cross sections is reduced to the determination of partial wave tunneling probabilities. To calculate these, the interaction potentials of the colliding atoms are needed. The energy dependence of these probabilities gives rise to an energy dependent ionization cross section for $S = 1$ and $S = 0$ that displays the quantum threshold behavior of the inelastic collisions.

To compare with experiments, the ion production rate $dN_{\rm ion}/dt$ in a (magneto-optically) trapped atomic sample can be expressed in terms of an ionization rate coefficient K (particle^{-1} cm^3/s):

$$\frac{dN_{\rm ion}(t)}{dt} = K \int n^2(r,t) d^3r. \tag{2}$$

K depends on the temperature T and can be calculated using the velocity dependent partial wave ionization cross sections for each of the potentials $^{(2S+1)}V(R)$. The contribution of the $^5\Sigma_g^+$ potential can then be neglected compared to contributions of the $^1\Sigma_g^+$ and $^3\Sigma_u^+$ potentials because it corresponds to a fully polarized electronic spin which cannot directly couple to the ionized states.

The interatomic interaction is almost identical in the case of $^3He^*$ and $^4He^*$ and partial wave contributions are therefore similar (Stas *et al.*, 2006). The composition of the total ionization cross section or rate coefficient from these contributions is different for the bosonic ($^4He^*$) and fermionic isotopes ($^3He^*$). Symmetrization requires that a scattering state describing a colliding pair of identical bosons has even symmetry under exchange of the atoms, while a state describing identical fermions has odd symmetry. As a result, partial waves with improper symmetry do not contribute to the total cross section or rate coefficient and are excluded from the summations. Also, the hyperfine structure of $^3He^*$ complicates the analysis as S is not a good quantum number for large internuclear distances, where atom pairs are characterized by F. However, S is a good quantum number for small internuclear distances, where the molecular interaction dominates and Wigner's spin-conservation rule applies. In a laser-cooled sample of He^* atoms, collisions occur for all values of the total atomic angular momentum, $F = 0$, 1, 2, and 3 in case of $^3He^*$ in the $f = \frac{3}{2}$ hyperfine level, and $S = 0$, 1, and 2 in the case of $^4He^*$. The contribution of each collision channel depends on the distribution of magnetic substates in the sample, where m is the azimuthal quantum number of the atom, which can take on values $m_f = -\frac{3}{2}, -\frac{1}{2}, \frac{1}{2}$, and $\frac{3}{2}$ in the case of $^3He^*$ and $m_s = -1$, 0, and 1 in the case of $^4He^*$. The unpolarized ionization rate coefficient $K^{(\rm unpol)}$ is obtained for a laser-cooled sample of He^* atoms where magnetic substates are uniformly populated. For samples with a temperature around 1 mK, only s and p waves need be taken into account.

The results of this theoretical model (Stas *et al.*, 2006) for $^4He^*$ turn out to agree well with the results of detailed close-coupling theory calculations (Leo *et al.*, 2001), as well as with a simpler calculation (Mastwijk *et al.*, 1998); at 1 mK $K^{(\rm unpol)} = 8.3 \times 10^{-11}$ cm^3/s which agrees with $K^{(\rm unpol)} = 8.9 \times 10^{-11}$ cm^3/s (Leo *et al.*, 2001) and $K^{(\rm unpol)} = 7.3 \times 10^{-11}$ cm^3/s (Mastwijk *et al.*, 1998).

1. Measurement of ionizing collisions in a MOT

The theoretical ionization rate constants can be compared to experimental values extracted from MOT data such as the ion production rate, number of atoms, and cloud size. For a MOT, the time dependence of the number of trapped atoms N can be described by the phenomenological equation (Bardou *et al.*, 1992; Stas *et al.*, 2006)

$$\frac{dN(t)}{dt} = L - \alpha N(t) - \beta \int n^2(r,t) d^3r. \tag{3}$$

The first term governing $N(t)$ is a constant loading rate L, representing the capture of atoms from the decelerated atomic beam into the MOT. The second and third terms are the linear and quadratic trap loss rates, respectively. If the loss is exclusively due to ionization, we can make a connection to Eq. (2) because $\beta = 2K$. For He^* samples in a 1083 nm MOT (Kumakura and Morita, 1999; Tol *et al.*, 1999; Browaeys *et al.*, 2000; Pereira Dos Santos, Perales *et al.*, 2001; Stas *et al.*, 2004, 2006; McNamara *et al.*, 2007) or 389 nm MOT (Koelemeij *et al.*, 2003, 2004; Tychkov *et al.*, 2004), collisional loss mechanisms give rise to significant trap loss. Quadratic trap loss is determined by collisions between trapped He^* atoms, while linear trap loss results from collisions with background gas particles. In a MOT, the density is generally small enough that three-body processes can be neglected.

For a Gaussian density distribution the ion current, measured on an MCP detector, can be written as (Tol *et al.*, 1999)

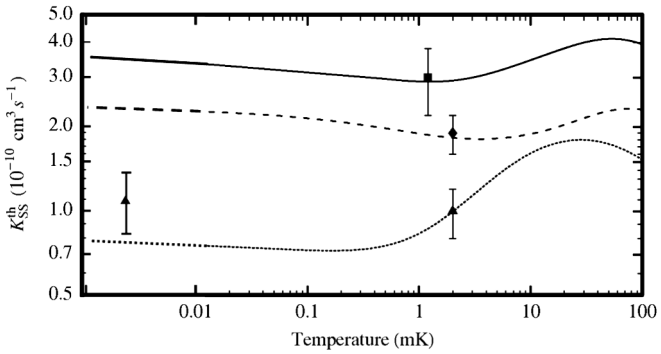

FIG. 10. Experimental Penning ionization loss rate coefficients for an unpolarized gas of helium atoms in the metastable $2\,^3S_1$ state, compared to single-channel theory (McNamara *et al.*, 2007). Dashed curve: theory for ^{3}He–^{3}He*, and experimental point at $T = 2$ mK (diamond); solid curve: theory for ^{4}He–^{3}He*, and experimental point at $T = 1$ mK (square); dotted curve: theory for ^{4}He–^{4}He*, and experimental points at $T = 2$ mK and $T = 3$ μK (triangle). The $T = 3$ μK point is from Partridge *et al.* (2010), deduced from experiments in an optical dipole trap; see Sec. III.B.2.

$$\varphi = \frac{V\beta}{4\sqrt{2}} n_0^2 + \varphi_{\mathrm{bgr}}. \tag{4}$$

Here n_0 is the central density in the MOT, and the effective volume V is defined by $V = (2\pi)^{3/2}\sigma_\rho^2\sigma_z$ (where σ_ρ and σ_z are the rms radii of the cloud).

An experimental value for K_{SS} in the absence of trapping light can be derived by measuring the ion production rate both in the MOT phase and while the trapping light is briefly turned off. For calibration one needs an independent measurement of the loss rate constant in the MOT (β_{MOT}) which can be deduced from measuring the decay of the MOT (see Sec. III.B.3). This procedure, and an analogous one for the heteronuclear case of a two-isotope MOT for ^{4}He* and ^{3}He* (McNamara *et al.*, 2007), provides values of the ionization loss rate constant at the temperature of the MOT. Inspection of Fig. 10 shows that experimental loss rate coefficients are well understood from the simplified theory described in the previous section in all cases.

As the theoretical model shows good agreement with other theoretical work and with the experimental results, cold ionizing collisions of He* atoms can be understood as single-channel processes that are determined by Wigner's spin-conservation rule, quantum threshold behavior, and the symmetrization postulate. Using the model, the difference between the ionization rate coefficients for ^{3}He* and ^{4}He* can be interpreted as an effect of the different quantum statistical symmetry of the two isotopes and the presence of a nuclear spin in the case of ^{3}He*. As the model is relatively simple, it is complementary to the more complete (and precise) close-coupling theory that has been developed for ^{4}He* collisions as well (Venturi *et al.*, 1999; Venturi and Whittingham, 2000; Leo *et al.*, 2001).

2. Two-body and three-body losses for spin-polarized ^{4}He*

The most important mechanism that causes decay of an ultracold gas of spin-polarized metastable ^{4}He atoms in the $m = +1$ state is Penning ionization due to spin relaxation, caused by the spin-dipole interaction (Shlyapnikov *et al.*, 1994; Leo *et al.*, 2001). At the temperatures and magnetic fields relevant for Bose-Einstein condensation experiments it turns out that the rate constant for this two-body process is $\sim 2 \times 10^{-14}$ cm^3/s, 4 orders of magnitude smaller than the Penning ionization loss rate for an unpolarized gas (see Fig. 10). This rate constant was also calculated for higher temperatures and magnetic fields (Fedichev *et al.*, 1996a). It was the prediction of this small loss rate constant, comparable in magnitude to two-body loss rates in the alkali atoms, that stimulated experimental research toward realization of BEC in several laboratories at the end of the 1990s.

The large suppression of Penning ionization has been measured in several studies on metastable ^{4}He*, first by spin polarizing a cloud of atoms from a MOT, where a suppression of at least 2 orders of magnitude was demonstrated (Herschbach *et al.*, 2000a), and later in studies of a spin-polarized cloud in a magnetic trap (Nowak *et al.*, 2000), close to or at quantum degeneracy (Sirjean *et al.*, 2002; Seidelin *et al.*, 2003, 2004; Tychkov *et al.*, 2006), where the calculated rate constant (Shlyapnikov *et al.*, 1994; Leo *et al.*, 2001) was experimentally confirmed.

Actually, at the high densities near BEC, the two-body losses are comparable in size to the three-body losses. One can study the decay of the condensate atom number as a function of time (Pereira Dos Santos, Léonard *et al.*, 2001; Tychkov *et al.*, 2006) or directly measure the ion rate as a function of the atom number (Sirjean *et al.*, 2002; Seidelin *et al.*, 2004). These experiments result in compatible values for the two- and three-body loss rate constants with the most accurate values being $\beta^{(\mathrm{pol})} = 2(1) \times 10^{-14}$ cm^3/s for the two-body loss rate constant and $\gamma^{(\mathrm{pol})} = 9(3) \times 10^{-27}$ cm^6/s for the three-body loss rate constant (Tychkov *et al.*, 2006) in good agreement with the theoretical predictions (Shlyapnikov *et al.*, 1994; Leo *et al.*, 2001). The amount of experimental data is limited and it shows a strong correlation between β and γ values. More measurements at different densities are required to improve the accuracy of the quoted numbers.

The lifetime of a mixture of quantum degenerate gases of ^{3}He* and ^{4}He* was also measured and is compatible with the theoretical three-body (boson-boson-fermion) inelastic rate constant estimation of 1.4×10^{-24} cm^6/s, 2 to 3 orders of magnitude larger than for the fully polarized bosonic case (McNamara *et al.*, 2006).

In a magnetic trap, only ^{4}He* atoms in the $m = +1$ state can be trapped. This automatically generates a spin-polarized gas. Recently, He* atoms were also optically trapped (Partridge *et al.*, 2010). In this case also $m = 0$ and $m = -1$ atoms as well as mixtures of different m states can be trapped. As only a spin-polarized gas of either $m = +1$ or $m = -1$ atoms is stable against Penning ionization, all other possibilities are expected to be considerably less stable. Indeed, they found that a gas of $m = 0$ atoms shows a loss rate constant of $6.6(1.7) \times 10^{-10}$ cm^3/s, while for a mixture of $m = +1$ and $m = -1$ atoms they found $7.4(1.9) \times 10^{-10}$ cm^3/s (25% error). In these cases Penning ionization can occur in the $^1\Sigma_g^+$ potential. At the temperatures where these experiments were performed (a few μK) Penning ionization in the $^3\Sigma_u^+$ potential is expected to contribute negligibly (Venturi and Whittingham, 2000). The measured

loss rate constants can be compared to the loss rate constants deduced in unpolarized clouds from a MOT as discussed previously and shown in Fig. 10. $K^{(\mathrm{unpol})} = 1.10(28) \times 10^{-10}$ cm^3/s and $K^{(\mathrm{unpol})} = 1.23(28) \times 10^{-10}$ cm^3/s are deduced from these $m = 0$, respectively, $m = \pm 1$ results, in agreement with the other experiments and theory.

Ionization rates for spin-polarized metastable helium have been studied theoretically in strongly confining traps, both isotropic and anisotropic. In isotropic traps, strong confinement reduces the trap lifetime due to spin-dipole interactions (Beams, Peach, and Whittingham, 2004). Surprisingly, in anisotropic traps, there are situations in which interference effects involving the anisotropic trapping potential and the spin-dipole interaction can dramatically change the trap lifetime due to ionization. The work of Beams, Whittingham, and Peach (2007) reported trap lifetime enhancements of 2 orders of magnitude for some, specific trap states at specific trap aspect ratios.

3. Collisions in the presence of light

Although the loss rate constant for Penning ionization collisions between unpolarized metastable helium atoms is of order 10^{-10} cm^3/s (see Sec. III.B.1), the dominant losses in a MOT are due to photoassociative collisions. During such a collision, a transition is made to a quasimolecular state with a potential, due to the resonant dipole-dipole interaction, scaling as $\pm C_3/R^3$ at long range, where R is the internuclear distance, and $C_3 \simeq \hbar\Gamma(\lambda/2\pi)^3$ is the squared atomic dipole matrix element of the transition, which has a line width $\Gamma/2\pi$ and wavelength λ. In the presence of light, red detuned by an amount Δ, a resonant transition to such an excited state is possible at the Condon radius R_C, where the molecular energy compensates the detuning:

$$R_C = \left(\frac{C_3}{2\pi\hbar|\Delta|}\right)^{1/3}. \tag{5}$$

At the Condon radius the van der Waals interaction between two noble gas atoms is small compared to the kinetic energy (if the detuning is not large) and has no noticeable effect on their relative motion. This contrasts with the situation in the excited state, for which the interaction is strongly attractive. Therefore, after excitation the two atoms are rapidly accelerated toward small internuclear distances, where couplings exist to loss channels involving autoionization or fine structure changing mechanisms. Before reaching this region, however, there is a probability that the molecule decays back to the lower state by spontaneous emission. This results in two fast He* atoms colliding, leading either to Penning ionization or to elastic scattering, after which the atoms may have sufficient kinetic energy to escape from the trap, a mechanism called radiative escape (Gallagher and Pritchard, 1989).

The loss rate constant can also be modified for blue-detuned light. This occurs by excitation of the colliding atom pair to the long-range repulsive part of the C_3/R^3 potential instead of the attractive part. In this case, optical shielding of cold collisions can occur since the atoms cannot reach a short internuclear distance where Penning ionization occurs. The loss rate constant can be several percent smaller than even in the dark (Katori and Shimizu, 1994; Walhout *et al.*, 1995; Orzel *et al.*, 1998). Weiner *et al.* (1999) reviewed these experiments, which are performed for the heavier noble gas atoms Kr and Xe. For metastable helium, optical shielding was demonstrated as well, although it is far less dramatic (Herschbach, 2003).

To measure the loss rate constant β_{MOT}, the time dependence of the number of trapped atoms N is determined by the loading of atoms into and/or loss of atoms from the trap. A cloud of N atoms, trapped in a MOT, can be characterized by a Gaussian density distribution with central density n_0, and the effective volume defined in Sec. III.B.1 for which $V = N/n_0(0)$. Equation (3) can then be written as

$$\frac{dN(t)}{dt} = L - \alpha N(t) - \frac{\beta_{\mathrm{MOT}} N^2(t)}{2\sqrt{2}V}. \tag{6}$$

If all parameters but N (or L) are known, the steady-state number of atoms (or the loading rate) follows from Eq. (6) by setting $dN/dt = 0$. Alternatively, any time dependence of, for instance, the volume may readily be included, and Eq. (6) can then be used to describe the resulting time dependence of N. Experimentally, one can deduce the loss rate constant β_{MOT} from the ionization signal in a MOT and, for instance, a measurement of the decay of the trap when the loading is stopped. When the central density in the MOT $n_0(0)$ is measured by absorption imaging and the linear decay rate is negligible or known, β_{MOT} is deduced from a fit of the trap loss rate $\beta_{\mathrm{MOT}} n_0(0)$.

In this way several groups have measured loss rate constants in a He* MOT at 1083 nm (Bardou *et al.*, 1992; Mastwijk *et al.*, 1998; Kumakura and Morita, 1999; Tol *et al.*, 1999; Browaeys *et al.*, 2000; Pereira Dos Santos, Perales *et al.*, 2001; Stas *et al.*, 2006) as well as 389 nm (Koelemeij *et al.*, 2003, 2004). These loss rate constants are at least 1 order of magnitude larger than for an unpolarized metastable helium cloud in the dark, ranging from 2×10^{-8} to 5×10^{-9} cm^3/s for a 1083 nm MOT (detuning -5 and -40 MHz respectively) and 2×10^{-9} cm^3/s for a 389 nm MOT (detuning -10 MHz). The numbers for a 1083 nm MOT at large detuning are the same within a factor of 2 for both isotopes.

In general, the loss rate constant increases with decreasing red detuning, until a certain value for the detuning [around ~ -5 MHz (Tol *et al.*, 1999; Herschbach *et al.*, 2000b)]. Beyond this detuning, the probability of decay by spontaneous emission starts to approach unity. Also the gradient and, therefore, the acceleration on the excited-state potential decreases with detuning. Consequently, the probability of reaching the short internuclear distances (in the excited state), where loss mechanisms reside, goes to zero. Additionally, resonances in the ionization rate may be observed. These are due to vibrational states in the excited-state potentials and will be discussed in more detail in Sec. IV.

C. Elastic and inelastic collisions in Ne

In the beginning, the research on cold collisions in metastable neon (the lightest noble gas atom after helium) was motivated by the quest for Bose-Einstein condensation. Initial theoretical research indicated that suppression of

Penning ionization in the metastable $^3P_2$ state, for atoms in the $m = +2$ state, might be sufficient (Doery *et al.*, 1998). But since *ab initio* calculations of scattering properties of all metastables except helium are demanding, these properties are best determined experimentally. Accordingly, groups in Eindhoven (Kuppens *et al.*, 2002) and Darmstadt (previously Hannover) (Zinner *et al.*, 2003; Spoden *et al.*, 2005; van Drunen, 2008) designed and built MOTs containing more than 10^9 atoms of the bosonic isotope ^{20}Ne, more than 10^8 atoms of the other bosonic isotope ^{22}Ne, and 3×10^6 atoms of the fermionic isotope ^{21}Ne.

In a MOT, where the atoms are unpolarized, a Penning ionization loss rate (in the dark) $\beta_{\mathrm{unpol}} = 5(3) \times 10^{-10}\,\mathrm{cm}^3/\mathrm{s}$ for ^{20}Ne was measured (Kuppens *et al.*, 2002) in an analogous way to He*. In an optical dipole trap, loss measurements on unpolarized atoms in the $^3P_2$ state gave Penning ionization loss rates $\beta_{\mathrm{unpol}} = 5^{+4}_{-3} \times 10^{-10}$ cm^3/s for ^{20}Ne and $\beta_{\mathrm{unpol}} = 10^{+4}_{-5} \times 10^{-10}$ cm^3/s for ^{22}Ne (van Drunen, 2008). These numbers are similar in a Ne* MOT (see Table I).

The rates of elastic and inelastic collisions of cold spin-polarized neon atoms in the metastable $^3P_2$ state for ^{20}Ne and ^{22}Ne were measured by transferring the atoms, after spin polarization, from a MOT to a magnetic trap. Penning ionization loss rates $\beta = 6.5(18) \times 10^{-12}$ cm^3/s for ^{20}Ne and $\beta = 1.2(3) \times 10^{-11}$ cm^3/s for ^{22}Ne were obtained. These losses thus indeed occur less frequently (a reduction by a factor of 77 for ^{20}Ne and 83 for ^{22}Ne) than for unpolarized atoms. This proves the suppression of Penning ionization due to spin polarization in Ne*, but the suppression factor is about 2 orders of magnitude smaller than for He*.

From cross-dimensional relaxation measurements in a magnetic trap, elastic scattering lengths of $a = -180(40)a_0$ for ^{20}Ne and $a = +150^{+80}_{-50}a_0$ for ^{22}Ne were obtained as well. These numbers show that concerning the magnitude and the sign of the elastic scattering length, ^{22}Ne would be a good candidate for pursuing BEC in metastable neon. Accordingly, evaporative cooling of ^{22}Ne in a magnetic trap has been demonstrated (van Drunen, 2008), but the small ratio of elastic to inelastic collisions has so far prevented realization of Bose-Einstein condensation in Ne*.

D. Ionizing collisions in Ar, Kr, and Xe

In the 1990s the heavier noble gas atoms were studied in MOT experiments. Detailed studies were performed on ionizing collisions in MOTs of Kr (Katori and Shimizu, 1994; Katori, Kunugita, and Ido, 1995) and Xe (Walhout *et al.*, 1995; Suominen *et al.*, 1996), in particular, in the presence of near-resonant light that may cause shielding of collisions. These studies have been reviewed (Weiner *et al.*, 1999) and we focus here only on the experimental results on rate constants, relevant when comparing noble gas atoms.

For metastable ^{40}Ar MOTs have been realized (Katori and Shimizu, 1993; Sukenik and Busch, 2002) and Penning ionization losses in the presence of the MOT light have been studied (Busch *et al.*, 2006). The homonuclear loss rate in the presence of MOT light turned out to be surprisingly small: $\beta^{(\mathrm{unpol})} = 5.8(1.7) \times 10^{-10}$ cm^3/s. These studies have so far not been extended to collisions in the dark.

More results were obtained for ^{84}Kr* and ^{83}Kr* (Katori and Shimizu, 1993, 1994; Katori, Kunugita, and Ido, 1995). For an unpolarized cloud of ^{84}Kr* an ionization rate constant in the dark $K^{(\mathrm{unpol})} = 2 \times 10^{-10}$ cm^3/s was reported (Katori and Shimizu, 1994), again of the same order of magnitude as for Ne* and He*. In the presence of near-resonant light this rate increased for negative detuning and decreased for small positive detuning (optical shielding) as discussed in Sec. III.B.3 for He*. Cooling and spin polarizing the fermionic isotope ^{83}Kr* demonstrated the effects of quantum statistics on the Penning ionization rate. It was shown (Katori, Kunugita, and Ido, 1995) that the rate constant for ionizing collisions decreased 10% when the temperature was decreased below the p-wave threshold in the case of the fermionic isotope while it remained constant for the bosonic isotope. Only marginal indications of suppression of ionization due to spin conservation in collisions were observed (Katori, Kunugita, and Ido, 1995).

Experiments in Xe* provide results that are similar to those in Kr*. Focused primarily on the effects of near-resonant light on collision dynamics in a MOT, the ^{132}Xe loss rate constant for ionizing collisions in the absence of light was measured: $\beta^{(\mathrm{unpol})} = 6(3) \times 10^{-11}$ cm^3/s (Walhout *et al.*, 1995). This value agreed well with a theoretical number of $\beta^{(\mathrm{unpol})} = 6.5 \times 10^{-11}$ cm^3/s (Orzel *et al.*, 1999), obtained using the same model as discussed in Sec. III.B, assuming unit ionization probability for atoms that have penetrated the centrifugal barriers. For the other even isotopes ^{134}Xe and ^{136}Xe identical rates were measured, in accordance with theory. The fermionic isotopes ^{129}Xe and ^{131}Xe showed the same loss rate constant $\beta^{(\mathrm{unpol})}$ (close to the p-wave threshold), also predicted by the model. Compared to Kr, in Xe a much larger difference in loss rate between bosons and fermions was found when comparing the ionization rate for a spin-polarized gas to that of an unpolarized gas. The two rates differed by a factor of 3 at temperatures far below the p-wave threshold (Orzel *et al.*, 1999), while they were equal at the p-wave threshold. Measuring the ratio $\beta^{(\mathrm{pol})}/\beta^{(\mathrm{unpol})}$ for the fermions as a function of temperature yielded a factor of 2 decrease, in perfect agreement with the predictions of the simple one-dimensional single-channel potential scattering model, also discussed in Sec. III.B. Interestingly, comparing the ionization rate for a spin-polarized gas to that of an unpolarized gas for the bosons ^{132}Xe*, ^{134}Xe*, and ^{136}Xe*, it was observed that instead of a suppression of Penning ionization an enhancement by 60% was found. This clearly shows that spin-conservation effects, seen in He* and Ne*, are absent in bosonic Xe. This result confirms that anisotropic interactions in the $np^5(n+1)s\ ^3P_2$ states may lift the spin-conservation restriction. It is, however, expected that these anisotropic interactions are strongest for heavier noble gas metastable atoms, explaining why for Ne* spin-conservation still holds to some extent.

E. Mixtures

Mixtures of different species (with at least one metastable noble gas atom) allow an extension of research possibilities. One can mix two isotopes of the same element or mix two different chemical species. *A priori* it may seem difficult to

simultaneously trap two different chemical species as most elements are easily ionizable by a metastable noble gas atom. Therefore Penning ionization may strongly affect the densities and lifetimes that can be realized. However, Penning ionization due to optically assisted heteronuclear collisions in a MOT is expected to be less important in comparison to the homonuclear case. The interaction is not a long-range resonant dipole interaction but a short-range van der Waals interaction. In the dark, an unpolarized mixture is therefore expected to show a two-body loss rate constant $\sim 10^{-10}$ cm^3/s, just as in the homonuclear case.

For a spin-polarized gas it is difficult to predict whether suppression of Penning ionization may occur. Based on the discussion on anisotropic interactions it seems that mixtures containing He* and an alkali atom (both in a symmetric S state) may be the most promising.

So far, mixtures with at least one metastable noble gas species have been realized experimentally for helium, neon, and argon. Since the study of collisions in the neon mixtures (^{20}Ne/^{21}Ne, ^{20}Ne/^{22}Ne, and ^{21}Ne/^{22}Ne) is still in progress (Feldker *et al.*, 2011; Schütz *et al.*, 2011), we focus on a qualitative discussion of the mixtures ^{3}He/^{4}He, ^{4}He/^{87}Rb, and ^{40}Ar/^{85}Rb in the subsequent sections.

1. ^{3}He/^{4}He

In Sec. III.B.1 we already discussed some collision properties of a mixture of the bosonic and fermionic isotope of helium in a MOT. Taking into account the quantum statistics in the collisions between unpolarized ^{3}He and ^{4}He atoms the Penning ionization losses can be well understood, in both the homonuclear and heteronuclear cases, as illustrated in Fig. 10.

It was expected that for a spin-polarized mixture of ^{3}He in the $|f, m_f\rangle = |3/2, +3/2\rangle$ state and ^{4}He in the $|j, m_j\rangle = |1, +1\rangle$ state a similar suppression of Penning ionization would hold as in the case of ^{4}He in the $|j, m_j\rangle = |1, +1\rangle$ state alone. Indeed, this was observed in a magnetic trap at $\sim$ mK temperatures (McNamara *et al.*, 2006). Cooling toward quantum degeneracy, however, a significant reduction in the lifetime of a condensate was observed in the presence of an $\sim\mu$K dense cloud of ^{3}He atoms. For a condensate of $|1, +1\rangle$, ^{4}He* atoms the lifetime was a few seconds while it was only $\sim$10 ms in the presence of $|3/2, +3/2\rangle$, ^{3}He* atoms (McNamara *et al.*, 2006). This reduction can be explained assuming large three-body losses for the heteronuclear mixture. It turns out that the heteronuclear scattering length is extremely large, $a_{34} = 27.2 \pm 0.5$ nm (Przybytek, 2008), calculated by mass scaling of the accurately known $^5\Sigma_g^+$ potential. As the three-body losses are proportional to the fourth power of the scattering length (Fedichev, Reynolds, and Shlyapnikov, 1996b), this explains the short lifetime that was observed (McNamara *et al.*, 2006).

2. ^{4}He/^{87}Rb and ^{40}Ar/^{85}Rb

Simultaneous trapping of alkali atoms with noble gas atoms has been studied for two cases. A dual-species MOT for Rb and Ar* was built (Sukenik and Busch, 2002) and Penning ionization was observed, of both Rb and Ar* (Busch *et al.*, 2006). This experiment was the first to identify the molecular ion RbAr$^+$ [associative ionization, see Eq. (1)], measured in a time-of-flight mass spectrometer. Two loss rates could be measured in the presence of light: the loss rate of Rb due to the presence of Ar* MOT light and the loss rate of Ar* due to the presence of Rb MOT light, $\beta^{(\mathrm{unpol})}_{\mathrm{Rb\text{-}Ar}} = 3.0(1.3) \times 10^{-11}$ cm^3/s and $\beta^{(\mathrm{unpol})}_{\mathrm{Ar\text{-}Rb}} = 1.9(0.9) \times 10^{-11}$ cm^3/s, respectively. These are much lower (by about 2 orders of magnitude) than loss rates in a single-isotope noble gas MOT.

Recently studies started on simultaneous trapping of Rb and He* (Byron *et al.*, 2010; Byron, Dall, and Truscott, 2010). Here, for the loss rates in the presence of light, analogous results were reported as in the Rb-Ar* case: the total two-body loss rate $\beta^{(\mathrm{unpol})}_{\mathrm{Rb\text{-}He}} = 6(2) \times 10^{-10}$ cm^3/s is relatively small (Byron, Dall, and Truscott, 2010). To investigate the possibilities of a dual-species BEC, both Rb and He* were spin polarized and the ion production was measured to see whether suppression of Penning ionization occurs. A suppression of Rb$^+$ ion production of at least a factor of 100 was observed, limited only by the detection sensitivity. This suppression is the largest measured for any noble gas boson except ^{4}He*, and is promising for future progress toward a dual-species BEC.

F. Feshbach resonances

The possibility to tune the scattering properties between atoms has pushed the research with ultracold and degenerate alkali atoms. For the metastable noble gases helium has been the subject of a recent study. Spin-polarized ^{4}He* has only limited possibilities to tune the scattering length as ^{4}He* has no hyperfine structure. This only allows resonances due to the weak magnetic dipole interaction which are expected to be narrow. For efficient coupling and experimentally accessible resonance widths at least one of the two collision partners should be ^{3}He*. As the fully spin-polarized mixtures do not allow efficient mixing at least one of the two atoms should be in a state with magnetic quantum number $|m| < m_{\max}$. This induces admixtures of molecular states with singlet and/or triplet character increasing the Penning ionization rate. Moreover, as the singlet and triplet potentials are not as accurately known as the quintet potential, this also leads to reduced accuracy in calculating the Feshbach resonances using knowledge of the molecular potentials. However, a detailed *ab initio* study of the possibilities to magnetically tune the scattering length in all isotopic mixtures of He* was performed recently (Goosen *et al.*, 2010). One promising broad Feshbach resonance was found for the case of a mixture of ^{4}He* and ^{3}He* atoms. For the single-isotope case narrow resonances are expected to exist; however, as the admixture of singlet and triplet character will be substantial in this case, accurate predictions could not be made.

In a second study the possibilities of optical Feshbach resonances were investigated for the case of spin-polarized ^{4}He* (Koelemeij and Leduc, 2004). It was found that a substantial modification of the scattering length can be realized experimentally applying laser radiation near the long-range states discussed in Sec. IV, however, only for a time of less than a millisecond, as strong losses and heating of trapped atoms are anticipated at this time scale.

IV. PHOTOASSOCIATION

A. General features for metastable atoms

Photoassociation processes involve two colliding atoms that absorb a photon to form an excited molecule. Photoassociation has been used for a long time in the field of molecular physics. It attracted renewed interest when cooling methods appeared [see Jones *et al.* (2006) and references therein]. Long-range molecules can be created from ultracold atoms and photoassociation resonances also provide a tool to modify the atomic collisional properties via optical Feshbach resonances. Finally, photoassociation spectra can be used to determine elastic scattering lengths as discussed in Sec. V.

Photoassociation has been successfully applied to cold and ultracold gases of metastable helium providing spectroscopical data of unprecedented accuracy for many different studies. Photoassociation with metastable atoms has some special features. First, noble gases are almost chemically inert and it is quite counterintuitive to be able to form dimers of such species. Moreover, each atom in the dimer has a high internal electronic energy. Thus the molecules also carry this energy. Nevertheless, photoassociation of ^{4}He* atoms has been demonstrated by different groups (Herschbach *et al.*, 2000b; Pieksma *et al.*, 2002; Kim *et al.*, 2004; van der Zwan *et al.*, 2006) and first results on photoassociation of ^{20}Ne* have been reported (van Drunen, 2008). For helium, these molecules are of special interest for the simplicity of the atom. The interaction potential between two colliding metastable atoms can be calculated *ab initio* with good accuracy (Przybytek and Jeziorski, 2005); this makes the comparison between experimental and calculated values a stimulating challenge.

B. One-photon photoassociation of metastable helium

The relevant molecular levels of helium are shown in Fig. 11. Starting from two atoms in the $2\,^3S_1$ state, a resonant laser can be tuned to excite the pair of atoms to a molecular state. Two photoassociation spectroscopy experiments reaching the molecular $J = 0$ and $J = 2$ levels were performed.

The first one (Herschbach *et al.*, 2000b) used a MOT at a temperature $\sim$1 mK and with atomic densities $\sim 5 \times 10^9$ cm^{-3}. A probe laser was scanned over a frequency range of 20 GHz below the atomic $2\,^3S_1 - 2\,^3P_2$ transition. Photoassociation spectra were recorded by measuring the variation of the ion rate induced by the photoassociation beam. The molecules are in an excited state and decay faster by Penning ionization rather than by radiative decay. This is especially true for a molecular state with total spin 0 or 1: These are ionized with a probability close to unity. The autoionization effect is reduced for molecules with a total spin 2 due to spin-conservation rules, as in the atomic case. However, the spin-orbit interaction causes spin mixing and the spin 2 molecules can also create ions. Three vibrational series were identified and many lines could be interpreted, in spite of the fact that the short-range part of the interaction potential is not well known (Herschbach *et al.*, 2000b).

Other photoassociation studies were later performed (Kim *et al.*, 2004), with two main differences with the previous experiments: First, an ultracold gas in a magnetic trap was used, just above the BEC threshold at a few μK, thus enhancing the photoassociation rate because of higher densities; second, spectra were recorded through the temperature changes of the cloud. The improved accuracy was used to determine the scattering length (see Sec. V).

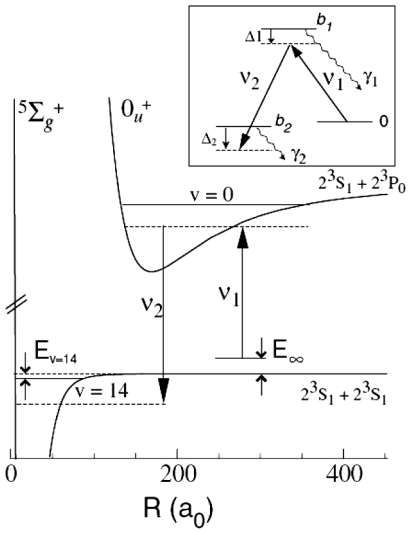

FIG. 11. Relevant molecular potentials for photoassociation of spin-polarized metastable ^{4}He atoms (not to scale). The 0_u^+ potential is purely long range and shallow. The arrows represent the two laser frequencies involved in the two-photon photoassociation experiment. From Moal *et al.*, 2006.

C. Formation of long-range helium molecules

The long-range part of the interaction potentials between two metastable helium atoms is well known, in contrast with its short-range part. Then, it was possible and interesting to search for purely long-range potentials. One such potential could be found within the manifold of molecular potentials linking to the $2\,^3S_1 - 2\,^3P_0$ asymptote: It is a 0_u^+ potential, with a steep inner wall at 150 a_0 and a weak attractive part at long distance. This potential well can support five molecular bound states that can be excited by photoassociation.

The excited dimers in the 0_u^+ potential are large molecules with classical inner turning points at about 150 a_0 and outer turning points as large as 1150 a_0. As a consequence of this extremely large size, the autoionization process is blocked because the two atoms cannot get close enough to Penning ionize (Léonard *et al.*, 2003). These molecules therefore decay by fluorescence.

A spectrocopic study of the giant photoassociated molecules provided a value of the binding energy of each of the five vibrationnal bound states of the 0_u^+ potential with an accuracy of 0.5 MHz. The results are in perfect agreement with calculations (Léonard *et al.*, 2003, 2004; Cocks, Whittingham, and Peach, 2010). The accuracy of the measurements was sufficient to clearly show the role of retardation effects in the interaction between the two atoms carried by the electromagnetic wave (Léonard *et al.*, 2004).

V. SCATTERING LENGTH MEASUREMENTS

In cold atom physics, the *s*-wave scattering length characterizes the strength of the interaction between the atoms. It is a crucial parameter for describing the physical properties of a condensate. In the case of metastable helium, several groups determined its value using different methods with increasing accuracy over the years. In the case of neon, collisional properties were used.

A. Determinations from collisional properties

The first idea is to deduce the scattering length a from the measurement of the chemical potential of the Bose-Einstein condensate. Within the Thomas-Fermi approximation, the chemical potential μ is estimated from the size of the condensate and the number of Bose-condensed atoms (Dalfovo *et al.*, 1999). The large uncertainty in the number of atoms gives a large error bar for the scattering length. For helium, the reported values for a were 20 ± 10 nm (Robert, 2001) and 16 ± 8 nm (Pereira Dos Santos, Léonard *et al.*, 2001). Another estimation, based on the temperature dependence of the collisional cross section in a thermal cloud, led to 10 ± 5 nm (Tol, Hogervorst, and Vassen, 2004).

The work of Seidelin *et al.* (2004) attempted to improve on the initial estimates which used measurements of the chemical potential. Instead of directly measuring the number of atoms in the condensate, they compared Penning ionization rates in an almost pure condensate and in a cloud at the BEC transition temperature. Observation of the ionization rate was also used to place the cloud close to the BEC transition (see Sec. IX). To a good approximation, the value of the critical temperature in a weakly interacting gas depends only on the trap geometry and the atom number (Stringari and Pitaevskii, 2003), thus the ionization production rate and detection efficiency could be calibrated. This calibration in turn gave the atom number, and the condensate expansion could again be used to find the scattering length. They found $a = 11.3^{+2.5}_{-1.0}$ nm.

For neon, studies of thermalizing collisions were used to determine the magnitude and sign of the scattering lengths of ^{20}Ne [$a = -9.5(2.1)$ nm] and ^{22}Ne ($a = 7.9^{+4.2}_{-2.7}$ nm) (see Sec. III.C).

B. Determinations using photoassociation

The basic idea in this method is to deduce the energy of the least bound state $v = 14$ in the $^5\Sigma_g^+$ molecular potential (see Fig. 11), from which the value of the scattering length can be derived. Because it is essentially a frequency measurement, its potential accuracy is much higher than those directly exploiting collisional effects. The first such measurement using He* was based on frequency shifts in a one-photon experiment, a second one used two-photon photoassociation.

In the one-photon photoassociation experiment, light-induced frequency shifts of the photoassociation spectra (Kim *et al.*, 2004) were found to be linearly dependent on the intensity of the photoassociation light beam. These light shifts depend on the scattering length a because the laser couples the excited vibrational states in the 0_u^+ potential to the continuum of free unbound scattering states above the dissociation limit, as well as to the bound states in the $^5\Sigma_g^+$ molecular potential. Consequently, the resulting shifts of the excited molecular levels depend on the value of the binding energy of the least-bound state and also on the Franck-Condon overlap between the excited and ground states. Both these parameters depend on the scattering length a. A reliable determination of a resulted from the measurement of the shifts and of a theoretical analysis (Portier *et al.*, 2006; Cocks and Whittingham, 2009, 2010). Uncertainties related to the laser intensity at the atom cloud were eliminated by comparing results for three different excited vibrational states in the 0_u^+ potential. The value $a = 7.2 \pm 0.6$ nm was deduced, significantly smaller than the determinations discussed in Sec. V.A. Recently this method to detect the photoassociation resonance was extended to observe collective dipole oscillations as a result of momentum transfer of the photoassociation laser to the cloud. This simple technique also allowed extraction of the scattering length with similar accuracy: $a = 7.4 \pm 0.4$ nm (Moal *et al.*, 2008).

In a one-photon photoassociation process, the created molecules have a lifetime limited by radiative decay, creating a pair of free atoms of high kinetic energy. However, the molecules can also decay to a bound state of the ground-state molecular potential. Interestingly, this decay can be stimulated using Raman transitions in a two-photon photoassociation process. This led to a new determination of a, which confirmed the first one (Moal *et al.*, 2006) and improved its accuracy. The principle of the measurement is illustrated in Fig. 11, showing the two laser beams simultaneously illuminating the sample. Here the binding energy of the least-bound state $v = 14$ in the $^5\Sigma_g^+$ molecular potential is directly deduced from the position of the resonance given by the Raman resonance condition $E_\infty + h\nu_1 - h\nu_2 = E_{v=14}$. A dark resonance spectrum of narrow width was recorded when scanning one of the two lasers, the other one being kept at a fixed

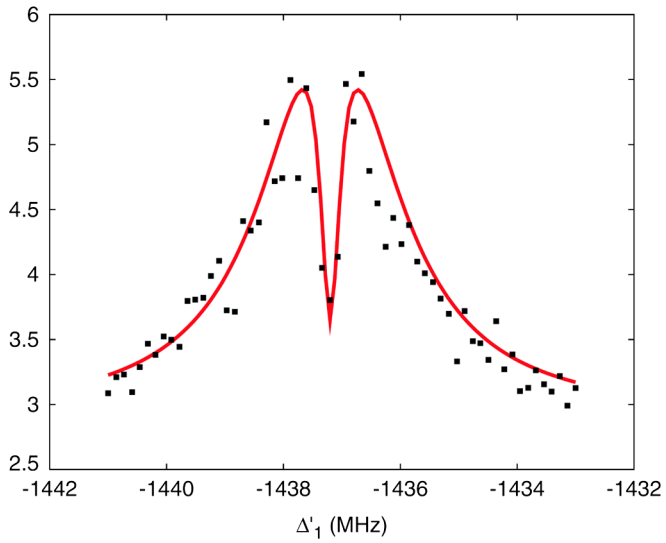

FIG. 12 (color online). Atom-molecule dark resonance in a two-photon photoassociation experiment with $2\,^3S_1$ metastable helium atoms. The resonance is detected by measuring the temperature increase of the cloud (vertical axis: temperature in μK unit). From Moal *et al.*, 2006.

frequency. Such bound-free dark resonance signals are shown in Fig. 12. The dependence on the relative kinetic energy E_∞ was eliminated by extrapolating to zero temperature.

The deduced binding energy is $E_{v=14} = -91.35 \pm 0.06$ MHz. The final determination of the scattering length then relied on the precise interaction potentials calculated *ab initio* (Przybytek and Jeziorski, 2005). This led to the accurate value $a = 7.512 \pm 0.005$ nm (Moal *et al.*, 2006).

VI. SPECTROSCOPIC MEASUREMENTS OF ATOMIC PROPERTIES

A. Metastable state lifetimes

As noted earlier, the long lifetimes of the noble gas metastable triplet states enable these species to act as effective ground states for atom optics experiments (Baldwin, 2005). The metastable behavior of these states arises from the doubly forbidden nature of the decay process to the $^1S_0$ ground state for each species: Both electric dipole and spin-flip (triplet-singlet) transitions are forbidden. As shown in Table I, the lifetimes of the metastable states range from ~15 to ~8000 s.

For the heavier noble gases (Ne, Ar, Kr, and Xe) the dominant decay process for the metastable $ns[3/2]_2(^3P_2)$ states is via a magnetic quadrupole ($M2$) transition. The He $2\,^3P_2$ state also decays to the ground state principally via an $M2$ transition, but its *lifetime* is dominated by electric dipole ($E1$) decay to the metastable $2\,^3S_1$ state. In contrast, the lifetime of the metastable $2\,^3S_1$ state itself is determined solely by decay to the ground state via a magnetic dipole ($M1$) transition.

In all the noble gases, the $^3P_1$ transition to the ground state is not forbidden by dipole selection rules (i.e., it can decay via an electric dipole transition), but the decay time is nevertheless relatively long since the transition is still spin-flip forbidden. Conversely, decay of the $^3P_0$ state to the ground state is strictly forbidden to all orders of the multipolar expansion since there is no change in the total quantum number $J = 0$.

The long lifetime of metastable atoms enables them to be laser cooled and trapped in ultrahigh vacuum environments for extended periods (comparable to their decay time). This allows the metastable state lifetime to be measured directly either by determining the decay rate of the atomic ensemble (Katori and Shimizu, 1993; Zinner *et al.*, 2003; Dall *et al.*, 2008) or by measuring the extreme ultraviolet (XUV) photon emission rate and calibrating that against another known XUV emission rate (Walhout *et al.*, 1995; Lefers *et al.*, 2002; Hodgman *et al.*, 2009a, 2009b). A schematic of such an experiment utilizing both techniques is shown in Fig. 13. However, measurement of the decay times of the metastable states is not simply motivated by their usefulness in atom optics. For example, the two-photon transition from the Xe $6s[3/2]_2$ state to the $6s[3/2]_0$ state is also potentially useful as an atomic clock transition (Walhout *et al.*, 1995), and the long lifetime of the He $2\,^3S_1$ state is important as an energy reservoir in electron collision-dominated plasmas for which this state has a large scattering cross section (Uhlmann *et al.*, 2005).

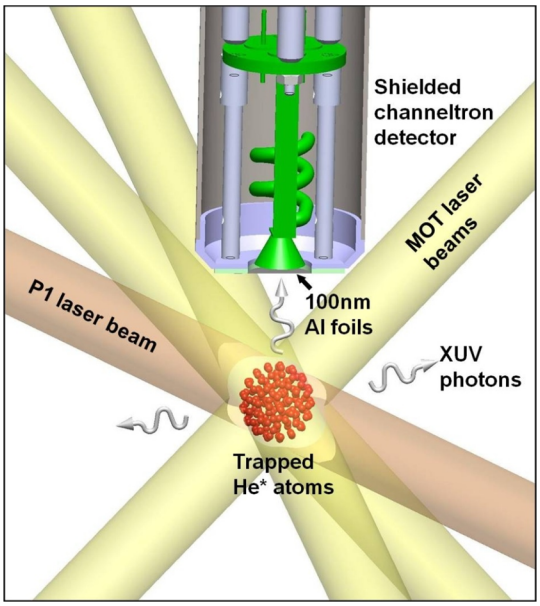

FIG. 13 (color online). Experimental schematic showing the trapped atomic ensemble whose decay rate can be determined directly from the trap number loss rate, or by measuring the emitted XUV photons incident on a shielded channeltron detector. Adapted from Hodgman *et al.*, 2009a.

Perhaps most importantly, the metastable state lifetimes are of significant interest as a test bed for quantum electrodynamics (QED), one of the most robust and long-standing theories in modern physics. However, QED calculations for atomic processes such as transition lifetimes are not as well determined as for atomic energy level differences (which can be accurate to one part in 10^{11}, see next section), with accuracies for lifetimes often no better than the percent level even in helium, the simplest multielectron atom. Surprisingly, the theoretical accuracy again closely matches the experimental uncertainty in measuring the transition rates, even though the measurement accuracy is up to 9 orders of magnitude worse than for the atomic energy level separations.

For the heavier noble gases, there are further complications due to the widely acknowledged uncertainties arising from the theoretical treatment of relativistic effects and electron correlations, to which the significant discrepancies between theory and experiment (see Table I) are attributed. In Ne, the lightest of these, the relativistic effects are relatively minor, making Ne a good test bed for studying electron correlations. However, while the agreement with theory is indeed somewhat better, the experimental value is still significantly less than predicted (Small-Warren and Chiu, 1975; Indelicato *et al.*, 1994; Tachiev and Froese Fischer, 2002). For the heavier species (Ar, Kr, and Xe) the discrepancy increases with Z (as does the lifetime), possibly due to inadequate treatment of relativistic effects. This disagreement between theory and experiment for the metastable lifetimes of the heavier noble gases has yet to be resolved. Indeed, a similar level of disagreement occurs for the decay of the metastable $2\,^3P$ state in Sr (Yasuda and Katori, 2004).

Theoretical attention has therefore focused more closely on He, the simplest multielectron atom. Being the lightest of the noble gases it is also less susceptible to computational

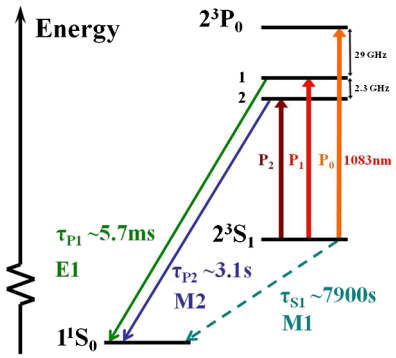

FIG. 14 (color online). Triplet states of ^{4}He showing XUV decay times to the ground state via the mechanisms indicated. Adapted from Hodgman *et al.*, 2009b.

uncertainty contributions from relativistic effects and electron correlations.

Until recently, no published measurements had been made for transition rates to the ground state from the He $2\,^3P$ manifold. Figure 14 summarizes the atomic energy level scheme for He and shows the primary decay mechanism to the ground state for each of the four lowest triplet states. Once again, decay of the $2\,^3P_0$ state to the ground state is strictly forbidden. Early attempts to measure the fastest ($2\,^3P_1$) decay rate in a helium discharge (Tang and Happer, 1972) remain unpublished, as were more recent attempts at the Institut d'Optique in Orsay using a He* trap (Poupard, 2000).

However, in the first of a series of experiments at the Australian National University in Canberra, the UHV capabilities of a well-characterized He BEC apparatus (Dall and Truscott, 2007) were exploited to produce the first published measurements of the He $2\,^3P_1$ transition rate to the ground state (Dall *et al.*, 2008). The initial experiment employed the Penning ionization of background gas atoms via (He*) single-body collisions as a diagnostic. In this way, a direct measurement could be made of the trap loss arising from decay to the ground state by atoms continually cycled into the $2\,^3P_1$ state from the metastable state via optical pumping with 1083 nm laser light.

This enabled the $2\,^3P_1$ transition rate to the ground state to be determined with an uncertainty of 4.4% (see Table II). The technique did not require any additional absolute measurements, only knowledge of the optical excitation fraction into the $2\,^3P_1$ state. The result was in excellent agreement with previous QED calculations (Drake, 1971; Johnson, Plante, and and Sapirstein, 1995; Łach and Pachucki, 2001) and anchored the isoelectronic sequence for this transition at low Z.

Furthermore, the $2\,^3P_1$ XUV flux can be used to accurately calibrate the decay of other transitions. Using a shielded channeltron detector, the transition rate for the $2\,^3P_1$ decay to the ground state was determined relative to the (now known) count rate of the XUV photons emitted via $2\,^3P_1$ decay to the ground state, with an absolute uncertainty of 5% (Hodgman *et al.*, 2009a). This was again in excellent agreement with the same QED frameworks as before (Drake, 1969; Johnson, Plante, and and Sapirstein, 1995; Łach and Pachucki, 2001), and was able to discount several others. An upper bound was also placed on the $2\,^3P_0$ decay rate of $0.01\ s^{-1}$ as determined by the channeltron background count rate.

Finally, the lifetime of the He $2\,^3S_1$ metastable state itself could be measured with improved accuracy using the same relative XUV flux technique. Earlier measurements using an electric discharge in a highly perturbed environment yielded error bars of at least 30% (Moos and Woodworth, 1973; Woodworth and Moos, 1975), compared with the most recent experimental uncertainty of 6.5% (Hodgman *et al.*, 2009b). It should be noted that the recent experiment covered a range of more than 6 orders of magnitude in XUV count rates. Again, the agreement with QED predictions was excellent. Summarizing, experiment and theory are in good agreement for all three decay rates at a level of accuracy of ~5%. The results are listed in Table II.

The value determined for the He metastable lifetime, 7870 (510) s (Hodgman *et al.*, 2009b), is the longest of any excited neutral atomic species yet measured. Once again, this experimental determination anchors the isoelectronic sequence for the heliumlike metastable lifetime at low Z and again confirms the previous three most consistent theories (Drake, 1971; Johnson, Plante, and Sapirstein, 1995; Łach and Pachucki, 2001). The excellent agreement between the calculated and recently measured decay rates to the ground state for the four lowest triplet states in He is another validation of the robustness of QED theory.

B. Precision spectroscopy of atomic structure

1. Precision spectroscopy on triplet levels of He*

As pointed out in the Introduction, helium has long been a favorite testing ground for fundamental two-electron QED theory and for new techniques in atomic physics, both experimental and theoretical. In this context, the spectroscopic measurements and theoretical determinations of the energies of low-lying triplet states have pushed the limits of precision. The readily accessible $2\,^3P$ and $3\,^3P$ manifolds have been the focus of much experimental activity, particularly following the introduction of optical frequency combs [see Maddaloni, Cancio, and De Natale (2009) for a recent review and Consolino *et al.* (2011)].

Among all triplet level transitions, that between the $2\,^3S$ and $2\,^3P$ states in ^{4}He at 1083 nm is by far the most experimentally studied. In a series of experiments (Frieze *et al.*, 1981; Minardi *et al.*, 1999; Castillega *et al.*, 2000; Storry, George, and Hessels, 2000; Giusfredi *et al.*, 2005; Zelevinsky, Farkas, and Gabrielse, 2005; Borbely *et al.*, 2009; Smiciklas and Shiner, 2010), 1083 nm light was used to access the ^{4}He $2\,^3P$ fine structure, with the prospect of obtaining an accurate value for the fine structure constant α. Assuming the QED theory of fine structure energies of an atomic system to be correct, a determination of α is possible by frequency measurements of these fine structure splittings, which are proportional to α^2. Although the possibility of using the helium $2\,^3P$ states to determine α was pointed out as early as 1969 (Hughes, 1969), serious experimental work only began in the 1980s. With the development of laser spectroscopy and improved calculations, helium was recognized as the best atom for an α determination which could compete with other methods. These methods use

many different physical systems and energy scales (Mohr, Taylor, and Newell, 2008), and thus a method based purely on atomic spectroscopy is of great interest.

Different high-precision spectroscopy approaches ranging from optically pumped magnetic resonance microwave spectroscopy (George, Lombardi, and Hessels, 2001; Borbely *et al.*, 2009) to heterodyne frequency differences of the 1083 nm transitions (Giusfredi *et al.*, 2005; Zelevinsky, Farkas, and Gabrielse, 2005; Smiciklas and Shiner, 2010) produced sub-kHz accuracy $2\,^3P$ fine structure measurements with a remarkable agreement among them. In particular, the recently reported 9 ppb accurate value for the largest interval $\Delta\nu_{2^3P_{0-2}} = 31\,908\,131.25\,(30)$ kHz, would lead to an uncertainty of 4.5 ppb in the inferred value of α if the theory were exact (Smiciklas and Shiner, 2010).

Unfortunately, theory of $2\,^3P$ fine structure (Drake, 2002; Pachucki and Yerokhin, 2009, 2010) has not experienced an accuracy improvement comparable to that of the experiments. Moreover, larger discrepancies between theory and measurements for the fine structure energies have prevented, up to now, an α value from helium competitive with determinations from other physical systems (Mohr, Taylor, and Newell, 2008). In fact, in the past, fine structure measurements were used to test the fine structure QED theory in He, rather than to determine α. However, the most recently published theoretical results (Pachucki and Yerokhin, 2010) almost resolved the discrepancies between measurements and theory for all three fine structure intervals, although the theoretical uncertainty is still almost 1 order of magnitude worse than the experimental one.

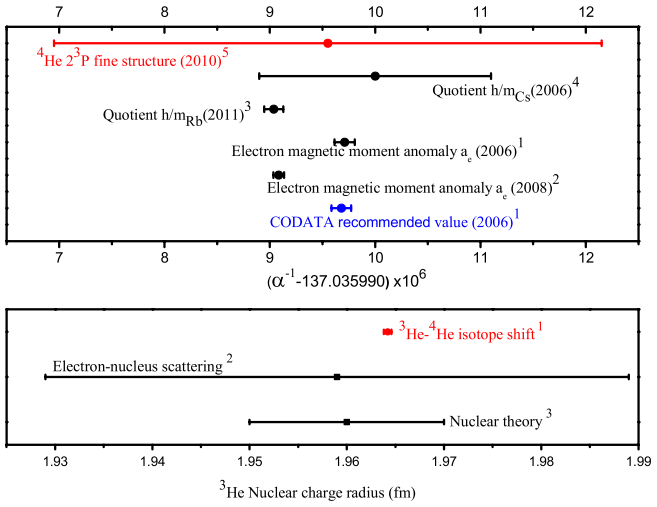

FIG. 15 (color online). Top: Comparison of most updated α determinations [(1) Mohr, Taylor, and Newell, 2008, and references therein; (2) Hanneke, Fogwell, and Gabrielse, 2008; (3) Bouchendira *et al.*, 2011; (4) Gerginov *et al.*, 2006] with the recent α value determined by ^{4}He $2\,^3P_0 - 2\,^3P_2$ fine structure [(5) Smiciklas and Shiner, 2010]. Bottom: Comparison of the ^{3}He nuclear charge radius measured from the ^{3}He–^{4}He isotope shift [(1) Marin *et al.*, 1995; Morton, Wu, and Drake, 2006b; Shiner, Dixson, and Vedantham, 1995; Zhao, Lawall, and Pipkin, 1991] and by electron-nucleus scattering [(2) Amroun *et al.*, 1994] and calculated with nuclear theory [(3) Pieper and Wiringa, 2001].

Combining the above cited $\Delta\nu_{2^3P_{0-2}}$ measurement (Smiciklas and Shiner, 2010) and QED corrections from the recent theory (Pachucki and Yerokhin, 2010), an α value from the He fine structure with an uncertainty of 31 ppb is determined. Such an uncertainty is mainly due to uncalculated high-order QED terms of the fine structure splittings. In the upper graph of Fig. 15, the agreement between this determination and the most recent α values from other physical systems is shown. The weight of this result in a new adjustment of α is still weak, as the accuracy from helium spectroscopy is more than 1 order of magnitude lower than its competitors. Finally, we mention some similar spectroscopic measurements of the $3\,^3P$ fine structure by using the $2\,^3S \rightarrow 3\,^3P$ transitions at 389 nm (Pavone *et al.*, 1994; Mueller *et al.*, 2005). These measurements provided an independent test of He fine structure QED theory, albeit with lower accuracy.

Precise frequency measurements of larger energy intervals, such as $2\,^3S \rightarrow 3\,^3P$ (Shiner, Dixson, and Zhao, 1994; Cancio Pastor *et al.*, 2004, 2006), provide a unique opportunity to test two-electron Lamb-shift calculations, which, of course, are absent in one-electron atoms. The most precise Lamb-shift contribution to a transition frequency in a simple atomic system, including hydrogen and deuterium, was determined by the optical frequency comb assisted frequency measurements of the 1083 nm ^{4}He transitions (Cancio Pastor *et al.*, 2004, 2006). Here $2\,^3S_1 \rightarrow 2\,^3P_{2,1,0}$ transitions were probed by saturated fluorescence spectroscopy in the absence of external magnetic fields, where the frequency of the exciting 1083 nm laser was measured against a quartz-GPS (Global Positioning System) disciplined optical frequency comb. The $2\,^3S - 2\,^3P$ centroid frequency was measured with an accuracy of about 2 kHz (8×10^{-12}), representing the best known optical frequency difference in helium (Morton, Wu, and Drake, 2006a). Theoretical calculations of such frequencies (Yerokhin and Pachucki, 2010) are in reasonable agreement with measurements, taking into account the larger uncertainty of theoretical energies (1–10 MHz). In fact, a QED test at the accuracy of the measurement is challenging due to the difficulty of calculating all high-order QED contributions for S and P states.

In addition to testing QED, the frequency measurements at 1083 nm contribute to improving the $2\,^3P$ level ionization energy, assuming the $2\,^3S$ ionization energy is well known. Unfortunately, the final $2\,^3P$ accuracy in the ionization energy is still limited to 60 kHz as a result of the uncertainty in the ionization energy of the $2\,^3S$ state. Surprisingly, the widely cited value for the $2\,^3S$ ionization energy is not a conventional experimental determination based on extrapolation of a Rydberg series, but instead a hybrid result obtained by combining an accurate measurement of the $2\,^3S \rightarrow 3\,^3D$ transition (Dorrer *et al.*, 1997) with QED and relativistic theoretical corrections for the $3\,^3D$ state (Morton, Wu, and Drake, 2006a). As recently proposed (Eyler *et al.*, 2008), highly accurate measurements of transitions from the $2\,^3S$ state to high-n Rydberg states can help to improve our knowledge of the ionization energy both by increasing the experimental accuracy and by using Rydberg levels with negligible QED and relativistic corrections. In particular, an optical frequency comb assisted measurement of the two-step transition

$2\,^3S \rightarrow 3\,^3P \rightarrow 40\,^3S$ in a cooled and trapped ensemble of He^* atoms may take the $2\,^3S$ accuracy in the ionization energy to the kHz level.

Another important fundamental physics parameter which can be extracted from precision spectroscopy of helium triplet levels is the determination of the nuclear charge radius (r_c) of helium isotopes. This and the nuclear mass are the two basic atomic physics observables defining the structure of an atomic nucleus, and hence provide a link to the nuclear theory of helium. Nuclear mass and volume differences between atomic isotopes determine the isotope shift of spectral lines. Precise isotope shift frequency measurements, together with a calculation of the nuclear mass contribution, extract the nuclear volume contribution, and thus the difference of the square charge radius of both isotopes (Morton, Wu, and Drake, 2006b). Since the r_c of the α particle has been measured independently (Borie and Rinker, 1978; Sick, 2008), measurements of the isotope shift of other helium isotopes, with respect to ^{4}He, give a determination of r_c of these isotopes. In a light atom such as helium, the difference in nuclear mass contributes more than 99.99% to the isotope shift. However, the isotope shift is calculated with an uncertainty of a few tens of ppb (Morton, Wu, and Drake, 2006b). By making measurements of comparable accuracy, uncertainties in r_c of 1×10^{-3} fm can be achieved, limited only by the accuracy of the r_c of the α particle.

The above method was applied for the first time to determine the ^{3}He r_c by measuring the isotope shift for the transitions at 1083 nm (Zhao, Lawall, and Pipkin, 1991) and at 389 nm (Marin *et al.*, 1995). More accurate results were obtained by using isotope shift measurements at 1083 nm by Shiner, Dixson, and Vedantham (1995). The determined ^{3}He r_c from these measurements are in good agreement even though isotope shifts of different helium transitions were used (Morton, Wu, and Drake, 2006b). The agreement provides validity to the method. In the lower graph of Fig. 15, the weighted mean of r_c for ^{3}He determined by ^{3}He/^{4}He isotope shift measurements is compared with the calculated value from nuclear theory (Pieper and Wiringa, 2001), and with the electron-nucleus scattering measurement (Amroun *et al.*, 1994). The potential of this method is demonstrated by the good agreement and the more than an order of magnitude higher accuracy. In fact, precise measurements of the size of halo nuclei of rare ^{6}He and ^{8}He isotopes were performed by using isotope shift measurements at 389 nm in $2\,^3S$ cooled and trapped in a MOT (Wang *et al.*, 2004; Mueller *et al.*, 2007). Moreover, another strength of this method is that, unlike electron-nucleus scattering, the resulting charge radius is independent of the theoretical model for the nucleus.

2. Precision spectroscopy on heavier metastable noble gases

Precision spectroscopy involving metastable levels of noble gases other than helium was mainly devoted to measuring isotope shifts and hyperfine structure in the case of fermionic isotopes (Cannon and Janik, 1990; Walhout *et al.*, 1993; Klein *et al.*, 1996; Blaum *et al.*, 2008; Feldker *et al.*, 2011). These measurements have not allowed precision levels as in helium due to the fact that metrology tools such as the optical frequency comb have not yet been used.

Particularly interesting from the point of view of this review are the spectroscopic measurements in Ne^* and Xe^*, performed in magneto-optical traps. For neon (Feldker *et al.*, 2011), the isotope shift of the $^3P_2 \rightarrow {}^3D_3$ transition at 640.2 nm for all combinations of the three stable isotopes was measured, as well as the hyperfine structure of the $^3D_3$ level of ^{21}Ne. The potential of two different spectroscopic techniques, absorption imaging and MOT fluorescence, used to realize these measurements was demonstrated, also for the rare isotope ^{21}Ne. The realized accuracy improves previous results by about 1 order of magnitude. Similar improvement was reported for isotope shift measurements on the $^3P_2 \rightarrow {}^3D_3$ transition at 882 nm for all possible combinations of the nine stable xenon isotopes, including the most rare ones (^{124}Xe and ^{126}Xe) (Walhout *et al.*, 1993). In addition, hyperfine structure measurements in the upper level ($^3D_3$) were performed for the two stable fermions (^{129}Xe and ^{131}Xe). As for neon, MOT fluorescence spectroscopy was used.

Although magneto-optical trapping of Ar^* and Kr^* has been demonstrated (see Sec. III.D), measurements of properties other than the metastable lifetime have not been performed with such samples.

VII. ATOM OPTICS EXPERIMENTS

A. Interferometry

Shortly after the development of laser-cooling techniques, and before the advent of BEC, atom interferometry developed as an important application of cold atoms. These developments are extensively described in a recent review (Cronin, Schmiedmayer, and Pritchard, 2009). That review also discusses interferometry experiments using conventional beams of metastable atoms. This topic is beyond the scope of this review; we restrict ourselves to a brief description of some interferometry experiments done with cold metastable atoms.

The first interferometry experiment using laser-cooled metastable atoms was reported in 1992 (Shimizu, Shimizu, and Takuma, 1992). Neon atoms from a MOT passed through a double slit and propagated to an MCP. High-contrast interference fringes were observed on a phosphor screen. The experiment introduced an important technique to enhance the spatial coherence of the source. In neon, it is possible to optically pump atoms from the $^3P_2$ state to the $^3P_0$ with 50% efficiency. The optically pumped atoms have no magnetic moment and are insensitive to the lasers creating the MOT; they therefore fall out and create a beam. The source size is approximately the pumping laser waist (smaller than 20 μm in this case), and much smaller than the size of the MOT itself. This technique is crucial for obtaining good fringe contrast with reasonable propagation distances. The same experimental technique was subsequently used by the same group to realize an amplitude hologram (Morinaga *et al.*, 1996), a phase hologram (Fujita, Mitake, and Shimizu, 2000), and a reflecting hologram (Shimizu and Fujita, 2002b) for neon atoms.

B. Metastable helium atom laser

Since the observation of BEC, the ability to coherently outcouple atoms to form a coherent beam of matter waves, or

"atom laser" (Mewes *et al.*, 1997), has attracted much attention, in part because of its potential applications in atom interferometry. Coherent matter wave optics is reviewed in Bongs and Sengstock (2004). Similar to its optical counterpart, the atom laser is interesting from both a fundamental and applied point of view. From a fundamental perspective, atom lasers can be used to study atom-atom interactions (Döring *et al.*, 2008) as well as coherent properties (Bloch, Hänsch, and Esslinger, 2000) of matter waves. Atomic scattering is responsible for nonlinearities in atom laser formation, which can generate nonclassical matter waves such as entangled beams (Dall *et al.*, 2009). Such beams are of interest for tests of quantum mechanics (Reid *et al.*, 2009), and for performing Heisenberg-limited interferometry (Dowling, 1998). From an applied perspective, the atom laser has the potential to revolutionize future atom interferometric sensors (Cronin, Schmiedmayer, and Pritchard, 2009), in which a high flux of collimated atoms is required. Ultimately the performance of such sensors will depend on the signal-to-noise ratio with which atoms in the atom laser beam can be detected. Thus the unique detection possibilities offered by metastable atoms (see Sec. II.G) may prove important for future atom laser applications.

1. Atom laser spatial profiles

Because of their low mass and large *s*-wave scattering length, trapped He^* atoms experience only a small gravitational displacement (relative to the cloud size) away from the magnetic trap minima, compared to an atom such as Rb. For such a system, rf output coupling leads to output coupling surfaces that are oblate spheres rather than planes, as is the case of previously studied atom lasers (Bloch, Hänsch, and Esslinger, 1999). Atoms which are outcoupled above the trap center experience an upward force and therefore travel upward and then drop back through the condensate. The resulting transverse atom laser profiles exhibit a central shadowed region (see Fig. 16), cast by the condensate, since atoms passing back through the condensate are pushed off axis due to the strong mean-field repulsion.

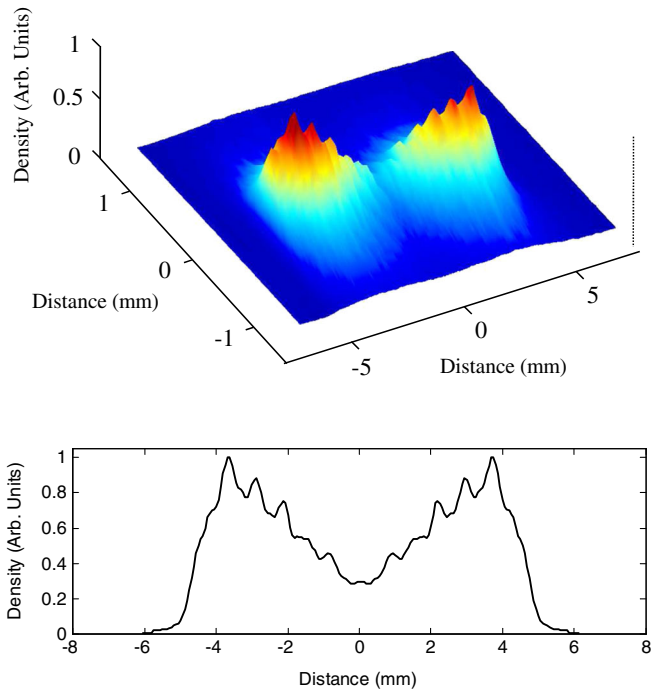

FIG. 16 (color online). Image (upper plot) and cross section (lower plot) showing interference fringes of a metastable ^{4}He atom laser. From Dall *et al.*, 2007.

Besides these large-scale classical effects, it has been predicted that interference fringes should be present on an atom laser beam. Atoms starting from rest at different transverse locations within the outcoupling surface can end up at a later time with different velocities at the same transverse position, leading to interference (Busch *et al.*, 2002). In the case of He^* these interference fringes are readily observable in the spatial profile of the atom laser (see Fig. 16) (Dall *et al.*, 2007).

For the purposes of atom interferometry, the complicated structure exhibited by the helium atom laser is likely to be a hindrance. In principle atom laser beams can be guided in the lowest mode of a confining potential in much the same way that optical fibers guide laser light. Recent experiments with ^{87}Rb atoms outcoupled from BECs into optical waveguides (Guerin *et al.*, 2006; Couvert *et al.*, 2008; Gattobigio *et al.*, 2009) achieved up to 85% single-mode occupancy. The mode population in these experiments was inferred by observing the propagation of atoms along the waveguide via absorption imaging, which also permits the transverse energy of the guided atoms to be determined and compared with that expected for various transverse mode combinations.

Recent experiments with an optically guided He^* BEC allowed direct imaging of the transverse mode structure of the guided matter waves (see Fig. 17) (Dall *et al.*, 2010). The laser beam used to confine the BEC is vertical, so that by adiabatically reducing the intensity of the optical trap atoms are pulled out of the trap and into the waveguide by gravity. Since this process is adiabatic, or nearly so, an almost 100% single-mode guided beam should be possible. This idea is

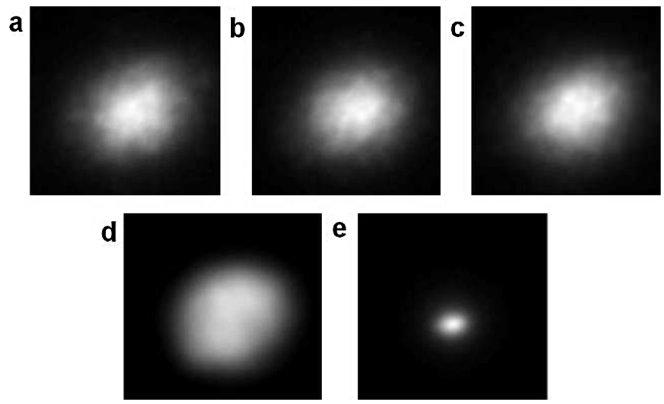

FIG. 17. Multimode speckle images: (a)–(c) Successive experimental realizations produced by guiding only the thermal component of the trapped atoms, showing interference between the thermal modes (speckle). Each panel is a single experimental run, and the pattern is seen to change between images due to the somewhat random nature of the speckle. (d) Average of 20 runs of the experiment; (e) image of a predominantly single-mode profile. All five images show a 3 mm window. From Dall, Hodgman, Manning, Johnsson *et al.*, 2011.

confirmed by simulations. Guiding the atom laser beam results in a smooth Gaussian mode profile [see Fig. 17(e)], avoiding the formation of structure that is often present in atom laser beams (see Fig. 16). In the case of He^* 65% of the atoms have been shown to be guided in the fundamental mode, while the coherence of the guided atom laser was demonstrated by the high visibility interference pattern generated from a transmission diffraction grating.

In some recent experiments (Dall, Hodgman, Manning, Johnsson *et al.*, 2011; Doll, Hodgman, Manning, and Truscott, 2011), atom guiding for several lowest-order modes was achieved by loading thermal atoms into the guide in a controlled fashion. Interference between the modes created atomic speckle which was imaged for the first time [see Figs. 17(a)–17(c)]. In addition, measurement of the second-order correlation function (see Sec. VIII) demonstrated atom bunching associated with the speckle pattern, while no atom bunching was observed for single-mode guiding [see Fig. 17(e)], as expected for a coherent atomic wave front.

2. Feedback control of an atom laser beam

Many precision applications of the optical laser involve active control, in which an error signal is used in a feedback loop to control the laser output (Drever *et al.*, 1983). Similarly, the success of the atom laser as a practical instrument may well depend on feedback control. For a beam of matter waves, flight times from the source to the detector are typically of the order of many milliseconds, rather than the nanosecond times possible with light waves. This difference renders feedback for most atom lasers less useful. In the case of helium, however, there is a way around this problem by probing the atom laser beam at the source rather than monitoring the atoms in the beam itself. An error signal can be derived from the ion signal which accompanies the outcoupling. This error signal can be fed back to the rf-outcoupling frequency. When this scheme was implemented (Dall, Dedman, and Truscott, 2008), a significant reduction in the intensity fluctuations of the atom laser beam was observed as shown in Fig. 18. Since presumably the feedback mechanism is acting on the position in the BEC where atoms are being outcoupled, the beam energy and its spatial structure may be stabilized as well.

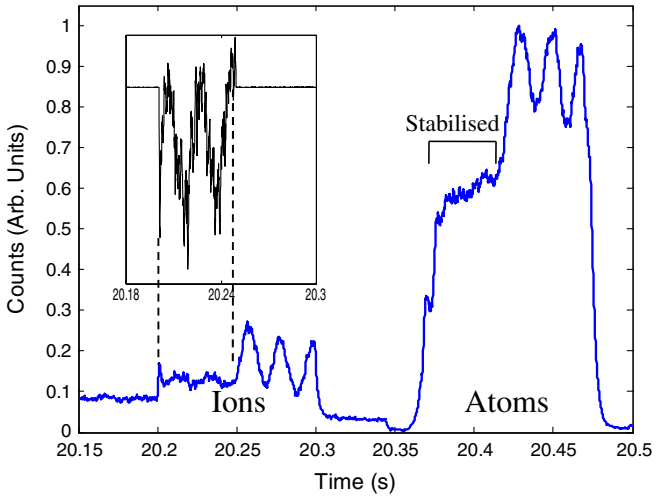

FIG. 18 (color online). Electron multiplier signal demonstrating stabilization of the atom laser beam. The electron multiplier detects both the ions, which arrive first, and the beam of atoms, which arrives after a 150 ms time of flight. Feedback control is implemented only for the first half of the atom laser signal. The inset shows the closed-loop error signal. From Dall, Dedman, and Truscott, 2008.

VIII. PAIR CORRELATION EXPERIMENTS

The particle counting techniques that naturally accompany the use of metastable atoms enabled and encouraged explorations of particle correlation effects in cold gases (see Sec. II.G.2). Analogous experiments using optical imaging techniques have also been carried out (Fölling *et al.*, 2005; Greiner *et al.*, 2005; Rom *et al.*, 2006), but in the following sections we concentrate on results obtained with metastable atoms.

Correlation measurements involve measuring at least two particles and answering the question, given the detection of one particle at point r_1 and time t_1, what is the probability of finding a second one at point r_2 and time t_2? The correlation is generally expressed in terms of second quantized field operators by the second-order correlation function (Naraschewski and Glauber, 1999; Gomes *et al.*, 2006):

$$g^{(2)}(r_1,t_1;r_2,t_2)=\frac{\langle\psi^\dagger(r_2,t_2)\psi^\dagger(r_1,t_1)\psi(r_1,t_1)\psi(r_2,t_2)\rangle}{\langle\psi^\dagger(r_1,t_1)\psi(r_1,t_1)\rangle\langle\psi^\dagger(r_2,t_2)\psi(r_2,t_2)\rangle}. \tag{7}$$

If this function is different from unity, particles are somehow correlated. In the first section we describe experiments emphasizing the role of the quantum statistical properties of atomic clouds through the Hanbury Brown and Twiss (HBT) effect. In the second section this same function will allow us to charaterize atomic sources produced by a four-wave mixing process which have nonclassical properties and potential applications in quantum information processing.

A. Correlation effects in equilibrium ensembles

Correlation measurements go to the heart of many quantum effects because, as has been shown in the field of quantum optics (Glauber, 2006), it is in the two-particle correlation effects that a second quantized field becomes truly necessary to adequately treat a system of particles or photons. Thus one often speaks of the beginning of modern quantum optics as coinciding with the experiments of Hanbury Brown and Twiss (HBT) (Hanbury Brown and Twiss, 1956) and their elucidation by Glauber (1963, 1965). We refer the interested reader to several works which give introductions and simple explanations of the HBT effect for both photons and particles (Baym, 1998; Loudon, 2000; Westbrook and Boiron, 2009).

In the field of atom optics, the first experimental work on HBT was done using metastable neon atoms (Yasuda and Shimizu, 1996). Figure 19 shows a schematic diagram of their experiment. The experiment was a tour de force, because the correlation length (or time) for thermal atoms in a MOT is short and, since an atom cloud in a MOT is far from quantum degeneracy, the probability of finding two particles within a coherence volume is small. It was necessary to acquire data

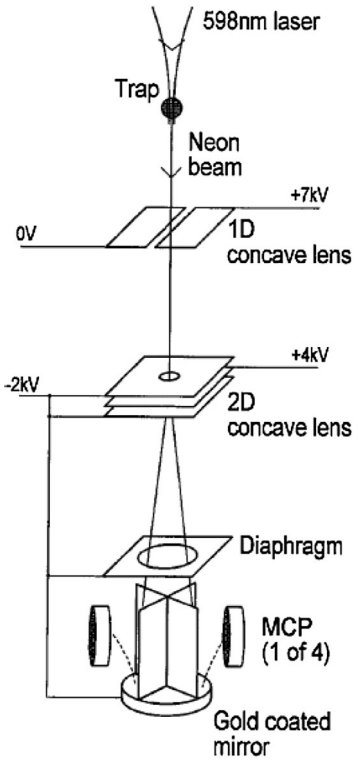

FIG. 19. Schematic diagram of the atom correlation experiment of Yasuda and Shimizu (1996). Metastable neon atoms are ejected from a MOT with a focused laser which pumps atoms into an untrapped state. Below the trap is a metallic plate (gold coated mirror) which can emit an electron when struck by a metastable atom. Four microchannel plates collect the ejected electrons from different parts of the plate. The Hanbury Brown–Twiss effect corresponds to an enhanced probability of detecting coincident electrons with zero delay, compared to the coincidence rate with a delay greater than the correlation time, about 100 ns. The electrodes between the source and the detector act as lenses and allow one to modify the source size as seen from the detector and thus modify the transverse coherence length of the beam.

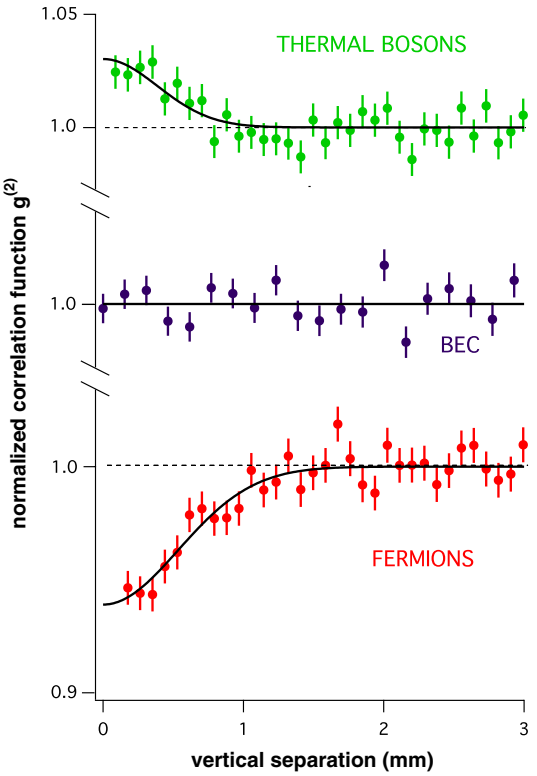

FIG. 20 (color online). Data on bunching and antibunching as shown by the normalized second-order correlation function (7). The vertical scale of each plot is the same. The upper plot shows bunching of a thermal gas of bosons (^{4}He). The lower plot shows antibunching of a thermal gas of fermions (^{3}He). The horizontal axis shows the spatial separation, but it can be converted into a temporal separation by multiplying by the mean velocity of the atoms (about 3 m/s). The middle plot shows the flat correlation function of atoms from a BEC. The upper and lower plots are derived from the data of Jeltes *et al.* (2007). The middle plot is derived from Schellekens *et al.* (2005).

for a time on the order of 50 h, and even with this amount of data, the signal-to-noise ratio was low, but the experimental result definitively exhibited the bunching behavior expected for the HBT effect of thermal bosons.

The situation became more favorable with the advent of evaporation techniques to achieve quantum degeneracy (see Sec. II). Quantum degeneracy corresponds to one particle per coherence volume, rendering the probability of finding two particles in the same coherence volume much higher. Thus, with the demonstration of BEC of He*, a more powerful version of the Yasuda and Shimizu experiment became an attractive possibility. In 2005, Schellekens *et al.* (2005) succeeded in observing HBT correlations with He*.

This work reported measurements both of a thermal gas slightly above the BEC threshhold and of a degenerate gas. As shown in the top two plots of Fig. 20, the thermal gas shows a HBT effect, while a BEC does not. The absence of HBT correlations in the BEC is an indication of the fact that, similar to the intensity of a laser, density fluctuations are suppressed. The positions of the particles in an ideal BEC are entirely uncorrelated with each other. In contrast to the work of Yasuda and Shimizu (1996), which used a continuous beam of atoms, the inherently cyclical nature of evaporative cooling experiments imposed a pulsed mode of operation on the work of Schellekens *et al.* (2005): An entire trapped sample was released and allowed to ballistically expand. Another difference between the two experiments is the observed correlation time which was 3 orders of magnitude larger than in the Ne* experiment. The difference is in part due to the smaller mass of helium, but also to the fact that in a ballistically expanding cloud, the slow and fast atoms separate during propagation leading to a local momentum spread which is smaller than that of the initial source. The spatial correlation length at the detector is inversely proportional to the momentum spread, and thus the correlation length increases as the cloud propagates. The correlation time is given by the longitudinal correlation length divided by the mean velocity of the atoms (Gomes *et al.*, 2006).

Recently a new thermal gas–BEC comparison was published (Manning *et al.*, 2010). In that work, atoms were rf outcoupled from a trap in roughly 30 small bunches, each containing only a fraction of the total atom number. This technique permitted the use of a higher atom number in the BEC without saturating the detector. The data showed that the

second-order coherence properties both of a thermal cloud and of a BEC are not perturbed by the operation of an rf outcoupler. This work was extended to the measurement of the three-body correlation function (Hodgman *et al.*, 2011). It demonstrated the long-range coherence of the BEC for correlation functions to third order, which supports the prediction that similar to coherent light, a BEC possesses long-range coherence to all orders.

The achievement of quantum degeneracy of a gas of metastable ^{3}He, the fermionic isotope of this atom, was reported by McNamara *et al.* (2006). In the fermion case, the exclusion principle, or alternatively the antisymmetry of fermion wave functions under exchange of particles, leads to an antibunching effect rather than a bunching effect as with bosons. Antibunching has no classical wave analog and thus by observing the HBT effect with fermions, one is truly entering the domain of what might be called quantum-atom optics in which we can have a nonclassical interference effect. A clear antibunching signal using ^{3}He* was reported in 2007 (Jeltes *et al.*, 2007). This work also repeated the experiment for a thermal bose gas (^{4}He*) of nearly the same temperature and density. The comparison, shown in Fig. 20, shows the dramatic effect of the different quantum statistics.

B. Four-wave mixing of matter waves

After the experiment of Hanbury Brown and Twiss, the field of quantum optics developed further with the availability of nonclassical photonic sources (Scully and Zubairy, 1997). One well-known example is the source produced in spontaneous parametric downconversion where photons are created in pairs through a nonlinear process (Burnham and Weinberg, 1970). Strongly correlated states are now at the heart of quantum information processing and of future interferometers (Giovannetti, Lloyd, and Maccone, 2004, 2011). Quantum *atom* optics is only at its early stages but is progressing rapidly. The fact that the atomic nonlinearity is intrinsically present due to atomic interactions and could be several orders of magnitude larger than optical nonlinearity (Mølmer *et al.*, 2008) has attracted considerable interest. The search for efficient nonclassical atomic sources is therefore both natural and desirable. There have been many proposals concerning atom pairs, especially the production and observation of individual entangled pairs of atoms through atomic collisions or the breakup of diatomic molecules (Band *et al.*, 2000; Duan *et al.*, 2000; Pu and Meystre, 2000; Opatrný and Kurizki, 2001; Kheruntsyan and Drummond, 2002; Ziń *et al.*, 2005; Naidon and Masnou-Seeuws, 2006; Norrie, Ballagh, and Gardiner, 2006; Savage, Schwenn, and Kheruntsyan, 2006; Ziń, Chwedeńczuk, and Trippenbach, 2006; Deuar and Drummond, 2007). As emphasized by Duan *et al.* (2000), pair production can be studied in two limits. If many atoms are created in a single pair of modes, stimulated emission of atoms is important and one speaks of two-mode squeezing in analogy with Heidmann *et al.* (1987). The opposite limit, in which the occupation number of the modes is much less than unity, corresponds to the spontaneous production of individual, entangled atom pairs, in either spin or momentum states in analogy with Ou and Mandel (1988), Shih and Alley (1988), and Rarity and Tapster (1990).

1. Pair production in the spontaneous regime

The correlation among scattered atoms has been studied experimentally in the spontaneous limit in the breakup of K_2 molecules (Greiner *et al.*, 2005), using the technique of noise correlation in absorption images (Grondalski, Alsing, and Deutsch, 1999; Altman, Demler, and Lukin, 2004), and in the collision between two Bose-Einstein condensates of metastable helium atoms (Perrin, 2007; Perrin *et al.*, 2007) using a 3D single atom detector (Schellekens *et al.*, 2005). The performance of such a detector (see Sec. II.G) has enabled a careful characterization of the pair production mechanism.

The collision between two BECs produces scattered particles by elastic collision and can be viewed as a spontaneous four-wave mixing process. This can be shown using the Hamiltonian governing the system

$$\hat{H} = \int d\mathbf{r}\hat{\Psi}^\dagger(\mathbf{r})\left(-\frac{\hbar^2}{2m}\Delta + V(\mathbf{r}) + g\hat{\Psi}^\dagger(\mathbf{r})\hat{\Psi}(\mathbf{r})\right)\hat{\Psi}(\mathbf{r}),$$

with V the trapping potential and g the interaction coupling constant. In a simple picture one can write $\hat{\Psi}(\mathbf{r})$ as

$$\hat{\Psi}(\mathbf{r}) = \phi_{\mathbf{Q}}(\mathbf{r}) + \phi_{-\mathbf{Q}}(\mathbf{r}) + \hat{\delta}(\mathbf{r}),$$

with $\phi_{\pm\mathbf{Q}}$ representing the two coherent colliding condensates of relative momentum $\pm\hbar\mathbf{Q}$ and $\hat{\delta}$ is the scattered field. When the depletion of the condensates can be ignored, the Hamiltonian contains a term of the form $g\phi_{\mathbf{Q}}\phi_{-\mathbf{Q}}\hat{\delta}^\dagger\hat{\delta}^\dagger$ + H.c. similar to the one found in spontaneous parametric downconversion or molecular dissociation. One then expects that the scattered field has also similar quantum properties.

In the experiment of Perrin (2007), two stimulated Raman transitions transfer the atoms from a condensate confined in a magnetic trap (magnetic substate $m = 1$) to the magnetic insensitive state $m = 0$. Since the laser beams of the Raman transitions are different, the momentum they transfer to the atoms is also different. The two ''daughter'' condensates have a relative velocity of $2v_{\mathrm{rec}} \approx 18.4$ cm/s, at least 8 times larger than the speed of sound in the initial condensate. Since the collisions are elastic, the scattered particles are

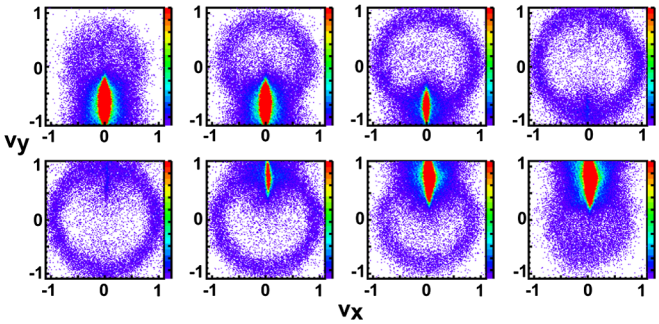

FIG. 21 (color online). Slices in vertical velocity v_z of the spherical shell of atoms in velocity space (in units of v_{rec}) for a collision of two BECs. The data are similar to that of Perrin (2007). All plots use the same linear false color scale. The scattering halo is the circular shell which intersects the BECs.

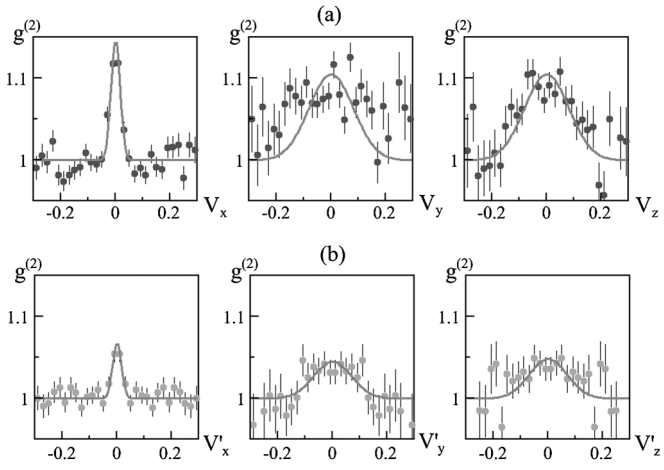

FIG. 22. (a) Back to back and (b) collinear correlation peaks observed in the collision of two BECs. (a) Projection of the normalized two-body correlation function along the different axes of the experiment and around $\mathbf{v}+\mathbf{v}'=\mathbf{0}$. The projection consists of averaging the correlation in the two other directions over a surface equal to the products of the corresponding correlation lengths. The peak is the signature for correlated atoms with opposite velocities. (b) Similar to (a) but for $\mathbf{v}-\mathbf{v}'=\mathbf{0}$. This peak is due to the Hanbury Brown and Twiss bunching effect. In all the graphs, velocities are expressed in units of the recoil velocity. From Perrin, 2007.

expected to lie approximately (Krachmalnicoff *et al.*, 2010) on a spherical shell in velocity space of radius v_{rec}, as shown in Fig. 21. Since atoms are expected to be scattered in pairs with opposite velocities (in the center of mass frame), the normalized two-body correlation function $g^{(2)}(\mathbf{v},\mathbf{v}')$ [the equivalent of Eq. (7) in velocity space] peaks at $\mathbf{v}'=-\mathbf{v}$; this is demonstrated in Fig. 22(a).

In addition to the correlations of opposite momenta, Fig. 22(b) shows the correlation for $\mathbf{v}'\approx\mathbf{v}$. Momentum conservation forbids two atoms to be scattered with the same velocity, but, since the experiment is performed with bosonic atoms, bunching between pairs of atoms is expected in analogy with the Hanbury Brown–Twiss effect (see Sec. VIII.A) (Mølmer *et al.*, 2008). The local correlation can hence be explained by a four-body process. As seen in Fig. 22, the correlation function is anisotropic with a width along x much shorter than along the yz plane. A perturbative approach (Chwedeńczuk *et al.*, 2008) confirms that the widths of the opposite and collinear correlation are mainly controlled by the spatial size of the BECs as in the Hanbury Brown–Twiss experiment (Gomes *et al.*, 2006). Since the trap is anisotropic with a long axis along x, the correlation along that axis is the shortest as expected. Numerical calculations are in good agreement with the experiment. The local correlation function can also be used to define a mode volume; this leads to a mode population of the order of 0.1, indicating the spontaneous nature of the collision. To fully understand the results, the BEC collision is also simulated using a fully quantum, first-principles numerical calculation based on the positive-P representation method (Deuar and Drummond, 2007; Perrin *et al.*, 2008). The good agreement between these calculations and the experimental data shows that the physical picture is correct and exemplifies the power of this method.

One expects that a zone in momentum space centered at $\mathbf{k}$ should have exactly the same atom number as the corresponding zone centered at $-\mathbf{k}$. Subshot noise number differences have indeed been observed in such a BEC collision experiment (Jaskula *et al.*, 2010). Although the measured noise reduction (0.5 dB) was modest, it has been shown to be completely dominated by the finite detection efficiency of the detector (see Sec. II.G), demonstrating that the collision between two BECs indeed produces a good nonclassical atomic source. The result is not entirely trivial because the presence of correlations in opposite momenta does not guarantee a sub-Poissonian number difference [see Buchmann *et al.* (2010) for an example].

2. Paired atom laser beams in the stimulated regime

Stimulated four-wave mixing in a trapped BEC was first demonstrated in 1999 (Deng *et al.*, 1999), using three matter waves to generate a fourth. More recently, twin atomic beams were created using a similar process (Vogels, Xu, and Ketterle, 2002). Although phase coherence of these matter waves was demonstrated, correlation properties were not observed.

In the case of a He* atom laser, pairs of beams can be produced simply by the process of rf outcoupling from a He* BEC (Dall *et al.*, 2009; RuGway *et al.*, 2011). Unlike the previous methods, which required pairs of atoms traveling at high kinetic energies as a source, this process involves scattering between atoms in the same zero momentum state to states with nonzero momentum. At the heart of the method are the different scattering lengths that are available for the different magnetic sublevels of He* (Leo *et al.*, 2001). As atoms are outcoupled in a different magnetic sublevel, their interaction energy abruptly changes, driving collisional processes consisting of atom pairs moving in opposite directions.

Stimulated four-wave mixing occurs if the outcoupling surface is chosen to be an ellipsoidal shell, for example, by detuning the outcoupling from the center of the condensate by 2 kHz. This causes a range of densities in the trapped and untrapped fields to exist over the surface. Atoms accelerated in the mean-field and trap potentials by initial four-wave mixing scattering are amplified, allowing resonant stimulated

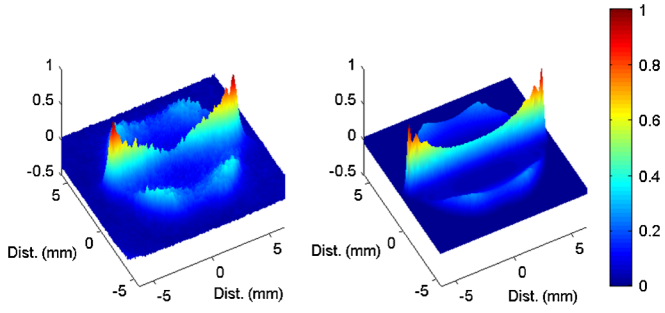

FIG. 23 (color online). Spatial profiles of the He* atom laser when the conditions for stimulated four-wave mixing are met (experimental image, left; theoretical simulation, right). Four extra peaks, resulting from four-wave mixing, are observed around the usual He* profile. Adapted from Dall *et al.*, 2009.

scattering into higher and higher final momentum modes. This sweeps out the halo shown in Fig. 23, and finally reaches the momentum corresponding to the well-defined peaks (shown on the outskirts of the halo in Fig. 23) which then become heavily populated.

Quantum and semiclassical models indicate that these peaks are formed from the scattering of pairs of atoms in a BEC and should be therefore entangled upon formation. It remains to be seen whether correlation and useful entanglement remain after the outcoupling process.

IX. OTHER EXPERIMENTS USING COLD, METASTABLE NOBLE GASES

In this section we discuss several other experiments that have been performed in recent years using cold noble gases.

A. Reflection of slow metastable atoms from surfaces

Using cooling techniques, atoms can be rendered sufficiently slow that they probe the weak, long-range interactions with surfaces corresponding to the Casimir-Polder force (Casimir and Polder, 1948). Since the potential in this regime is *attractive*, the reflection of atoms from a surface is remarkable. The phenomenon is a wave effect, analogous to the partial reflection of an electromagnetic wave at a dielectric interface, and is generally referred to as ''quantum reflection.'' The low noise electronic detection methods, discussed in Sec. II, rendered metastable atoms useful for such experiments because reflection coefficients, and thus the available signal, can be small. Shimizu (2001) reported the observation of specular reflection of Ne^* atoms from both a silicon and a glass surface. A grazing incidence geometry permitted incident velocities as low as 1 mm/s normal to the surface. For Ne^*, this velocity corresponds to a de Broglie wavelength of approximately 20 μm. For incident normal velocities between 1 and 35 mm/s, the observed reflectivities varied from above 0.3 to below 10^{-3}. A careful study of the velocity dependence showed that, within the estimated uncertainties, the data agreed well with the Casimir-Polder theory. This work was followed up by a study of reflection and diffraction from a Si surface with a periodic structure of parallel ridges with heights of a few microns (Shimizu and Fujita, 2002a). Using the same atomic source geometry, they demonstrated somewhat higher reflectivities at 1 mm/s incident velocity and much higher reflectivity at 30 mm/s. The group later experimented with reflection of He^* from a flat silicon surface (Oberst *et al.*, 2005). The lowest incident normal velocity was higher in this case (30 mm/s), but at this velocity a reflectivity above 10% was nevertheless observed. They also compared the velocity dependence with that of Ne^* and showed that it scaled with the mass and polarizability of the atoms.

Interaction of He^* with surfaces was also studied theoretically. Yan and Babb (1998) made detailed calculations of the polarizability and gave interaction potentials for a perfectly conducting or dielectric surface. Marani *et al.* (2000) used these results to analyze how the atom surface interaction would modify the behavior of atom diffraction effects at an evanescent wave atomic mirror. Halliwell *et al.* (2003) determined the reflection probability for He^* atoms inside hollow optical fibers to determine the contribution to the atomic transmission efficiency.

B. Birth and death of a Bose-Einstein condensate

As pointed out in Secs. I and III, inelastic collisions with a metastable atom usually lead to production of ions and electrons. Since charged particles are efficiently detected with an MCP detector, the corresponding ionization signal can be used to monitor the metastable atomic cloud in real time. We have already seen how such a signal can be used in a feedback loop (see Sec. VII). The ion signal can also serve to monitor condensation dynamics. At low density, the ion rate is due to Penning collisions with background gas and thus allows one to monitor the metastable atom number. At a higher density, which is reached for clouds close to quantum degeneracy, two- and three-body inelastic collisions dominate the observed ion rate. This, in turn, gives information about the atomic density. Because the N-body correlation functions are different in a thermal cloud and a condensate (see Sec. VIII), inelastic N-body collisions occur with a rate constant $N!$ smaller for a condensate than for a thermal sample (Kagan, Svistunov, and Shlyapnikov, 1985; Burt *et al.*, 1997). Nevertheless, in contrast to a homogeneous gas, the ion rate of a trapped condensate is still significantly higher than for a thermal sample in the same trap because of its higher density.

Therefore, in a trap one can observe a gas crossing the threshold for Bose-Einstein condensation as a sudden increase in the ion production rate (Robert *et al.*, 2001; Seidelin *et al.*, 2003; Tychkov *et al.*, 2006). This phenomenon is illustrated in Fig. 24. This signal is a good indicator to pinpoint the BEC threshold and reproducibly place a gas close to that threshold. In addition, since for a given trap and temperature the threshold corresponds to a well-defined

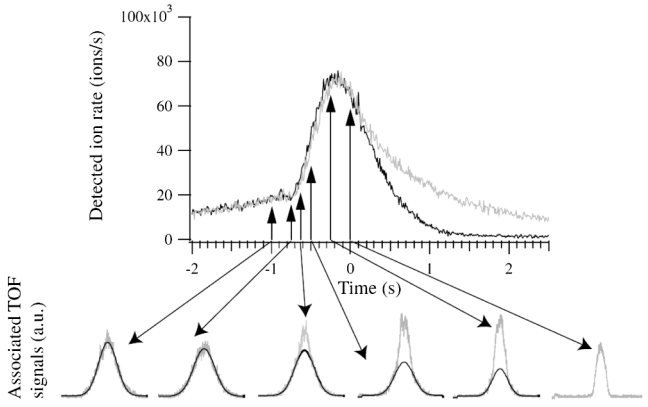

FIG. 24. Ion signal during the last stage of rf evaporation. Its sharp increase at $t_{\rm th} = -0.7$ s indicates that the cloud crosses the Bose-Einstein threshold. This is confirmed by switching off the trap at various times and measuring the time-of-flight signal. For $t > t_{\rm th}$ a double structure is clearly visible indicating the presence of a Bose-Einstein condensate. The upper lighter curve corresponds to a situation where the rf shield is always on, whereas it is off after BEC formation for the lower darker curve. The difference indicates that without an rf shield, the condensate heats up rapidly (see text). From Seidelin *et al.*, 2003.

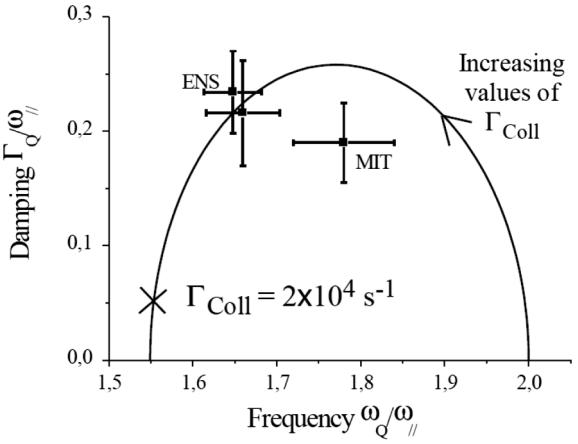

FIG. 25. Damping of the quadrupole-monopole mode as a function of its frequency in units of the longitudinal frequency of the trap. In the collisionless regime, there is no damping. As the elastic collision rate increases, the frequency of the mode is shifted and damping is present. MIT and ENS correspond, respectively, to the measurements performed by Stamper-Kurn *et al.* (1998) at Massachusetts Institute of Technology and Leduc *et al.* (2002) at Ecole Normale Superieure. From Leduc *et al.*, 2002.

number of atoms, locating the BEC threshold can be used to calibrate the number of atoms. This idea was used in an experiment to measure the scattering length (Seidelin *et al.*, 2004), as discussed in Sec. V. Figure 24 also shows that the ion rate permits monitoring of condensate decay. Such a study was also carried out by Tychkov *et al.* (2006), and modeled by Zin ́ *et al.* (2003), Gardiner *et al.* (1997), and Söding *et al.* (1999). It has been shown that under the assumption of rapid thermalization, a transfer of atoms from the condensate to the thermal component should occur, enhancing the condensate decay.

C. Hydrodynamic regime close to the bosonic degenerate regime

Usually, ultracold clouds are in the collisionless regime in which the atomic motion is described by a single particle Hamiltonian. On the other hand, if the mean free path between colliding atoms is small compared to dimensions of the trapped cloud, the atomic cloud is in the hydrodynamic regime. In this regime the oscillation frequencies of the excited modes of the gas are modified and exhibit damping (Griffin, Wu, and Stringari, 1997; Guéry-Odelin *et al.*, 1999). Since the scattering length is notably larger in metastable helium than in alkali atoms, this regime should be easier to observe in metastable helium (Stamper-Kurn *et al.*, 1998; Leduc *et al.*, 2002). Leduc *et al.* (2002) studied the quadrupole-monopole mode for several elastic collision rates, and indeed a regime close to the hydrodynamic limit was reached in which a shift of ~20% of the mode frequency was observed (see Fig. 25). This regime was later also observed in a sodium BEC (van der Stam *et al.*, 2007).

X. OUTLOOK

A significant part of this review was devoted to the substantial body of work on collision processes between metastable atoms. This work has led to our ability to routinely cool helium to quantum degeneracy. It has indicated that for neon, although evaporatively cooled samples of bosonic and fermionic samples have been produced, the conventional path to quantum degeneracy remains difficult, but not hopeless. Work is currently concentrating on the detailed investigation and the possible modification of the elastic and inelastic collisional properties. For the heavier metastable noble gases, inelastic collision rates are so high that we see little hope of achieving degeneracy with them without radical innovations. As discussed, the study of cold collisions in helium has led to the prediction of a magnetic Feshbach resonance. We expect to see attempts to observe and exploit these resonances in the near future. The demonstration of stable mixtures of ^{4}He* and ^{87}Rb (Byron *et al.*, 2010; Byron, Dall, and Truscott, 2010) leads us to speculate that useful Feshbach resonances may turn up in this system as well.

The investigation of scattering resonances in heteronuclear mixtures also opens the possibility of studying Efimov states (Kraemer *et al.*, 2006; Knoop *et al.*, 2009; Ferlaino and F., 2010) in such mixtures. It was suggested (D'Incao and Esry, 2006) that a heteronuclear Efimov state might permit a demonstration of universality in the spacing of Efimov resonances. This spacing, which is given by the factor of 22.7 in homonuclear systems, is predicted to have a smaller ratio the greater the mass ratio in a heteronuclear system. Thus, the observation of a series of states in the same system may be easier. A system consisting of one He* and two Rb atoms appears to be a good candidate for such a study (Knoop, 2011).

For the purposes of more traditional spectroscopy, we expect that future investigations could further challenge QED by measuring the decay rates of the $3\,^3P$ states to the ground state using a 389 nm laser to access these states from the $2\,^3S_1$ metastable state for comparison with theoretical calculations (Morton and Drake, 2011). Singlet states can be accessed via direct laser transition from the $2\,^3S_1$ metastable state to the $2\,^1S_0$ metastable state (van Leeuwen and Vassen, 2006; van Rooij *et al.*, 2011). As an alternative, high-lying $l > 1$ triplet states near the ionization limit can be excited; these exhibit a mixed singlet-triplet character and can, as a result of this mixing, decay into the singlet state manifold (Eyler *et al.*, 2008). This strategy may allow a more accurate determination of the two-photon decay of the $2\,^1S_0$ state [19.7(1.0) ms] (Van Dyck, Johnson, and Shugart, 1971), and enable a more stringent test of QED predictions (Derevianko and Johnson, 1997).

Spectroscopic measurements can also be performed from the metastable triplet state to singlet states. In particular, two different proposals have recently been made to measure the $2\,^3S - 2\,^1S$ doubly forbidden transition (van Leeuwen and Vassen, 2006; Eyler *et al.*, 2008). In the first (van Leeuwen and Vassen, 2006), one-photon spectroscopy with a high power cw laser at 1557 nm was proposed to exploit the weak magnetic dipole transition between these two states. This transition was observed recently in Amsterdam in a quantum degenerate gas and its frequency was measured, for both ^{3}He and ^{4}He, applying an optical frequency comb (van Rooij *et al.*, 2011). In the second (Eyler *et al.*, 2008), direct, two-photon optical frequency comb spectroscopy at

886 and 2060 nm was proposed, to drive a Raman transition in the $2^3S \rightarrow 2^1P \rightarrow 2^1S$ levels. In both cases, cooled, trapped atoms are needed to ensure narrow linewidths and to obtain measurable signal-to-noise ratios.

From the point of view of atom optics, it seems clear that the three-dimensional single atom detection capability afforded by metastable noble gas atoms will continue to inspire many investigations. We have seen the first successful production of atom pairs and macroscopically occupied twin beams via variants of four-wave mixing of matter waves, but other variants are possible. Four-wave mixing enabled by modification of dispersion relations using an optical lattice (Hilligsøe and Mølmer, 2005) was demonstrated in alkali atoms (Gemelke *et al.*, 2005; Campbell *et al.*, 2006). In that work twin beams were generated but their degree of correlation, or intensity squeezing, was not measured. In a more recent experiment using Rb (Bücker *et al.*, 2011), workers used an intermediate excited state in a nearly one-dimensional gas to produce twin beams and were able to demonstrate a high degree of relative intensity squeezing between the beams. These two techniques can be adapted to metastable atoms, and we expect that the ability to make observations in three dimensions with good spatial resolution will improve our knowledge of the details of four-wave mixing in matter waves. For example, it remains to be seen whether the atoms in the correlated beams are sufficiently coherent to permit their use in interferometry experiments. Recent experiments showing the effects of mean-field interactions (Krachmalnicoff *et al.*, 2010) may be showing that uncontrolled phase shifts can be present.

If twin beams can be made sufficiently coherent, the experience of the quantum optics community suggests several possible experiments. In Sec. VIII, we already alluded to several theoretical proposals to observe the entanglement which should be present among the atoms in pair creation experiments. These proposals seem technically challenging but we believe that some of them will be realized eventually. Another possibility inspired by quantum optics is to realize an atomic analog of the famous experiment of Hong, Ou, and Mandel (1987). Using atoms in such experiments will add a new twist on this effect because one can use either bosons or fermions. The results are different in the two cases.

Another important recent trend in cold atom physics is the study of strongly correlated many-body systems. To give some examples, Feshbach resonances in Fermi gases have been used to explore the BEC-BCS crossover regime (Greiner, Regal, and Jin, 2003; Jochim *et al.*, 2003; Bourdel *et al.*, 2004), and the implementation of optical lattices has allowed the exploration of other many-body states and quantum phase transitions, the first of which was the celebrated superfluid-to-Mott insulator transition (Greiner *et al.*, 2002). The physics of many-body systems realized in quantum gases is too rich to summarize here and we refer the interested reader to a recent review (Bloch, Dalibard, and Zwerger, 2008). It seems to us, however, that the correlation techniques that have been developed in the context of metastable helium experiments will probably help to shed light on these systems especially in the study of quantum phase transitions, where the behavior of correlation functions is often a crucial signature.

ACKNOWLEDGMENTS

This work was initiated by the project CIGMA (Controlled Interactions in quantum Gases of Metastable Atoms), partly financed by the European Science Foundation EuroQUAM Programme. We thank all students and co-workers for their contribution to the research presented in this work. W. V. and G. B. acknowledge support from the Dutch Foundation for Fundamental Research on Matter (FOM) and the German Research Foundation (DFG), respectively.

REFERENCES

Altman, E., E. Demler, and M. D. Lukin, 2004, Phys. Rev. A **70**, 013603.
Amroun, A., *et al.*, 1994, Nucl. Phys. **A579**, 596.
Anderson, M. H., J. R. Ensher, M. R. Matthews, C. E. Wieman, and E. A. Cornell, 1995, Science **269**, 198.
Aspect, A., E. Arimondo, R. Kaiser, N. Vansteenkiste, and C. Cohen-Tannoudji, 1988, Phys. Rev. Lett. **61**, 826.
Aspect, A., N. Vansteenkiste, R. Kaiser, H. Haberland, and M. Karrais, 1990, Chem. Phys. **145**, 307.
Baldwin, K. G. H., 2005, Contemp. Phys. **46**, 105.
Band, Y. B., M. Trippenbach, J. P. Burke, and P. S. Julienne, 2000, Phys. Rev. Lett. **84**, 5462.
Bardou, F., J. P. Bouchaud, A. Aspect, and C. Cohen-Tannoudji, 2002, *Levy Statistics and Laser Cooling. How Rare Events Bring Atoms to Rest* (Cambridge University Press, Cambridge, England).
Bardou, F., O. Emile, J.-M. Courty, C. I. Westbrook, and A. Aspect, 1992, Europhys. Lett. **20**, 681.
Barrett, M. D., J. A. Sauer, and M. S. Chapman, 2001, Phys. Rev. Lett. **87**, 010404.
Baym, G., 1998, Acta Phys. Pol. B **29**, 1839.
Beams, T. J., G. Peach, and I. B. Whittingham, 2004, J. Phys. B **37**, 4561.
Beams, T. J., I. B. Whittingham, and G. Peach, 2007, Phys. Rev. A **76**, 062707.
Blaum, K., W. Geithner, J. Lassen, P. Lievens, K. Marinova, and R. Neugart, 2008, Nucl. Phys. **A799**, 30.
Bloch, I., 2005, Nature Phys. **1**, 23.
Bloch, I., J. Dalibard, and W. Zwerger, 2008, Rev. Mod. Phys. **80**, 885.
Bloch, I., T. W. Hänsch, and T. Esslinger, 1999, Phys. Rev. Lett. **82**, 3008.
Bloch, I., T. W. Hänsch, and T. Esslinger, 2000, Nature (London) **403**, 166.
Bongs, K., and K. Sengstock, 2004, Rep. Prog. Phys. **67**, 907.
Borbely, J. S., M. C. George, L. D. Lombardi, M. Weel, D. W. Fitzakerley, and E. A. Hessels, 2009, Phys. Rev. A **79**, 060503.
Borie, E., and G. A. Rinker, 1978, Phys. Rev. A **18**, 324.
Bouchendira, R., P. Cladé, S. Guellati-Khélifa, F. Nez, and F. Biraben, 2011, Phys. Rev. Lett. **106**, 080801.
Bourdel, T., L. Khaykovich, J. Cubizolles, J. Zhang, F. Chevy, M. Teichmann, L. Tarruell, S. J. J. M. F. Kokkelmans, and C. Salomon, 2004, Phys. Rev. Lett. **93**, 050401.
Bradley, C. C., C. A. Sackett, J. J. Tollett, and R. G. Hulet, 1995, Phys. Rev. Lett. **75**, 1687.
Browaeys, A., J. Poupard, A. Robert, S. Nowak, W. Rooijakkers, E. Arimondo, L. Marcassa, D. Boiron, C. I. Westbrook, and A. Aspect, 2000, Eur. Phys. J. D **8**, 199.
Browaeys, A., A. Robert, O. Sirjean, J. Poupard, S. Nowak, D. Boiron, C. I. Westbrook, and A. Aspect, 2001, Phys. Rev. A **64**, 034703.

Buchmann, L. F., G. M. Nikolopoulos, O. Zobay, and P. Lambropoulos, 2010, Phys. Rev. A **81**, 031606.
Bücker, R., J. Grond, S. Manz, T. Berrada, T. Betz, C. Koller, U. Hohenester, T. Schumm, A. Perrin, and J. Schmiedmayer, 2011, Nature Phys. **7**, 608.
Burnham, D. C., and D. L. Weinberg, 1970, Phys. Rev. Lett. **25**, 84.
Burt, E. A., R. W. Ghrist, C. J. Myatt, M. J. Holland, E. A. Cornell, and C. E. Wieman, 1997, Phys. Rev. Lett. **79**, 337.
Busch, H. C., M. K. Shaffer, E. M. Ahmed, and C. I. Sukenik, 2006, Phys. Rev. A **73**, 023406.
Busch, T., M. Köhl, T. Esslinger, and K. Mølmer, 2002, Phys. Rev. A **65**, 043615.
Byron, L. J., R. G. Dall, W. Rugway, and A. G. Truscott, 2010, New J. Phys. **12**, 013004.
Byron, L. J., R. G. Dall, and A. G. Truscott, 2010, Phys. Rev. A **81**, 013405.
Campbell, G. K., J. Mun, M. Boyd, E. W. Streed, W. Ketterle, and D. E. Pritchard, 2006, Phys. Rev. Lett. **96**, 020406.
Cancio Pastor, P., G. Giusfredi, P. De Natale, G. Hagel, C. de Mauro, and M. Inguscio, 2004, Phys. Rev. Lett. **92**, 023001.
Cancio Pastor, P., G. Giusfredi, P. De Natale, G. Hagel, C. de Mauro, and M. Inguscio, 2006, Phys. Rev. Lett. **97**, 139903.
Cannon, B., and G. Janik, 1990, Phys. Rev. A **42**, 397.
Carnal, O., and J. Mlynek, 1991, Phys. Rev. Lett. **66**, 2689.
Carr, L. D., D. DeMille, R. V. Krems, and J. Ye, 2009, New J. Phys. **11**, 055049.
Cashen, M., and H. Metcalf, 2003, J. Opt. Soc. Am. B **20**, 915.
Cashen, M. T., and H. Metcalf, 2001, Phys. Rev. A **63**, 025406.
Casimir, H. B. G., and D. Polder, 1948, Phys. Rev. **73**, 360.
Castillega, J., D. Livingston, A. Sanders, and D. Shiner, 2000, Phys. Rev. Lett. **84**, 4321.
Chen, C. Y., K. Bailey, Y. M. Li, T. P. O'Connor, Z.-T. Lu, X. Du, L. Young, and G. Winkler, 2001, Rev. Sci. Instrum. **72**, 271.
Chin, C., R. Grimm, P. Julienne, and E. Tiesinga, 2010, Rev. Mod. Phys. **82**, 1225.
Chu, S., 1998, Rev. Mod. Phys. **70**, 685.
Chu, S., 2002, Nature (London) **416**, 206.
Chwedeńczuk, J., P. Ziń, M. Trippenbach, A. Perrin, V. Leung, D. Boiron, and C. I. Westbrook, 2008, Phys. Rev. A **78**, 053605.
Cocks, D. G., and I. B. Whittingham, 2009, Phys. Rev. A **80**, 023417.
Cocks, D. G., and I. B. Whittingham, 2010, Phys. Rev. A **81**, 033406.
Cocks, D. G., I. B. Whittingham, and G. Peach, 2010, J. Phys. B **43**, 135102.
Cohen-Tannoudji, C. N., 1998, Rev. Mod. Phys. **70**, 707.
Consolino, L., G. Giusfredi, P. De Natale, M. Inguscio, and P. Cancio, 2011, Opt. Express **19**, 3155.
Cornell, E. A., and C. E. Wieman, 2002, Rev. Mod. Phys. **74**, 875.
Couvert, A., M. Jeppesen, T. Kawalec, G. Reinaudi, R. Mathevet, and D. Guéry-Odelin, 2008, Europhys. Lett. **83**, 50 001.
Cronin, A. D., J. Schmiedmayer, and D. E. Pritchard, 2009, Rev. Mod. Phys. **81**, 1051.
Dalfovo, F., S. Giorgini, L. P. Pitaevskii, and S. Stringari, 1999, Rev. Mod. Phys. **71**, 463.
Dalibard, J., and C. Cohen-Tannoudji, 1985, J. Opt. Soc. Am. B **2**, 1707.
Dall, R. G., S. S. Hodgman, A. G. Manning, M. T. Johnsson, K. G. H. Baldwin, and A. G. Truscott, 2011, Nature Commun. **2**, 291.
Dall, R. G., S. S. Hodgman, A. G. Manning, and A. G. Truscott, 2011, Opt. Lett. **36**, 1131.
Dall, R., and A. Truscott, 2007, Opt. Commun. **270**, 255.
Dall, R. G., K. G. H. Baldwin, L. J. Byron, and A. G. Truscott, 2008, Phys. Rev. Lett. **100**, 023001.
Dall, R. G., L. J. Byron, A. G. Truscott, G. R. Dennis, M. T. Johnsson, and J. J. Hope, 2009, Phys. Rev. A **79**, 011601.
Dall, R. G., L. J. Byron, A. G. Truscott, G. R. Dennis, M. T. Johnsson, M. Jeppesen, and J. J. Hope, 2007, Opt. Express **15**, 17673.
Dall, R. G., C. J. Dedman, and A. G. Truscott, 2008, Opt. Express **16**, 14716.
Dall, R. G., S. S. Hodgman, M. T. Johnsson, K. G. H. Baldwin, and A. G. Truscott, 2010, Phys. Rev. A **81**, 011602.
Davis, K. B., M. O. Mewes, M. R. Andrews, N. J. van Druten, D. S. Durfee, D. M. Kurn, and W. Ketterle, 1995, Phys. Rev. Lett. **75**, 3969.
Dedman, C. J., J. Nes, T. M. Hanna, R. G. Dall, K. G. H. Baldwin, and A. G. Truscott, 2004, Rev. Sci. Instrum. **75**, 5136.
DeMarco, B., and D. Jin, 1999, Science **285**, 1703.
Deng, L., E. Hagley, J. Wen, M. Trippenbach, Y. Band, P. Julienne, J. Simsarian, K. Helmerson, S. Rolston, and W. Phillips, 1999, Nature (London) **398**, 218.
Derevianko, A., and W. R. Johnson, 1997, Phys. Rev. A **56**, 1288.
Derevianko, A., and H. Katori, 2011, Rev. Mod. Phys. **83**, 331.
Deuar, P., and P. D. Drummond, 2007, Phys. Rev. Lett. **98**, 120402.
Dickinson, A. S., F. X. Gadea, and T. Leininger, 2004, J. Phys. B **37**, 587.
D'Incao, J. P., and B. D. Esry, 2006, Phys. Rev. A **73**, 030703.
Doery, M. R., E. J. D. Vredenbregt, S. S. Op de Beek, H. C. W. Beijerinck, and B. J. Verhaar, 1998, Phys. Rev. A **58**, 3673.
Doret, S. C., C. B. Connolly, W. Ketterle, and J. M. Doyle, 2009, Phys. Rev. Lett. **103**, 103005.
Döring, D., N. P. Robins, C. Figl, and J. D. Close, 2008, Opt. Express **16**, 13893.
Dorrer, C., F. Nez, B. de Beauvoir, L. Julien, and F. Biraben, 1997, Phys. Rev. Lett. **78**, 3658.
Dowling, J. P., 1998, Phys. Rev. A **57**, 4736.
Doyle, J. M., B. Friedrich, J. Kim, and D. Patterson, 1995, Phys. Rev. A **52**, R2515.
Drake, G. W. F., 1969, Astrophys. J. **158**, 1199.
Drake, G. W. F., 1971, Phys. Rev. A **3**, 908.
Drake, G. W. F., 2002, Can. J. Phys. **80**, 1195.
Drever, R. W. P., J. L. Hall, F. Kowalski, G. Hough, J. Ford, A. Munley, and H. Ward, 1983, Appl. Phys. B **31**, 97.
Duan, L.-M., A. Sørensen, J. I. Cirac, and P. Zoller, 2000, Phys. Rev. Lett. **85**, 3991.
Eyler, E., D. Chieda, M. Stowe, M. Thorpe, T. Schibli, and J. Ye, 2008, Eur. Phys. J. D **48**, 43.
Faulstich, A., A. Schnetz, M. Sigel, T. Sleator, O. Carnal, V. Balykin, H. Takuma, and J. Mlynek, 1992, Europhys. Lett. **17**, 393.
Fedichev, P. O., M. W. Reynolds, U. M. Rahmanov, and G. V. Shlyapnikov, 1996a, Phys. Rev. A **53**, 1447.
Fedichev, P. O., M. W. Reynolds, and G. V. Shlyapnikov, 1996b, Phys. Rev. Lett. **77**, 2921.
Feldker, T., J. Schütz, H. John, and G. Birkl, 2011, Eur. Phys. J. D **65**, 257.
Ferlaino, F., and R. Grimm, 2010, Physics **3**, 9.
Fölling, S., F. Gerbier, A. Widera, O. Mandel, T. Gerike, and I. Bloch, 2005, Nature (London) **434**, 481.
Frieze, W., E. Hinds, V. Hughes, and F. Pichanick, 1981, Phys. Rev. A **24**, 279.
Fujita, J., S. Mitake, and F. Shimizu, 2000, Phys. Rev. Lett. **84**, 4027.
Gallagher, A., and D. E. Pritchard, 1989, Phys. Rev. Lett. **63**, 957.
Gardiner, C. W., P. Zoller, R. J. Ballagh, and M. J. Davis, 1997, Phys. Rev. Lett. **79**, 1793.

Gattobigio, G. L., A. Couvert, M. Jeppesen, R. Mathevet, and D. Guéry-Odelin, 2009, Phys. Rev. A **80**, 041605.
Gay, T. J., 1996, *Sources of Metastable Atoms and Molecules*, Experimental Methods in the Physical Sciences: Atomic, Molecular and Optical Physics: Atoms and Molecules Vol. 29B (Academic Press, New York), p. 95.
Gemelke, N., E. Sarajlic, Y. Bidel, S. Hong, and S. Chu, 2005, Phys. Rev. Lett. **95**, 170404.
George, M. C., L. Lombardi, and E. Hessels, 2001, Phys. Rev. Lett. **87**, 173002.
Gerginov, V., K. Calkins, C. Tanner, J. McFerran, S. Diddams, A. Bartels, and L. Holberg, 2006, Phys. Rev. A **73**, 032504.
Giovannetti, V., S. Lloyd, and L. Maccone, 2004, Science **306**, 1330.
Giovannetti, V., S. Lloyd, and L. Maccone, 2011, Nature Photon. **5**, 222.
Giusfredi, G., P. De Natale, D. Mazzotti, P. Cancio Pastor, C. de Mauro, L. Fallani, G. Hagel, V. Krachmalnicoff, and M. Inguscio, 2005, Can. J. Phys. **83**, 301.
Glauber, R. J., 1963, Phys. Rev. **130**, 2529.
Glauber, R. J., 1965, in *Quantum Optics and Electronics*, edited by C. de Witt, A. Blandin, and C. Cohen-Tannoudji (Gordon and Breach, New York).
Glauber, R. J., 2006, Rev. Mod. Phys. **78**, 1267.
Gomes, J. V., A. Perrin, M. Schellekens, D. Boiron, C. I. Westbrook, and M. Belsley, 2006, Phys. Rev. A **74**, 053607.
Goosen, M. R., T. G. Tiecke, W. Vassen, and S. J. J. M. F. Kokkelmans, 2010, Phys. Rev. A **82**, 042713.
Greiner, M., O. Mandel, T. Esslinger, T. W. Hänsch, and I. Bloch, 2002, Nature (London) **415**, 39.
Greiner, M., C. A. Regal, and D. S. Jin, 2003, Nature (London) **426**, 537.
Greiner, M., C. A. Regal, J. T. Stewart, and D. S. Jin, 2005, Phys. Rev. Lett. **94**, 110401.
Griffin, A., W.-C. Wu, and S. Stringari, 1997, Phys. Rev. Lett. **78**, 1838.
Grimm, R., M. Weidemuller, and Y. B. Ovchinnikov, 2000, Adv. At. Mol. Opt. Phys. **42**, 95.
Grondalski, J., P. M. Alsing, and I. H. Deutsch, 1999, Opt. Express **5**, 249.
Guerin, W., J.-F. Riou, J. P. Gaebler, V. Josse, P. Bouyer, and A. Aspect, 2006, Phys. Rev. Lett. **97**, 200402.
Guéry-Odelin, D., F. Zambelli, J. Dalibard, and S. Stringari, 1999, Phys. Rev. A **60**, 4851.
Hack, J., L. Liu, M. Olshanii, and H. Metcalf, 2000, Phys. Rev. A **62**, 013405.
Halliwell, X. W., H. Friedrich, S. T. Gibson, and K. G. H. Baldwin, 2003, Opt. Commun. **224**, 89.
Hanbury Brown, R., and R. Q. Twiss, 1956, Nature (London) **177**, 27.
Hanneke, D., S. Fogwell, and G. Gabrielse, 2008, Phys. Rev. Lett. **100**, 120801.
Harada, Y., S. Masuda, and H. Ozaki, 1997, Chem. Rev. **97**, 1897.
Heidmann, A., R. J. Horowicz, S. Reynaud, E. Giacobino, C. Fabre, and G. Camy, 1987, Phys. Rev. Lett. **59**, 2555.
Herschbach, N., 2003, "Trapped Triplet Helium Atoms: Inelastic Collisions and Evaporative Cooling," Ph.D. thesis, Vrije Universiteit Amsterdam, The Netherlands.
Herschbach, N., P. Tol, A. Tychkov, W. Hogervorst, and W. Vassen, 2003, J. Opt. B **5**, S65.
Herschbach, N., P. J. J. Tol, W. Hogervorst, and W. Vassen, 2000a, Phys. Rev. A **61**, 050702(R).
Herschbach, N., P. J. J. Tol, W. Vassen, W. Hogervorst, G. Woestenenk, J. W. Thomsen, P. van der Straten, and A. Niehaus, 2000b, Phys. Rev. Lett. **84**, 1874.
Hess, H. F., 1986, Phys. Rev. B **34**, 3476.
Hill, J. C., L. L. Hatfield, N. D. Stockwell, and G. K. Walters, 1972, Phys. Rev. A **5**, 189.
Hilligsøe, K. M., and K. Mølmer, 2005, Phys. Rev. A **71**, 041602.
Hodgman, S. S., R. G. Dall, K. G. H. Baldwin, and A. G. Truscott, 2009a, Phys. Rev. A **80**, 044501.
Hodgman, S. S., R. G. Dall, L. J. Byron, K. G. H. Baldwin, S. J. Buckman, and A. G. Truscott, 2009b, Phys. Rev. Lett. **103**, 053002.
Hodgman, S. S., R. G. Dall, A. G. Manning, K. G. H. Baldwin, and A. G. Truscott, 2011, Science **331**, 1046.
Hong, C. K., Z. Y. Ou, and L. Mandel, 1987, Phys. Rev. Lett. **59**, 2044.
Hoogerland, M. D., J. P. J. Driessen, E. J. D. Vredenbregt, H. J. L. Megens, M. P. Schuwer, H. C. W. Beijerinck, and K. A. H. van Leeuwen, 1996, Appl. Phys. B **62**, 323.
Hoogerland, M. D., D. Milic, W. Lu, H.-A. Bachor, K. G. H. Baldwin, and S. J. Buckman, 1996, Aust. J. Phys. **49**, 567.
Hotop, H., 1996, *Detection of Metastable Atoms and Molecules*, Experimental Methods in the Physical Sciences: Atomic, Molecular and Optical Physics: Atoms and Molecules Vol. 29B (Academic Press, New York), p. 191.
Hughes, V. W., 1969, Comments At. Mol. Phys. **1**, 5.
Indelicato, P., J. Desclaux, and Y.-K. Kim, 1994 (unpublished), cited in M. Walhout*et al.*, Phys. Rev. Lett. **72**, 2843 (1994).
Jagutzki, O., V. Mergel, K. Ullmann-Pfleger, L. Spielberger, U. Spillmann, R. Dörner, and H. Schmidt-Böking, 2002, Nucl. Instrum. Methods Phys. Res., Sect. A **477**, 244.
Jaskula, J.-C., M. Bonneau, G. B. Partridge, V. Krachmalnicoff, P. Deuar, K. V. Kheruntsyan, A. Aspect, D. Boiron, and C. I. Westbrook, 2010, Phys. Rev. Lett. **105**, 190402.
Jeltes, T., *et al.*, 2007, Nature (London) **445**, 402.
Jessen, P. S., and I. H. Deutsch, 1996, Adv. At. Mol. Opt. Phys. **37**, 95.
Jochim, S., M. Bartenstein, A. Altmeyer, G. Hendl, S. Riedl, C. Chin, J. H. Denschlag, and R. Grimm, 2003, Science **302**, 2101.
Johnson, W., J. Plante, and D. R. Sapirstein, 1995, Adv. At. Mol. Opt. Phys. **35**, 255.
Jones, K. M., E. Tiesinga, P. D. Lett, and P. S. Julienne, 2006, Rev. Mod. Phys. **78**, 483.
Julienne, P. S., and F. H. Mies, 1989, J. Opt. Soc. Am. B **6**, 2257.
Jung, R., S. Gerlach, R. Schumann, G. von Oppen, and U. Eichmann, 2003, Eur. Phys. J. D **23**, 415.
Kagan, Y., B. V. Svistunov, and G. V. Shlyapnikov, 1985, JETP Lett. **42**, 209.
Katori, H., H. Kunugita, and T. Ido, 1995, Phys. Rev. A **52**, R4324.
Katori, H., and F. Shimizu, 1993, Phys. Rev. Lett. **70**, 3545.
Katori, H., and F. Shimizu, 1994, Phys. Rev. Lett. **73**, 2555.
Kawanaka, J., M. Hagiuda, K. Shimizu, F. Shimizu, and H. Takuma, 1993, Appl. Phys. B **56**, 21.
Ketterle, W., 2002, Rev. Mod. Phys. **74**, 1131.
Ketterle, W., D. Durfee, and D. Stamper-Kurn, 1999, in *Bose-Einstein Condensation in Atomic Gases*, Proceedings of the International School of Physics Enrico Fermi, Course CXL, edited by M. Inguscio, S. Stringari, and C. E. Wieman (IOS Press, Amsterdam), p. 67.
Ketterle, W., and N. J. van Druten, 1996, Adv. At. Mol. Opt. Phys. **37**, 181.
Kheruntsyan, K. V., and P. D. Drummond, 2002, Phys. Rev. A **66**, 031602.
Killian, T., and S. Rolston, 2010, Phys. Today **63**, 46.
Kim, J., U. Rapol, S. Moal, J. Leonard, M. Walhout, and M. Leduc, 2004, Eur. Phys. J. D **31**, 227.

Klein, A., B. Brown, U. Georg, M. Keim, P. Lievens, R. Neugart, M. Neuroth, R. Silverans, and L. Vermeeren, 1996, Nucl. Phys. **A607**, 1.
Knoop, S., 2011 (private communication).
Knoop, S., F. Ferlaino, M. Mark, M. Berninger, H. Schobel, H.-C. Nagerl, and R. Grimm, 2009, Nature Phys. **5**, 227.
Koelemeij, J. C. J., and M. Leduc, 2004, Eur. Phys. J. D **31**, 263.
Koelemeij, J. C. J., R. J. W. Stas, W. Hogervorst, and W. Vassen, 2003, Phys. Rev. A **67**, 053406.
Koelemeij, J. C. J., A. S. Tychkov, T. Jeltes, W. Hogervorst, and W. Vassen, 2004, J. Phys. B **37**, 3501.
Köhler, T., K. Góral, and P. S. Julienne, 2006, Rev. Mod. Phys. **78**, 1311.
Koolen, A. E. A., G. T. Jansen, K. F. E. M. Domen, H. C. W. Beijerinck, and K. A. H. van Leeuwen, 2002, Phys. Rev. A **65**, 041601.
Krachmalnicoff, V., 2009, "Two Experiments on Quantum Correlations in Gases of Metastable Helium: Fermion Antibunching and a Study of Boson Pair Correlations in the Collision of Two Condensates," Ph.D. thesis, Université de Paris-Sud.
Krachmalnicoff, V., *et al.*, 2010, Phys. Rev. Lett. **104**, 150402.
Kraemer, T., *et al.*, 2006, Nature (London) **440**, 315.
Kumakura, M., and N. Morita, 1992, Jpn. J. Appl. Phys. **31**, L276.
Kumakura, M., and N. Morita, 1999, Phys. Rev. Lett. **82**, 2848.
Kunugita, H., T. Ido, and F. Shimizu, 1997, Phys. Rev. Lett. **79**, 621.
Kuppens, S. J. M., J. G. C. Tempelaars, V. P. Mogendorff, B. J. Claessens, H. C. W. Beijerinck, and E. J. D. Vredenbregt, 2002, Phys. Rev. A **65**, 023410.
Labeyrie, G., A. Browaeys, W. Rooijakkers, D. Voelker, J. Grosperrin, B. Wanner, C. I. Westbrook, and A. Aspect, 1999, Eur. Phys. J. D **7**, 341.
Łach, G., and K. Pachucki, 2001, Phys. Rev. A **64**, 042510.
Lapington, J., 2004, Nucl. Instrum. Methods Phys. Res., Sect. A **525**, 361.
Lawall, J., F. Bardou, B. Saubamea, K. Shimizu, M. Leduc, A. Aspect, and C. Cohen-Tannoudji, 1994, Phys. Rev. Lett. **73**, 1915.
Lawall, J., S. Kulin, B. Saubamea, N. Bigelow, M. Leduc, and C. Cohen-Tannoudji, 1995, Phys. Rev. Lett. **75**, 4194.
Lawall, J., C. Orzel, and S. L. Rolston, 1998, Phys. Rev. Lett. **80**, 480.
Lawall, J., and M. Prentiss, 1994, Phys. Rev. Lett. **72**, 993.
Leduc, M., J. Leonard, F. dos Santos, E. Jahier, S. Schwartz, and C. Cohen-Tannoudji, 2002, Acta Phys. Pol. B **33**, 2213.
Lefers, J., N. Miller, D. Rupke, D. Tong, and M. Walhout, 2002, Phys. Rev. A **66**, 012507.
Lemonde, P., 2009, Eur. Phys. J. Special Topics **172**, 81.
Leo, P. J., V. Venturi, I. B. Whittingham, and J. F. Babb, 2001, Phys. Rev. A **64**, 042710.
Léonard, J., A. P. Mosk, M. Walhout, P. van der Straten, M. Leduc, and C. Cohen-Tannoudji, 2004, Phys. Rev. A **69**, 032702.
Léonard, J., M. Walhout, A. P. Mosk, T. Müller, M. Leduc, and C. Cohen-Tannoudji, 2003, Phys. Rev. Lett. **91**, 073203.
Lindquist, K., M. Stephens, and C. Wieman, 1992, Phys. Rev. A **46**, 4082.
Loudon, R., 2000, *The Quantum Theory of Light* (Oxford University Press, Oxford, England), 3rd ed.
Lu, W., M. D. Hoogerland, D. Milic, K. G. H. Baldwin, and S. J. Buckman, 2001, Rev. Sci. Instrum. **72**, 2558.
Luiten, O. J., M. W. Reynolds, and J. T. M. Walraven, 1996, Phys. Rev. A **53**, 381.
Maddaloni, P., P. Cancio, and P. De Natale, 2009, Meas. Sci. Technol. **20**, 052001.
Manning, A. G., S. S. Hodgman, R. G. Dall, M. T. Johnsson, and A. G. Truscott, 2010, Opt. Express **18**, 18712.
Marani, R., L. Cognet, V. Savalli, N. Westbrook, C. I. Westbrook, and A. Aspect, 2000, Phys. Rev. A **61**, 053402.
Marin, F., F. Minardi, F. S. Pavone, M. Inguscio, and G. W. F. Drake, 1995, Z. Phys. D **32**, 285.
Mastwijk, H. C., J. W. Thomsen, P. van der Straten, and A. Niehaus, 1998, Phys. Rev. Lett. **80**, 5516.
McNamara, J. M., T. Jeltes, A. S. Tychkov, W. Hogervorst, and W. Vassen, 2006, Phys. Rev. Lett. **97**, 080404.
McNamara, J. M., R. J. W. Stas, W. Hogervorst, and W. Vassen, 2007, Phys. Rev. A **75**, 062715.
Metcalf, H., 1989, J. Opt. Soc. Am. B **6**, 2206.
Metcalf, H. J., and P. van der Straten, 1999, *Laser Cooling and Trapping* (Springer, New York).
Mewes, M.-O., M. R. Andrews, D. M. Kurn, D. S. Durfee, C. G. Townsend, and W. Ketterle, 1997, Phys. Rev. Lett. **78**, 582.
Mewes, M.-O., M. R. Andrews, N. J. van Druten, D. M. Kurn, D. S. Durfee, and W. Ketterle, 1996, Phys. Rev. Lett. **77**, 416.
Milic, D., M. D. Hoogerland, K. G. H. Baldwin, and S. J. Buckman, 2001, Appl. Opt. **40**, 1907.
Minardi, F., G. Bianchini, P. Cancio Pastor, G. Giusfredi, F. Pavone, and M. Inguscio, 1999, Phys. Rev. Lett. **82**, 1112.
Moal, S., M. Portier, J. Kim, E. Arimondo, and M. Leduc, 2008, Europhys. Lett. **83**, 23 001.
Moal, S., M. Portier, J. Kim, J. Dugué, U. D. Rapol, M. Leduc, and C. Cohen-Tannoudji, 2006, Phys. Rev. Lett. **96**, 023203.
Mohr, P. J., B. N. Taylor, and D. B. Newell, 2008, Rev. Mod. Phys. **80**, 633.
Mølmer, K., A. Perrin, V. Krachmalnicoff, V. Leung, D. Boiron, A. Aspect, and C. I. Westbrook, 2008, Phys. Rev. A **77**, 033601.
Moos, H. W., and J. R. Woodworth, 1973, Phys. Rev. Lett. **30**, 775.
Morinaga, M., M. Yasuda, T. Kishimoto, F. Shimizu, J.-i. Fujita, and S. Matsui, 1996, Phys. Rev. Lett. **77**, 802.
Morita, N., and M. Kumakura, 1991, Jpn. J. Appl. Phys. **30**, L1678.
Morton, D. C., Q. X. Wu, and G. W. F. Drake, 2006a, Can. J. Phys. **84**, 83.
Morton, D., Q. Wu, and G. Drake, 2006b, Phys. Rev. A **73**, 034502.
Morton, D. C., and G. Drake, 2011, Phys. Rev. A **83**, 042503.
Mueller, P., *et al.*, 2007, Phys. Rev. Lett. **99**, 252501.
Mueller, P., L. B. Wang, G. W. F. Drake, K. Bailey, Z. T. Lu, and T. P. OConner, 2005, Phys. Rev. Lett. **94**, 133001.
Müller, M. W., A. Merz, M. W. Ruf, H. Hotop, W. Meyer, and M. Movre, 1991, Z. Phys. D **21**, 89.
Naidon, P., and F. Masnou-Seeuws, 2006, Phys. Rev. A **73**, 043611.
Naraschewski, M., and R. J. Glauber, 1999, Phys. Rev. A **59**, 4595.
Nguyen, S. V., S. C. Doret, C. B. Connolly, R. A. Michniak, W. Ketterle, and J. M. Doyle, 2005, Phys. Rev. A **72**, 060703.
Norrie, A. A., R. J. Ballagh, and C. W. Gardiner, 2006, Phys. Rev. A **73**, 043617.
Nowak, S., A. Browaeys, J. Poupard, A. Robert, D. Boiron, C. I. Westbrook, and A. Aspect, 2000, Appl. Phys. B **70**, 455.
Oberst, H., Y. Tashiro, K. Shimizu, and F. Shimizu, 2005, Phys. Rev. A **71**, 052901.
Opatrný, T., and G. Kurizki, 2001, Phys. Rev. Lett. **86**, 3180.
Orzel, C., S. D. Bergeson, S. Kulin, and S. L. Rolston, 1998, Phys. Rev. Lett. **80**, 5093.
Orzel, C., M. Walhout, U. Sterr, P. S. Julienne, and S. L. Rolston, 1999, Phys. Rev. A **59**, 1926.
Ou, Z. Y., and L. Mandel, 1988, Phys. Rev. Lett. **61**, 50.
Pachucki, K., and V. A. Yerokhin, 2009, Phys. Rev. A **79**, 062516.
Pachucki, K., and V. A. Yerokhin, 2010, Phys. Rev. Lett. **104**, 070403.

Palmer, A. J., M. Baker, and R. T. Sang, 2004, Rev. Sci. Instrum. **75**, 5056.
Partlow, M., X. Miao, J. Bochmann, M. Cashen, and H. Metcalf, 2004, Phys. Rev. Lett. **93**, 213004.
Partridge, G. B., J.-C. Jaskula, M. Bonneau, D. Boiron, and C. I. Westbrook, 2010, Phys. Rev. A **81**, 053631.
Pavone, F., F. Marin, P. De Natale, M. Inguscio, and F. Biraben, 1994, Phys. Rev. Lett. **73**, 42.
Pereira Dos Santos, F., J. Léonard, J. Wang, C. J. Barrelet, F. Perales, E. Rasel, C. S. Unnikrishnan, M. Leduc, and C. Cohen-Tannoudji, 2001, Phys. Rev. Lett. **86**, 3459.
Pereira Dos Santos, F., F. Perales, J. Léonard, A. Sinatra, J. M. Wang, F. S. Pavone, E. Rasel, C. S. Unnikrishnan, and M. Leduc, 2001, Eur. Phys. J. D **14**, 15.
Perrin, A., 2007, ''Observation de paires d'atomes corrélés au travers de la collision de deux condensats de Bose-Einstein,'' Ph.D. thesis, Université Paris et Marie Curie.
Perrin, A., H. Chang, V. Krachmalnicoff, M. Schellekens, D. Boiron, A. Aspect, and C. I. Westbrook, 2007, Phys. Rev. Lett. **99**, 150405.
Perrin, A., C. M. Savage, D. Boiron, V. Krachmalnicoff, C. I. Westbrook, and K. Kheruntsyan, 2008, New J. Phys. **10**, 045021.
Pethick, C. J., and H. Smith, 2002, *Bose-Einstein Condensation in Dilute Gases* (Cambridge University Press, Cambridge, England).
Phillips, W. D., 1998, Rev. Mod. Phys. **70**, 721.
Phillips, W. D., and H. Metcalf, 1982, Phys. Rev. Lett. **48**, 596.
Pieksma, M., M. Čížek, J. W. Thomsen, P. van der Straten, and A. Niehaus, 2002, Phys. Rev. A **66**, 022703.
Pieper, S. C., and R. B. Wiringa, 2001, Annu. Rev. Nucl. Part. Sci. **51**, 53.
Portier, M., S. Moal, J. Kim, M. Leduc, C. Cohen-Tannoudji, and O. Dulieu, 2006, J. Phys. B **39**, S881.
Poupard, J., 2000, ''Mesure de deux caracteristiques de l'helium metastable importantes pour le refroidissement radiatif,'' Ph.D. thesis, Université Paris-Sud.
Przybytek, M., 2008, ''Correlation, Relativistic, and Adiabatic Effects in the Interaction of Metastable Helium Atoms,'' Ph.D. thesis, University of Warsaw, Poland.
Przybytek, M., and B. Jeziorski, 2005, J. Chem. Phys. **123**, 134315.
Pu, H., and P. Meystre, 2000, Phys. Rev. Lett. **85**, 3987.
Raab, E. L., M. Prentiss, A. Cable, S. Chu, and D. E. Pritchard, 1987, Phys. Rev. Lett. **59**, 2631.
Rarity, J. G., and P. R. Tapster, 1990, Phys. Rev. Lett. **64**, 2495.
Rasel, E., F. Pereira Dos Santos, F. Saverio Pavone, F. Perales, C. Unnikrishnan, and M. Leduc, 1999, Eur. Phys. J. D **7**, 311.
Rasel, E. M., M. K. Oberthaler, H. Batelaan, J. Schmiedmayer, and A. Zeilinger, 1995, Phys. Rev. Lett. **75**, 2633.
Rauner, M., S. Kuppens, M. Schiffer, G. Birkl, K. Sengstock, and W. Ertmer, 1998, Phys. Rev. A **58**, R42.
Reid, M. D., P. D. Drummond, W. P. Bowen, E. G. Cavalcanti, P. K. Lam, H. A. Bachor, U. L. Andersen, and G. Leuchs, 2009, Rev. Mod. Phys. **81**, 1727.
Robert, A., 2001, ''Réalisation d'un condensat de Bose-Einstein d'Hélium métastable,'' Ph.D. thesis, Université Paris-Sud.
Robert, A., O. Sirjean, A. Browaeys, J. Poupard, S. Nowak, D. Boiron, C. I. Westbrook, and A. Aspect, 2001, Science **292**, 461.
Rom, T., T. Best, D. van Oosten, U. Schneider, S. Fölling, B. Paredes, and I. Bloch, 2006, Nature (London) **444**, 733.
Rooijakkers, W., W. Hogervorst, and W. Vassen, 1995, Phys. Rev. Lett. **74**, 3348.
Rooijakkers, W., W. Hogervorst, and W. Vassen, 1996, Opt. Commun. **123**, 321.
Rooijakkers, W., W. Hogervorst, and W. Vassen, 1997a, Phys. Rev. A **56**, 3083.
Rooijakkers, W., W. Hogervorst, and W. Vassen, 1997b, Opt. Commun. **135**, 149.
RuGway, Wu, S. S. Hodgman, R. G. Dall, M. T. Johnsson, and A. G. Truscott, 2011, Phys. Rev. Lett. **107**, 075301.
Samson, J. A. R., and D. Ederer, 2000, ''Experimental Methods in the Physical Sciences: Vacuum Ultraviolet Spectroscopy ii.''
Savage, C. M., P. E. Schwenn, and K. V. Kheruntsyan, 2006, Phys. Rev. A **74**, 033620.
Schellekens, M., 2007, ''The Hanbury Brown and Twiss Effect for Cold Atoms'', Ph.D. thesis, Université Paris-Sud.
Schellekens, M., R. Hoppeler, A. Perrin, J. Viana Gomes, D. Boiron, A. Aspect, and C. I. Westbrook, 2005, Science **310**, 648.
Schiffer, M., M. Christ, G. Wokurka, and W. Ertmer, 1997, Opt. Commun. **134**, 423.
Schmidt, P. O., S. Hensler, J. Werner, T. Binhammer, A. Görlitz, T. Pfau, and A. Simoni, 2003, J. Opt. Soc. Am. B **20**, 960.
Scholz, A., M. Christ, D. Doll, J. Ludwig, and W. Ertmer, 1994, Opt. Commun. **111**, 155.
Schreck, F., L. Khaykovich, K. L. Corwin, G. Ferrari, T. Bourdel, J. Cubizolles, and C. Salomon, 2001, Phys. Rev. Lett. **87**, 080403.
Schumann, R., C. Schubert, U. Eichmann, R. Jung, and G. von Oppen, 1999, Phys. Rev. A **59**, 2120.
Schütz, J., T. Feldker, H. John, and G. Birkl, 2011 (unpublished).
Scully, M. O., and M. S. Zubairy, 1997, *Quantum Optics* (Cambridge University Press, Cambridge, England).
Seidelin, S., J. V. Gomes, R. Hoppeler, O. Sirjean, D. Boiron, A. Aspect, and C. I. Westbrook, 2004, Phys. Rev. Lett. **93**, 090409.
Seidelin, S., O. Sirjean, J. V. Gomes, D. Boiron, C. I. Westbrook, and A. Aspect, 2003, J. Opt. B **5**, S112.
Shih, Y. H., and C. O. Alley, 1988, Phys. Rev. Lett. **61**, 2921.
Shimizu, F., 2001, Phys. Rev. Lett. **86**, 987.
Shimizu, F., and J. Fujita, 2002a, J. Phys. Soc. Jpn. **71**, 5.
Shimizu, F., and J.-i. Fujita, 2002b, Phys. Rev. Lett. **88**, 123201.
Shimizu, F., K. Shimizu, and H. Takuma, 1987, Jpn. J. Appl. Phys. **26**, L1847.
Shimizu, F., K. Shimizu, and H. Takuma, 1989, Phys. Rev. A **39**, 2758.
Shimizu, F., K. Shimizu, and H. Takuma, 1990, Chem. Phys. **145**, 327.
Shimizu, F., K. Shimizu, and H. Takuma, 1991, Opt. Lett. **16**, 339.
Shimizu, F., K. Shimizu, and H. Takuma, 1992, Phys. Rev. A **46**, R17.
Shiner, D., R. Dixson, and V. Vedantham, 1995, Phys. Rev. Lett. **74**, 3553.
Shiner, D., R. Dixson, and P. Zhao, 1994, Phys. Rev. Lett. **72**, 1802.
Shlyapnikov, G. V., J. T. M. Walraven, U. M. Rahmanov, and M. W. Reynolds, 1994, Phys. Rev. Lett. **73**, 3247.
Sick, I., 2008, Phys. Rev. C **77**, 041302.
Sirjean, O., S. Seidelin, J. V. Gomes, D. Boiron, C. I. Westbrook, A. Aspect, and G. V. Shlyapnikov, 2002, Phys. Rev. Lett. **89**, 220406.
Siska, P., 1993, Rev. Mod. Phys. **65**, 337.
Small-Warren, N. E., and L.-Y. C. Chiu, 1975, Phys. Rev. A **11**, 1777.
Smiciklas, M., and D. Shiner, 2010, Phys. Rev. Lett. **105**, 123001.
Söding, J., D. Guery-Odelin, P. Desbiolles, F. Chevy, H. Inamori, and J. Dalibard, 1999, Appl. Phys. B **69**, 257.
Spoden, P., M. Zinner, N. Herschbach, W. J. van Drunen, W. Ertmer, and G. Birkl, 2005, Phys. Rev. Lett. **94**, 223201.
Stamper-Kurn, D. M., H.-J. Miesner, S. Inouye, M. R. Andrews, and W. Ketterle, 1998, Phys. Rev. Lett. **81**, 500.
Stärck, J., and W. Meyer, 1994, Chem. Phys. Lett. **225**, 229.
Stas, R. J. W., J. M. McNamara, W. Hogervorst, and W. Vassen, 2004, Phys. Rev. Lett. **93**, 053001.

Stas, R. J. W., J. M. McNamara, W. Hogervorst, and W. Vassen, 2006, Phys. Rev. A **73**, 032713.
Stenger, J., S. Inouye, A. P. Chikkatur, D. M. Stamper-Kurn, D. E. Pritchard, and W. Ketterle, 1999, Phys. Rev. Lett. **82**, 4569.
Storry, C., M. C. George, and E. Hessels, 2000, Phys. Rev. Lett. **84**, 3274
Stringari, S., and L. Pitaevskii, 2003, *Bose-Einstein Condensation* (Oxford University Press, London, England).
Sukenik, C. I., and H. C. Busch, 2002, Phys. Rev. A **66**, 051402.
Suominen, K.-A., K. Burnett, P. S. Julienne, M. Walhout, U. Sterr, C. Orzel, M. Hoogerland, and S. L. Rolston, 1996, Phys. Rev. A **53**, 1678.
Swansson, J. A., K. G. H. Baldwin, M. D. Hoogerland, A. G. Truscott, and S. J. Buckman, 2004, Appl. Phys. B **79**, 485.
Swansson, J. A., R. G. Dall, and A. G. Truscott, 2006, Rev. Sci. Instrum. **77**, 046103.
Swansson, J. A., R. G. Dall, and A. G. Truscott, 2007, Appl. Phys. B **86**, 485.
Tachiev, G., and C. Froese Fischer, 2002, ''Method: MCHF (energy adjusted), http://nlte.nist.gov/MCHF/index.html.
Tang, H. Y. S., and W. Happer, 1972, Bull. Am. Phys. Soc. **17**, 476.
Tempelaars, J., R. Stas, P. Sebel, H. Beijerinck, and E. Vredenbregt, 2002, Eur. Phys. J. D **18**, 113.
Tol, P., 2005, ''Trapping and Evaporative Cooling of Metastable Helium'', Ph.D. thesis, VU University, Amsterdam.
Tol, P. J. J., N. Herschbach, E. A. Hessels, W. Hogervorst, and W. Vassen, 1999, Phys. Rev. A **60**, R761.
Tol, P. J. J., W. Hogervorst, and W. Vassen, 2004, Phys. Rev. A **70**, 013404.
Townsend, C. G., N. H. Edwards, C. J. Cooper, K. P. Zetie, C. J. Foot, A. M. Steane, P. Szriftgiser, H. Perrin, and J. Dalibard, 1995, Phys. Rev. A **52**, 1423.
Truscott, A., K. Strecker, W. McAlexander, G. Partridge, and R. Hulet, 2001, Science **291**, 2570.
Tychkov, A., 2008, ''Bose-Einstein Condensation of Metastable Helium Atoms,'' Ph.D. thesis, VU University, Amsterdam.
Tychkov, A. S., J. M. Jeltes, J. M. McNamara, P. J. J. Tol, N. Herschbach, W. Hogervorst, and W. Vassen, 2006, Phys. Rev. A **73**, 031603(R).
Tychkov, A. S., J. C. J. Koelemeij, T. Jeltes, W. Hogervorst, and W. Vassen, 2004, Phys. Rev. A **69**, 055401.
Uhlmann, L. J., R. Dall, A. G. Truscott, M. D. Hoogerland, K. G. H. Baldwin, and S. J. Buckman, 2005, Phys. Rev. Lett. **94**, 173201.
van der Stam, K. M. R., R. Meppelink, J. M. Vogels, and P. van der Straten, 2007, Phys. Rev. A **75**, 031602.
van der Zwan, E., D. van Oosten, D. Nehari, P. van der Straten, and H. Stoof, 2006, J. Phys. B **39**, S825.
van Drunen, W. J., 2008, ''Collisional Interactions Between Metastable Neon Atoms'', Ph.D. thesis, Technische Universität Darmstadt, Germany.
van Drunen, W. J., N. Herschbach, J. Schütz, and G. Birkl, 2011, unpublished.
Van Dyck, R. S., C. E. Johnson, and H. A. Shugart, 1971, Phys. Rev. A **4**, 1327.
van Leeuwen, K. A. H., and W. Vassen, 2006, Europhys. Lett. **76**, 409.
van Rooij, R., J. S. Borbely, J. Simonet, M. D. Hoogerland, K. S. E. Eikema, R. A. Rozendaal, and W. Vassen, 2011, Science **333**, 196.
Vansteenkiste, N., C. Gerz, R. Kaiser, L. Hollberg, C. Salomon, and A. Aspect, 1991, J. Phys. II (France) **1**, 1407.
Vassen, W., 1996, in *OSA TOPS Volume 7: Ultracold Atoms and BEC*, edited by K. Burnett (OSA, Washington, DC), p. 20.
Vassen, W., T. Jeltes, J. McNamara, and A. Tychkov, 2007, in *Ultracold Fermi Gases*, Proceedings of the International School of Physics ''Enrico Fermi,'' Course CLXIV, edited by M. Inguscio, W. Ketterle, and C. Salomon (IOS Press, Amsterdam), p. 817.
Venturi, V., and I. B. Whittingham, 2000, Phys. Rev. A **61**, 060703.
Venturi, V., I. B. Whittingham, P. J. Leo, and G. Peach, 1999, Phys. Rev. A **60**, 4635.
Vogels, J. M., K. Xu, and W. Ketterle, 2002, Phys. Rev. Lett. **89**, 020401.
Walhout, M., H. J. L. Megens, A. Witte, and S. L. Rolston, 1993, Phys. Rev. A **48**, R879.
Walhout, M., U. Sterr, C. Orzel, M. Hoogerland, and S. L. Rolston, 1995, Phys. Rev. Lett. **74**, 506.
Walhout, M., U. Sterr, A. Witte, and S. L. Rolston, 1995, Opt. Lett. **20**, 1192.
Walhout, M., A. Witte, and S. L. Rolston, 1994, Phys. Rev. Lett. **72**, 2843.
Walker, T., D. Sesko, and C. Wieman, 1990, Phys. Rev. Lett. **64**, 408.
Wang, L.-B., *et al.*, 2004, Phys. Rev. Lett. **93**, 142501.
Weiner, J., V. S. Bagnato, S. Zilio, and P. S. Julienne, 1999, Rev. Mod. Phys. **71**, 1.
Westbrook, C. I., and D. Boiron, 2009, in *Proceedings of Science, Quantum of Quasars Workshop*, edited by C. Foellmi (Trieste International School of Advanced Studies, Triest, Italy), Vol. PoS (QQ09), p. 005 [http://pos.sissa.it/archive/conferences/101/005/QQ09_005.pdf].
Westbrook, C. I., A. Robert, O. Sirjean, A. Browaeys, J. Poupard, D. Boiron, and A. Aspect, 2002, in *Laser Spectroscopy, Proceedings of the XV International Conference*, edited by S. Chu, V. Vuletic, A. Kerman, and C. Chin (World Scientific, Singapore), p. 12.
Woestenenk, G., J. Thomsen, M. van Rijnbach, and P. van der Straten, 2001, Rev. Sci. Instrum. **72**, 3842.
Woodworth, J. R., and H. W. Moos, 1975, Phys. Rev. A **12**, 2455.
Yan, Z.-C., and J. F. Babb, 1998, Phys. Rev. A **58**, 1247.
Yasuda, M., and H. Katori, 2004, Phys. Rev. Lett. **92**, 153004.
Yasuda, M., and F. Shimizu, 1996, Phys. Rev. Lett. **77**, 3090.
Yerokhin, V. A., and K. Pachucki, 2010, Phys. Rev. A **81**, 022507.
Zelevinsky, T., D. Farkas, and G. Gabrielse, 2005, Phys. Rev. Lett. **95**, 203001.
Zhao, P., J. R. Lawall, and F. M. Pipkin, 1991, Phys. Rev. Lett. **66**, 592.
Ziń, P., J. Chwedeńczuk, and M. Trippenbach, 2006, Phys. Rev. A **73**, 033602.
Ziń, P., J. Chwedeńczuk, A. Veitia, K. Rzazewski, and M. Trippenbach, 2005, Phys. Rev. Lett. **94**, 200401.
Ziń, P., A. Dragan, S. Charzyński, N. Herschbach, W. Hogervorst, and W. Vassen, 2003, J. Phys. B **36**, L149.
Zinner, M., P. Spoden, T. Kraemer, G. Birkl, and W. Ertmer, 2003, Phys. Rev. A **67**, 010501.